COMBUSTION EFFICIENCY IMPROVEMENT IN A ROTARY FURNACE USING A POST COMBUSTION CHAMBER

BY

LUWAYA EDWIN

THE UNIVERSITY OF ZAMBIA

LUSAKA

2000

COMBUSTION EFFICIENCY IMPROVEMENT IN A ROTARY FURNACE USING A POST COMBUSTION CHAMBER

BY

LUWAYA EDWIN

A DISSERTATION SUBMITTED TO
THE UNIVERSITY OF ZAMBIA IN PARTIAL FULFILMENT OF THE REQUIREMENTS FOR THE DEGREE OF MASTER OF ENGINEERING IN THERMOFLUIDS

THE UNIVERSITY OF ZAMBIA

LUSAKA

2000

To My Family

DECLARATION

I Luwaya Edwin do hereby solemnly declare that this dissertation represents my own work, and that it has not previously been submitted for a degree at the University of Zambia or any other University.

Signature: .....

Date: 8/11/00

APPROVAL

This dissertation of Luwaya Edwin is approved as fulfilling the partial requirements for the award of the degree of Master of Engineering in Thermofluids by the University of Zambia.

Name	Signature	Date
Dr P.N. Kioni External Examiner	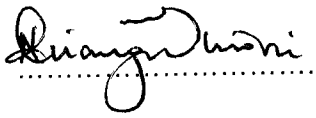	8th August 2000
Dr. N.J. Kwenda Kwema Internal Examiner	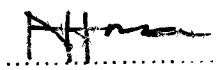	7.11.2000
..... Supervisor	.....	.....
Dr S.B. Kanyanga Dissertation Chairperson	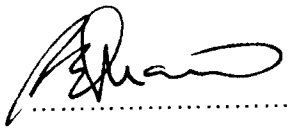	8/11/2000
.....	.....	.....

ABSTRACT

Combustion Efficiency Improvement in a Rotary Furnace using a Post Combustion Chamber. Luwaya Edwin. Department of Mechanical Engineering, University of Zambia.

Geometric parameters, of a rotary furnace, necessary for the improvement of combustion efficiency are analysed using Computational Fluid Dynamics (CFD). The simulation is based on a real Rotary Furnace at Kabwe Power and Metals Limited in Kabwe. A Post Combustor Chamber (PCC) was incorporated in the numerical model at the exit of the combustor and the results compared with the case where no post combustor was used. Performance optimisation of the furnace was done by varying the fuel-air ratio and the size of the PCC. The flow characteristic results obtained, for the case of PCC and no PCC incorporated were contrasted. Flow characteristics were looked at in the wake of combustion, focusing on convection, temperature distribution, conduction, and radiative heat transfer.

The k-ε model is used for turbulence flow prediction. Combustion of premixed fuel is simulated by the Simple Chemical Reacting Scheme (SCRS). The eddy break-up (EBU) model is used to determine the rate of the reaction. The six-flux model is used for the radiative heat transfer without turbulence-radiation interaction i.e. only the products of combustion are participating in radiative heat transfer. The SIMPLEST algorithm is employed to solve the transport equations of momentum and other scalar variables. Radiation field is determined using a modification of the SIMPLEST scheme.

The computation has shown that improvement of the thermal performance of the Rotary Furnace can be done using the post combustion chamber. The PCC improves the thermal performance of the furnace by increasing the intensity of recirculation and mixing of hot vitiated products with fresh charge in the primary combustion zone thus increasing residence time of combusting materials in the furnace space. This reduces the exhaust gas loss therefore increasing the useful heat value in the combustor. The heat flux to the sink is equally increased. The combustion efficiency improved by 0.53 percent. For the rotary furnace at Kabwe the PCC should be optimised as demonstrated in this study

Keywords: Combustion efficiency, EBU model, Post Combustion Chamber, Premixed fuel, Recirculation, Rotary furnace, Six-flux model, SCRS, SIMPLEST.

ACKNOWLEDGEMENTS

It is a great pleasure to acknowledge the people who contributed their support, time and physical energy to this project. Foremost, I acknowledge the inestimable guidance, advice and encouragement Dr. Chisale P.C. ceaselessly provided throughout this study, which spanned for a year and some months.

I also acknowledge the help rendered by Professor Francis Yamba, for the expertise in combustion and Ir. Lamers A.P.G.G. for the expertise in numerical computations. I also extend my gratitude to my friends and colleagues, with whom I shared many wonderful experiences and friendly diversions.

The financial aid, from the MHO program of the Netherlands' Ministry of Higher Education, for the scholarship is also greatly appreciated. The support was just more than monetary.

All this work would have been neither possible nor meaningful without the understanding, patience and unflagging support from my family and my parents. They tolerated amazingly well the time spent on the project for days at end, time that I could have spent with them.

TABLE OF CONTENTS

Page

DECLARATION....(iv)
APPROVAL....(v)
ABSTRACT....(vi)
ACKNOWLEDGEMENTS....(vii)
LIST OF FIGURES....(xi)
LIST OF TABLES....(xiv)

1.0 INTRODUCTION

1.1 Background....1
1.2 Literature Review....2
1.2.1 Turbulence Models....2
1.2.2 Combustion Models....3
1.2.3 Radiation Models....4
1.2.4 Heat Recovery Methods....5
1.2.5 Experimental Studies....7
1.3 Problem Statement....8
1.4 Objectives of the Study....9
1.5 Methodology of the Study....10

2.0 MATHEMATICAL MODELS

2.1 Introduction....11
2.2 Formulation of Governing Equations of Fluid Flow and Heat Transfer....12
2.3 Flux Laws and Source Laws....25
2.4 Turbulence and its Modelling....30
2.4.1 Turbulence....30
2.4.2 Time Averaged Conservation Equations for Turbulence....34
2.4.3 Turbulence Modelling....40
2.5 Combustion Analysis and its Modelling....44
2.5.1 Combustion Analysis....44
2.5.2 Simplification of Species Conservation Equations....50

2.5.3 Combustion Rate in Premixed Flames and the Eddy-Break-Up Model....55
2.6 Radiation and its Modelling....58
2.6.1 Introduction....58
2.6.2 Radiation Energy Balance....61
2.6.3 Radiation Models....62

3.0 METHOD OF SOLUTION

3.1 Introduction....67
3.2 Summary of the Solution Scheme....68
3.2.1 Numerical Procedure for the Three-Dimensional Flow....68
3.2.2 The Computer Code used....76
3.3 Miscellaneous Details....78
3.4 Formulations and Boundary Conditions for a Three-Dimensional Furnace....80
3.5 Simultaneous Predictions of Flow Patterns and Radiation for Three-Dimensional Flames....86

4.0 NUMERICAL RESULTS AND DISCUSSIONS

4.1 Overview and Problem Description....89
4.2 Effect of Post Combustion Chamber: Results and Discussions....92
4.2.1 Flow Field....92
4.2.2 Combustion and Temperature field....107
4.2.3 Radiation Field....114
4.3 Effect of Optimisation of Post Combustion Chamber Results and Discussions....119
4.3.1 Model Parameters....119
4.3.2 Flow Field....121
4.3.3 Combustion and Temperature field....124
4.3.4 Radiation Field....127
4.4 Heat Flux across Wall of Combustor....130
4.5 Exhaust Gas Loss....132
4.6 Combustion Efficiency....133
4.7 Summary....133

5.0 CONCLUSIONS AND RECOMMENDATIONS

5.1 Conclusions.....135

5.2 Recommendations.....136

APPENDIX A Specifications for Rotary Furnace.....139

APPENDIX B Lead Recoveries Data.....140

APPENDIX C Verification of Numerical Computer Program.....142

APPENDIX D Verification of Turbulent Model.....149

APPENDIX E Relaxation of Sources.....154

REFERENCES.....156

5.0 CONCLUSIONS AND RECOMMENDATIONS

5.1 Conclusions.....135

5.2 Recommendations.....136

APPENDIX A Specifications for Rotary Furnace.....139

APPENDIX B Lead Recoveries Data.....140

APPENDIX C Verification of Numerical Computer Program.....142

APPENDIX D Verification of Turbulent Model.....149

APPENDIX E Relaxation of Sources.....154

REFERENCES.....156

LIST OF FIGURES

2.1 Fluid Element for Fluid Conservation Laws....12
2.2 Mass Flow in and out of Fluid Element....14
2.3 Stress Components on Three Faces of Fluid Element....16
2.4 Stress Components in x-direction....16
2.5 Heat Flux Vector Components....21
2.6 Typical Point Property Measurement in a Turbulent Flow....36
2.7 Control Volume....45
2.8 Classical Combustion Analysis....46
2.9 Control Volume Energy Balance....47
2.10 Mixing and Fast Reaction between Fuel and Oxidant Streams....54
2.11 Radiant Energy Balance on a Monochromatic Beam passing a specific direction through Element in Absorbing, Emitting, Scattering Medium....52

3.1 Numerical Grid Arrangement in the Axisymmetrical Furnace....69
3.2 Integration Domain....69
3.3 Three-Dimensional Finite Difference Equation Grid (Y-Z plane)....70
3.4 Convention for the Neighbouring Nodes and Coefficients....73
3.5 Structure of PHOENICS....76
3.6 Schematic of the Rotary Furnace (a) Without PCC and (b) With PCC....82
3.7 The Problem: Statement....86
3.8 The Problem: Why Simultaneous Prediction is needed....86
3.9 The Problem: Physical Aspects, 1....86
3.10 The Problem: Physical Aspects, 2....86
3.11 The Problem: Physical Aspects, 3....87
3.12 The Problem: Mathematical Aspects, 1....87
3.13 The Problem: Mathematical Aspects, 2....87
3.14 The Solution Procedure, 1, Turbulence....87
3.15 The Solution Procedure, 2, Chemistry....88
3.16 The Solution Procedure, 3, Radiation....88
3.17 The Solution Procedure, 4, Mathematics....88

4.1 Adiabatic Flame Temperature Dependency on Equivalent Ratio [λ].....91

4.2 Velocity vector plots for furnace only in Z-Y plane:
(a) At θ=0° and 180 ° (b) At θ=90° and 270 °.....95

4.3 Velocity vector plots for furnace with PCC in Z-Y plane:
(a) At θ=0° and 180 ° (b) At θ=90° and 270 °.....96

4.4 Velocity vector plots for inlet section of furnace only in Z-Y plane:
(a) At θ=0° and 180 ° (b) At θ=90° and 270 °.....97

4.5 Velocity vector plots for inlet section of furnace with PCC in Z-Y plane:
(a) At θ=0° and 180 ° (b) At θ=90° and 270 °.....98

4.6 Velocity Vector plots in cross-stream of Furnace only in Y-Z plane
(a) At z/L = 0.01 (b) At z/L = 0.2 (c) At z/L = 0.4 (d) At z/L = 1.....99

4.7 Velocity Vector plots in cross-stream of Furnace with PCC in Y-Z plane
(a) At z/L = 0.01 (b) At z/L = 0.095 (c) At z/L = 0.196 (d) At z/L = 1.....100

4.8 Axial Velocity Distribution at various r/R and λ=1 in Y-Z plane atθ =0° and 180°:
(a) Furnace only (b) Furnace with PCC.....101

4.9 Turbulent Kinetic Energy (J) in Y-Z plane at λ=1
(a) Furnace only (b) Furnace with PCC.....104

4.10 Turbulent Dissipation (KJ/s) Y-Z plane at λ=1
(a) Furnace only (b) Furnace with PCC.....106

4.11 Mixture Fraction Distribution in Y-Z plane at λ=1
(a) Furnace only (b) Furnace with PCC.....110

4.12 Fuel Concentration [kg/m^3] Distribution in Y-Z plane at λ=1
(a) Furnace only (b) Furnace with PCC.....111

4.13 Temperature Distribution in Y-Z plane at λ=1
(a) Furnace only (b) Furnace with PCC.....112

4.14 Temperature Distribution at various r/R and λ = 1 in Y-Z plane at θ = 0°and 180°
(a)Furnace only (b) Furnace with PCC.....113

4.15 Radiation Flux Distribution for Furnace only
(a) x-direction (b) y-direction.....115

(c) z-direction.....116

4.16 Radiation Flux Distribution for Furnace with PCC
(a) x-direction (b) y-direction.....117

(c) z-direction.....118

4.17 Temperature Distribution at Centre line of Furnace at λ = 1:
For various lengths of PCC.....120

4.18 Axial Velocity Distribution at various r/R and λ = 1 in Y-Z plane at θ = 0°and 180°:
Furnace with Optimised PCC.....121

4.19 Turbulence in Furnace with Optimised PCC in Y-Z plane at λ=1
(a) Kinetic Energy *k* [KJ] (b) Dissipation ε [KJ/s].....123

4.20 Combustion in Furnace with Optimised PCC
(a) Mixture Fraction (b) Fuel Concentration [kg/m^3] 125

4.21 Temperature Distribution in Furnace with optimised PCC in Y-Z plane: 126

4.22 Temperature Distribution at various r/R and λ = 1 in Y-Z plane at θ = 0°and 180°:
For Furnace with optimised PCC 126

4.23 Radiation Flux Distribution for Furnace with Optimised PCC
(a) x-direction (b) y-direction 128

(c) z-direction 129

4.24 Heat Flux across Wall of Furnace at λ = 1 131

4.25 Heat Loss through Exhaust gas at λ = 1 132

B.1 Annual Lead Recoveries
(a) Before the PCC Project, (b) After the PCC Project 141

C.1 Test Problem for Verifying the Computer Code 142

C.2 Numerical and Exact Solution of the Problem shown in Figure C1 143

C.3 The Grid used for Discretisation 145

C.4 Numerical and Exact Solutions of the Problem shown in Figure C.1 148

D.1 Schematic Diagram of the (LLNL) Test Cell 150

D.2 Predicted Flow inside Compartment: Velocity Vectors Plots
in Z-Y Plane at X=5.25 m 151

D.3 Predicted Temperature (K) Field in the Y-Z plane at X=3.00 m 152

D.4 Comparison of Temperature Distribution between Experiment and k-ε 153

LIST OF TABLES

3.1 Summary of Important Features of PHOENICS....76
3.2 List of Variables for the Model Analysis....83
3.3 Boundary Conditions....84

4.1 System Parameters of the Reference Problem....89
4.2 System Parameters of the Post Combustion Chamber....89
4.3 Some Computational details of the Simulation for reference and real case....90
4.4 Some Computational details of the Simulation with optimised PCC....119
4.5 Combustion Efficiency....133
4.6 Effect of Post Combustion Chamber on Thermal Performance of Furnace....134

A.1 Specifications for Rotary Furnace....139
B.1 Results For the Lead Smelting Trials....140
C.1 Values of Coefficients....146
C.2 Results....147
E.1 Recommended Relaxation Factors (α)....155

1.0 GENERAL INTRODUCTION

1.1 Background

Furnace engineers have for a long time looked forward to predict successfully the flow, reactions and heat transfer in combustion chambers by numerically solving the fundamental transport equations of the related phenomena. The ultimate goal being to avoid the experimental approach which is time consuming and sometimes prohibitively expensive. It is worthy noting that numerically calculated distributions of properties of interest are a recent development. The problem has been compounded by the complexity of the transport equations, absence of knowledge of the detailed physics and chemistry of the processes and limitation of current computers. The development of stable numerical schemes, more fundamental understanding of the fluid physics, and availability of fast digital computers have given rise to the latest achievements.

For large-scale turbulent reacting flows, the problems associated with fluid dynamics and chemistry remain to be solved. This is particularly true in industrial combustion chambers where complex flows unfold [1, 2]. The turbulent structure of the flow has to be predicted first, but any finite number of correlation equations cannot exactly describe its time mean flow field. Though many models are available, they are not fully understood either. Well understood is the molecular transport of heat and mass transfer, but irreversible coupling effects still pose difficulties. Molecular transport processes are negligible compared to turbulent processes in furnace flows. Complicated problems do arise with chemical reactions because of the large number of intermediate reactions, most of which are not known. Sometimes non-chemical reactions like mixing of fuel and oxidiser govern the fuel-burning rate. These complications in turbulent flames impede the development of a complete combustion theory. Simplified approaches are commonly employed. These approaches, as practised, neglect all reaction times except for the most important one or two processes.

Infrared radiation to and from the gas increases due to existence of polyatomic or nonsymmetric molecules like CO_2, H_2O, CO and-or CH_4 in the products and fuel. Increased optical path length increases radiation contribution thus making it the dominant heat transfer mode for furnace dimensions of one meter or greater. For a gas downstream from the flame, radiation originates from a homogeneous medium. Near the flame, this is not the case, as the properties of the medium change rapidly along the path. Also

transport and other quantities in the medium fluctuate with time. Common products of combustion products at atmospheric pressure are strong selective emitters and absorbers of thermal radiation. Therefore the above factors make the problem of radiation transfer in combustion chambers extremely complicated. That is, the intensity of radiation is a function of the local co-ordinates, direction and wavelength with fluctuations that should be averaged. To account for all these effects in practical combustion calculations will entail a formidable task. Most sources neglect some factors like temperature fluctuations and spectral effects etc [3].

1.2 Literature Review

1.2.1 Turbulence Models

Mathematical modelling of turbulence has mostly been developed for incompressible flows. Some researchers [4, 5, 6] have used these models to simulate furnace flows that are compressible in nature due to large temperature variations and they have obtained reasonably good results. For furnace flows, the two-equation k-ε turbulence model has been successfully applied. The other types of turbulence models existing, i.e. mathematical or simulative, have not been verified for furnace flows and hence their validity is not known. The k-ε is widely accepted as the most reasonable compromise between accuracy and computational ease for flows in furnaces as they involve large number of dependent variables. For compressible high Reynolds number flows, the model has been modified in terms of density averaged quantities. Other researchers [7, 8, 9] used time-averaged quantities though they have complex expressions. Density averaged expressions are simpler, and mostly closer to experimental results than time averaged quantities. A fine grid is usually required in the near wall region for the k-ε model application. To reduce the computational effort the wall functions are used [10]. The Boussineq approximation is generally accepted for transport quantities other than the momentum. It regards the second order correlation of a scalar quantity and velocity as proportional to the gradient of the mean scalar quantity. The concept is also applied to the transport of correlation of scalar quantities.

1.2.2 Combustion Models

Chemically reacting turbulent flow has a complicated nature. Therefore numerical solutions for the combustion variables were attempted only after significant advances in modelling of turbulence. Several methods and models have been proposed, and they have been reviewed by Khalil [11]. Turbulent homogeneous flames fall into premixed, diffusion and general flames, according to the inlet composition of the fuel and oxidiser. They can be categorised into diffusion controlled or reaction controlled flames, depending on the Damkoehler number i.e. ratio of the diffusion time to the reaction time. Heterogeneous flames such as those which occur during droplet combustion are characterised by the additional feature of evaporation time. Since combustion involves many intermediate steps, most of the fast processes are neglected and only one or two slow processes are considered to govern combustion rate.

Spalding [12] proposed the eddy break up (EBU) model that is based on analogy and empirical observations and gives a reasonable approximation for diffusion flames [9]. Pope [13] showed that the EBU model does not guarantee a standard solution for the diffusion flames and hence is restricted to premixed flames [14]. Bray [15] has given a rigorous treatment of premixed flames. He obtained an expression similar to the EBU model for a case of high Damkoehler number. The probability density function (p.d.f.) is a fundamental concept in combustion analysis and Borghi [16] and O'Brien [17] have discussed it at some length. The two researchers derived the transport equation of the p.d.f. The method calls for the solution of a large number of transport equations for the many p.d.f. independent scalar variables. This will require very high computing capability. For practical calculations, assumed functional forms of the p.d.f are used and most important parameters of the p.d.f. are calculated. The use of clipped Gaussian or Gama function distribution of probability of mixture fraction is recommended. Spalding [18] has reviewed two-phase flows and combustion models. Khalil [11] and Jones [2] have surveyed the mechanisms of pollutant formation, which they found to be reaction controlled. Two-phase combustion and pollutant formations are not the subject of this work.

1.2.3 Radiation Models

Heat transfer is very important either to increase the thermal efficiency of the system or to prevent excessive heating of the combustor. Many industrial furnaces are used to transfer heat from products of combustion and space to a load in the furnace. Pure combustors like gas turbine combustors are used to burn fuel in order to raise the temperature of products of combustion. For a combustor of one meter or greater space, radiation is the dominant heat transfer mode compared to convection. Convection heat transfer rate at the wall is solved through the energy equation with the aid of wall functions, which express the effective turbulent viscosity and effective thermal diffusivity in the boundary layer. Radiation, however, requires special attention and treatment because of its integral nature. Various techniques for solving the Radiative Transfer Equations (RTE) are reviewed by Viskanta [19]. Khalil [11] has treated the commonly used methods for the combustion space heat transfer: zone method, spherical harmonics approximation, and discrete ordinate methods and flux method. Zone methods, first suggested by Hottel [20] are easy to apply but very expensive in memory and computing time for large number of zones. This is the main reason for its non usage in the kind of flow under consideration in this thesis. Other techniques available are the Monte Carlo method and Finite-Difference Method. These though are not used; instead most of the practical calculations are done using differential approximations due to their compatibility with the transport equations. The differential approximations are based on an assumed intensity distribution with direction, in order to derive second order differential equations as the model equation(s). The differential approximations for multidimensional geometries are the P_N-approximations, the flux methods and modified flux methods. Neither the P_N-approximations nor the spherical harmonics method has been used in combination with the other transport equations for momentum, turbulence and combustion, but it appears to have some advantages, namely, it has accuracy and requires relatively small number of equations for solution compared to other differential approximations.

The most widely used methods to model radiation transfer in combustion are the flux methods and their modifications. They have been found to yield reasonable predictions. DeMarco and Lockwood [21] have accounted for the variation of the intensity with the solid angle in terms of polynomials of the direction cosines. The discrete ordinate method, first proposed by Chandrasekhar [22], is simple physically and is useful for one or two-dimensional geometries and is appropriate for all opacities. The differential approximations albeit may be subject to greater errors as the optical thickness is

decreased [23]. Unfortunately, for complicated and-or three-dimensional geometries, the number of discrete ordinate equations becomes extremely large.

Of greater importance is the reduction in the number of radiation model equations to be consistent with the accuracy required. The reduction is generally achieved after assumptions have been made and this somehow affects the accuracy within the acceptable range. This is as a result of the spectral nature of gaseous radiation, which frequently requires the use of non-gray models. This may require solution of simultaneous radiation model equations for all the spectral bands. Crosbie and Viskanta [24] and Grant [25] studied the effect of single line shapes. To cover the numerous lines over the spectrum, narrow or wide band model, weighted sum of gray gases model, and the mean absorption and emission coefficient are being used. To account for the inhomogeneity of participating medium Curtis Godson approximation [26], series-expanded formulation [27] and total transmittance technique [28], have been developed. These methods require knowledge of the temperature, concentration and-or pressure distribution along the radiation path and therefore cannot be directly used for gases with fluctuating properties along the path.

Normally the turbulence interacts with the radiation. Because of the high intense fluctuations of local temperature resulting from combustion, the emission of radiation is higher than that which is calculated at the mean temperature. The turbulence-absorption interaction has been accounted for by assuming that the medium is radiatively "cold". However, the effect of turbulence-emission interaction has not been investigated, and thus requires additional research effort. The turbulence-emission interaction is believed to have greater effect than the turbulence-absorption interaction for combustion chambers [29]. Therefore, the time-mean radiation intensity has not been obtained.

1.2.4 Heat Recovery Methods

Efficient combustion is bound up with the maintenance of suitable ambient conditions prevailing in the furnace. The most important factors to be controlled are the actual furnace temperature level, and uniform temperature throughout the furnace. The major control parameters are the rate of fuel input, flame characteristics and conditions of draught. The most ideal means of control though are a combination of instrumentation involving measurement of temperature, control of rate of fuel consumption from the results

of this measurement, coupled with control of fuel-air ratio and of draught, regulated from the measurement of the furnace pressure [30].

In practical combustors, heat losses are inevitable but can be controlled. The desirable thing in a furnace is to transfer the heat to the load for the purpose of raising its temperature and to enhance certain chemical or physical changes to take place in the material. But heat is lost in various ways. The common ones are: furnace wall losses, foundation losses, surroundings losses by radiation and convection through the outer surfaces of the walls. Some heat radiates away through cracks and openings. Furnace gases also pass out through doors. For a metallurgical furnace special loss by radiation from exposed liquid surface of a salt bath or lead bath can occur. Finally, heat passes out with the products of combustion, either in form of sensible heat or undeveloped heat of combustibles escaping unburned. In order to establish improved practise by modification of the furnace operation or design details, knowledge and analysis of the heat balance is necessary.

Heat Supplied = Useful Heat + Structure Loss + Exhaust Gases Loss

Therefore for constant fuel consumption and constant structure loss, an increase of useful heat can take place only by reduction of stack loss. From the heat balance an indication can then be obtained of the directions in which improvements can be made to increase useful heat [31].

Some items involved in the heat balance are unavoidable losses. Inevitably the flue gases would contain significant heat. The heat need not be lost if efficient methods of waste heat recovery are applied. Several devices have been developed over the years to recover waste heat like the recuperators (regenerators), and waste heat boilers. A recuperator is a heat exchanger in which energy from a steady flow of hot products of combustion i.e. waste gas is transferred to the air supplied to the combustion process. A wide variety of recuperators are used in practise, many of which employ radiation heat transfer from the waste gases as well as convection. A regenerator also transfers energy from the waste gases to the incoming combustion air, but in this case an energy storage medium, such as a corrugated steel sheet or ceramic matrix, is alternately heated by the hot gases and cooled by air. Other regenerators use the concept of switching alternately the flow paths to heat and cool the thermal storage medium. Waste heat boilers are sometimes added to

generate process steam or power. Air pre-heated by flue gases could be supplied to gas turbine to drive blowers or generate power. Such systems are only economical for continuously operated furnaces with operation temperatures above 870°C. For furnace temperatures greater than 1200°C, fuel chemical reaction continues even in the stack leading to heat losses and significant discrepancies in fuel usage [32, 33].

However improvement of combustion efficiency can be achieved using the Post Combustion Chamber (PCC). In contrast to regenerators, the PCC does not recover the lost heat for use. It just minimises the loss by effectively controlling the parameters promoting stack losses. These parameters are flue gas velocity, residence time of burning mixture in furnace, back pressure build-up and combustion characteristics of unburned particles, [34]. Therefore the current study will draw from literatures to set its investigatory work and come up with performance data that will be analysed to draw appropriate conclusions and recommendations.

1.2.5 Experimental Studies

More has been reported on theoretical studies of industrial furnaces and relatively little on experimental work in industrial furnaces. Because of the three-dimensional nature of the combustion furnace, many investigators have done studies on two-dimensional axisymmetric combustors. Khalil *et al.* [35] studied an axisymmetric combustor with a jacket. They computed the flow, combustion and heat transfer numerically and obtained reasonable agreement with the experimental data. In comparing the results, however, there are many unmeasured quantities, which makes the direct verification of the numerical prediction difficult. Jones and McGuirk [36] performed a series of experiments on two-dimensional and three-dimensional gas turbine combustors by neglecting heat transfer. These computations showed lower and less uniform temperature field than obtained experimentally, possibly because they neglected the radiative heat transfer in the gas. Essenhigh [37] and his co-workers reported a series of experiments on a test furnace. They concluded that the effect of thermal load, excess air, process temperature, flame-load temperature difference, load emissivity and heat loss through the wall are the most important, while the effect of gas emissivity is not as significant [37]. Patankar and Spalding [38] reported a calculation method for the three-dimensional turbulent reacting flow in a gas-turbine combustion chamber. They simultaneously predicted flow patterns and radiation for three-dimensional flames. The combined flow and radiation problem was

formulated in terms of finite-difference equations. The resulting predictions though showed only qualitative agreement with experiment.

1.3 Problem Statement

At the slag dump in the mine area of Kabwe Power and Metal Ltd (KPM), formerly Zambia Consolidated Copper Mines Ltd (ZCCM) Kabwe Division, there are over 500 tonnes high-grade slag containing 40 percent lead (Pb), and over 2 000 000 tonnes low-grade slag containing 18 to 40 percent Pb. This Pb bearing slag exists in form of sulphides (PbS), Sulphates ($PbSO_4$) and Oxides (PbO_2, PbO) as entrained metal in the dross. The mixture of these Pb compounds is known as *lead dross*. The slag, which accumulated from various refining processes, poses an environmental threat if left unprocessed. During the ZCCM era several trials to smelt the Pb from this slag were carried out unsuccessfully. The Pb recovery achieved then amounted to an average of only 26.6 percent. Two major causes for this poor recovery of Pb were identified. The first was the loss of useful heat from the furnace through the flue gases, resulting in high fuel consumption. The second was as a result of the loss of useful heat leading to low heat rise in the combustor, therefore preventing attainment of temperature of reaction (i.e. 1200 ^{0}C) for the slag. This in turn prolonged the smelting time to a period extending to 48 hours per batch. The KPM Ltd realised the need to improve production and exploit the lead bearing materials to produce lead for export and local use in the manufacture of starting sheets of Pb for the production of anodes for use in ZCCM Tank Houses. These factors led to pursuance of the lead-smelting project. Trials were carried out to establish the project viability. The trials proved that recovery of Pb could be improved by reducing the loss of useful heat to the stack, thus raising the temperature of reaction of the slag. This in turn would improve combustion efficiency (η_c) and result in low fuel consumption. To improve recovery, a Post Combustion Chamber was installed in the exhaust system of the old combustor. The recovery of Pb, due to installing of a Post Combustion Chamber, rose to an average of 74.96 percent. (Appendix B [34]).

With problems like these, studies of possible alternatives in furnace designs, modifications of existing equipment, constructions and operations to improve furnace performance can not be over emphasised, in view of the diminishing supplies of fossil fuels and accompanying rise in energy costs. These studies represent a much more economic way of increasing combustion efficiency in existing combustors at relatively low costs. To understand the intricacies leading to improved recovery of Pb by using a Post Combustion

Chamber, flow characteristics: combustion characteristics, and heat transfer characteristics have to be investigated.

1.4 Objectives of the Study

The purpose of this research, therefore, is to obtain a better understanding of an industrial rotary furnace incorporating a post combustor chamber by numerically simulating the flow, combustion and heat transfer in the furnace. An industrial furnace is a fairly large (dimensions in the range of 1m and above) high temperature furnace such as a cement kiln or metal smelting furnace. This study is limited to premixed flame of natural gas (methane CH_4) and air as the oxidiser. Scattering of radiation is negligible, as combustion products of gas-fired furnaces usually do not contain particulates. The study is for a three-dimensional cylindrical combustion chamber. The work is focused on the most important phenomena and their effects, which require additional understanding. While various methods have for long been used to recover waste heat from flue gases, more complete understanding of how the post combustor chamber help retain heat in the furnace by influencing the flow features is needed. The main focus of this research will be on the effects of the post combustor on these flow characteristics and the performance of the furnace. Specifically, the objectives of this study are:

1. To model numerically the furnace with the view of getting optimum flow features of turbulence, combustion and heat transfer without and with the Post Combustor Chamber and compare the results.

2. To determine the effects of geometric variations of post combustion chamber on the overall velocity patterns, temperature distribution and concentration distribution in various combustor regimes as well as heat loss through the walls of combustor and exhaust gases.

3. To determine the effect of the post combustion chamber on combustion efficiency of furnace.

The results of this study will furnish information necessary for the improvement of heat recovery in the furnace and hence improve combustion efficiency and fuel economy as well as minimise pollution of the environment.

1.5 Methodology of the Study

A numerical simulation of combustion characteristics is used to model the furnace. The governing differential equations of fluid flow, combustion and heat transfer are solved using a numerical code called PHOENICS. The performance of the furnace is modelled in two parts at an optimum fuel-air ratio to be determined. The reference model of the furnace is without the post combustion chamber. The second model incorporates the post combustion chamber in the exhaust system of the reference model. The two sets of results are contrasted. Finally, at the same optimum fuel-air ratio, the size of the post combustion chamber is varied in the simulation to obtain flow, combustion and heat transfer characteristics favouring high combustion efficiency.

The combustion efficiency in this study is defined as the measure of the extent to which energy in the combustor from reactants have been converted from chemical energy to thermal energy. This is characterised by the amount of energy in the effluent to the chemical energy contained in the fuel, namely calorific value. The combustion efficiency will be calculated on the energy basis given by:

$$\eta_C = \frac{\text{Net Rate of Energy Release}}{\text{Rate of Energy Supply}} = \frac{(\text{Rate of Energy Release}) - (\text{Rate of Energy Loss})}{\text{Rate of Energy Supply}}$$

$$\eta_C = \frac{(m_A C_{pA} + m_F C_{pF}) T_{tFA} - (m_p C_{pp} T_{tp} + m_F C_{pF} T_F)}{H_{FU}} \qquad \text{Eq. 1.}$$

Where:-m_A, m_F and m_p are the mass flow rates of air, fuel and products respectively [kg/s].

-T_{tFA} and T_{tp} are the total-head temperatures of fuel-air mixture and products of combustion respectively, [K].

-T_F is the fuel inlet temperature, [K].

-H_{FU} is the combustion value of the fuel, [MJ/kg].

-C_{pA}, C_{pF} and C_{pp} are the constant pressure mean specific heat capacities of air, fuel and products, [kJ/kgK]. For fuel the C_{pF} is from datum to T_F [39].

Finally, conclusions will be drawn and recommendations made based on the results so obtained.

2.0 MATHEMATICAL MODELS

2.1 Introduction

Combustion modelling is the simulation of a physical process on a scale, or by a method, which enables combustion investigations to be carried out which would be difficult, if not impossible, to perform on the real combustor. The model mimics selected aspects of the real combustor processes and therefore predicts or simulates its characteristics and responses to certain design or operating changes. This study uses mathematical modelling to simulate fluid flow and mixing, combustion and heat transfer phenomena, which govern the thermal behaviour of the plant. The model is written in form of computer program embodying a system of mathematical equations, text and-or data written in Fortran language, with defined input and output parameters. In the mathematical model simplifying assumptions have been made when formulating the phenomena in order to arrive at a near real problem. The simulated results need validation against reliable experimental data in order to evaluate its range of applicability and its predictive accuracy. Absolute predictive accuracy is not necessarily required as the model can be "calibrated" by sensible adjustment of some input parameters, to give agreement with existing plant data. This then becomes a reliable model of that particular plant, which can then be used to simulate the effects of design or operation changes [1].

The steady state flow of gases and liquids plays a vital role in many kinds of engineering applications and devices. The problem of flow and heat transfer in furnaces and combustors are of a multidisciplinary nature, and hence, attention is focused on the general principles which govern the behaviour of the flow in complex configurations. The conservation equations of mass, momentum, species and energy are expressed through partial differential forms. These equations form the foundation and represent mathematical statements of the conservation laws of physics upon which all prediction procedures are based either directly or indirectly. The governing equations do not themselves provide complete specification of the mathematical problem, as additional information is required. This first information deals with the turbulent nature of the flow necessary to solve the set of momentum equations in turbulent flows and generally form turbulence models. The second type of information deals with reactive flows i.e. the specification of the rate of fuel consumption, heat release and flame properties including geometry of the reaction chamber. The various ways of preparation techniques of fuel and air result in diffusion, premixed and arbitrarily fired flames. These flames differ fundamentally from each other right from flame initialisation, development and stability. The difference become even

more complex when these flames are analysed in turbulence regime. This information is important in understanding aspects of combustion modelling.

Heat transfer to the workload in the chamber, in many situations, is the main requirement from the combustion process. This heat transfer is utilised to heat up the workload. Radiation and convective heat transfer models take care of this aspect. Radiation contribution to the energy balance is needed to complete the specification of the energy balance equation. To complete specification of the problem, details of thermodynamic properties are needed. To solve the equations, boundary and inlet conditions should be specified [2].

2.2 Formulation of Governing Equations of Fluid Flow and Heat Transfer

In this section, the mathematical basis for a comprehensive general-purpose model of fluid flow, combustion and heat transfer is developed from the basic principles of conservation of mass, momentum and energy. This leads to the governing equations of fluid flow, combustion and heat transfer. The fluid is taken as a continuum. The molecular structure of matter and molecular motions are ignored for the analysis of fluid flows at macroscopic length scales (say 1μm and larger). Macroscopic properties (i.e. velocity, pressure, density and temperature; and their space and time derivatives) are used to describe the behaviour of the fluid. These are assumed as averages over suitably large number of molecules. A fluid particle or point in a fluid is then the smallest possible element of fluid whose macroscopic properties are not influenced by individual molecules. A small element of fluid with sides δx, δy and δz is considered here, (Fig. 2.1).

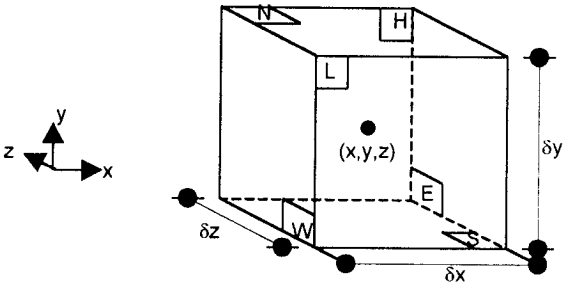

Figure 2.1 Fluid element for conservation laws.

For the six faces, the labels N, S, E, W, H and L stand for North, South, East, West, High and Low. Co-ordinate axes are given in the positive directions. Position (x, y, z) locates

the centre of element. All fluid properties are functions of space and time. To avoid unduly cumbersome notation, the dependence on space co-ordinates and time will not be explicitly stated. This practise will apply to all fluid properties throughout this work. The first two terms of the Taylor series expansion will express accurately enough the fluid properties at the faces of the element since they are very small [3].

2.2.1 Mass Conservation (Continuity)

In case of the mass balance for the fluid element: Rate of increase of mass in fluid element is equal to net rate of flow of mass into the fluid element. The rate of increase of mass in the fluid element is:

$$\frac{\partial}{\partial t}(\rho\ \delta x\ \delta y\ \delta z) = \frac{\partial \rho}{\partial t}\delta x\ \delta y\ \delta z \qquad \text{Eq.2.1}$$

The mass flow rate across a face of the element is given by product of density, area and the velocity component normal to the face. From Fig.2.2 the net rate of flow of mass into the element across its boundaries is given by:

$$\begin{aligned}
&\left(\rho u - \frac{\partial(\rho u)}{\partial x}\cdot\frac{1}{2}\delta x\right)\delta y\ \delta z - \left(\rho u + \frac{\partial(\rho u)}{\partial x}\cdot\frac{1}{2}\delta x\right)\delta y\ \delta z \\
&+\left(\rho v - \frac{\partial(\rho v)}{\partial y}\cdot\frac{1}{2}\delta y\right)\delta x\ \delta z - \left(\rho v + \frac{\partial(\rho v)}{\partial y}\cdot\frac{1}{2}\delta y\right)\delta x\ \delta z \\
&+\left(\rho w - \frac{\partial(\rho w)}{\partial z}\cdot\frac{1}{2}\delta z\right)\delta x\ \delta y - \left(\rho w + \frac{\partial(\rho w)}{\partial z}\cdot\frac{1}{2}\delta z\right)\delta x\ \delta y
\end{aligned} \qquad \text{Eq.2.2}$$

Flows into the element produce an increase of mass in the element and have a positive sign, while flows out of the element have a negative sign.

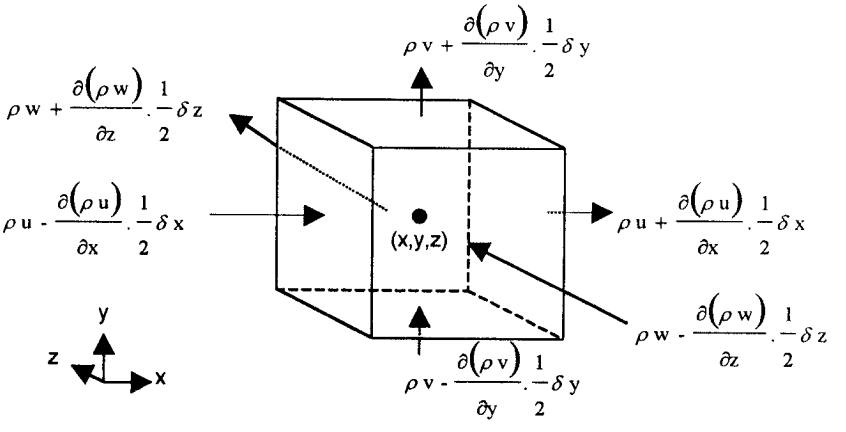

Figure 2.2 Mass flow in and out of a fluid element.

The rate of increase of mass inside the element, Eq.2.1, is equated to the net rate of flow of mass into the element across its faces, Eq.2.2. The expression is divided by the elemental volume ($\delta x\ \delta y\ \delta z$) throughout.

All terms of the resulting mass balance are arranged on the left hand side of the equation giving:

$$\frac{\partial \rho}{\partial t} + \frac{\partial(\rho u)}{\partial x} + \frac{\partial(\rho v)}{\partial y} + \frac{\partial(\rho w)}{\partial z} = 0 \qquad \text{Eq. 2.3}$$

In a more compact vector notation:

$$\frac{\partial \rho}{\partial t} + \mathrm{div}(\rho\, \mathbf{u}) = 0 \qquad \text{Eq. 2.4}$$

Equation 2.4 is the unsteady, three-dimensional mass conservation or continuity equation at a point in a compressible fluid. The first term on the left hand side is the rate of change in time of density (mass per unit volume). The second term describes the net flow of mass out of the element across its boundaries, and is known as the convective term.

For an incompressible fluid (i.e. a liquid) the density ρ is constant and Eq.2.3 in longhand notation becomes:

$$\frac{\partial u}{\partial x} + \frac{\partial v}{\partial y} + \frac{\partial w}{\partial z} = 0 \qquad \text{Eq.2.5}$$

Using Eq.2.4 for an incompressible fluid Eq.2.5 can be expressed as:

$$\operatorname{div}(\mathbf{u}) = 0$$

2.2.2 Momentum Conservation

Newton's second Law states that the rate of change of momentum of a fluid particle equals the sum of the forces on the particle. The rates of increase of x-, y-, or z-momentum per unit volume of a fluid particle are given by:

$$\rho \frac{Du}{Dt}, \ \rho \frac{Dv}{Dt}, \text{ and } \ \rho \frac{Dw}{Dt} \qquad \text{Eq.2.6}$$

Where the total derivative with respect to time or derivative of movement in the u, v, and w directions are as follows:

$$\frac{Du}{Dt} = \frac{\partial u}{\partial t} + \frac{\partial u}{\partial x}\frac{dx}{dt} + \frac{\partial u}{\partial y}\frac{dy}{dt} + \frac{\partial u}{\partial z}\frac{dz}{dt},$$

$$\frac{Dv}{Dt} = \frac{\partial v}{\partial t} + \frac{\partial v}{\partial x}\frac{dx}{dt} + \frac{\partial v}{\partial y}\frac{dy}{dt} + \frac{\partial v}{\partial z}\frac{dz}{dt},$$

$$\frac{Dw}{Dt} = \frac{\partial w}{\partial t} + \frac{\partial w}{\partial x}\frac{dx}{dt} + \frac{\partial w}{\partial y}\frac{dy}{dt} + \frac{\partial w}{\partial z}\frac{dz}{dt}$$

Forces on a fluid particle are divided into two types. The surface forces consist of pressure forces and viscous forces. The body forces are made up of gravity force, centrifugal force, coriolis force and electromagnetic force. The contributions due to surface forces are treated as separate terms in the momentum equation and the effects of body forces are included as source terms.

The stress of a fluid element is defined in terms of pressure (**P**), a normal stress, and nine viscous stress components (τ) as depicted in Fig.2.3. For direction of the viscous stresses, the suffix notation τ_{ij} is used, where suffices j and i indicate that stress component acts in j- direction on a surface normal to the i-direction.

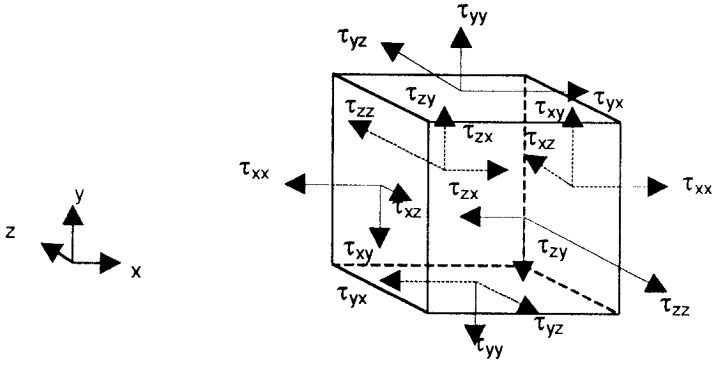

Figure 2.3 Stress components on three faces of a fluid element.

Now consider the x-component of the forces due to pressure **P** and stress components τ_{xx}, τ_{yx} and τ_{zx} shown in Fig.2.4. The product of stress and area gives the resulting force from a surface stress. Forces aligned with direction of co-ordinate axis have a positive sign and those in opposite direction have a negative sign. The Net force in the x-direction is the sum of the force components acting in that direction on the fluid element.

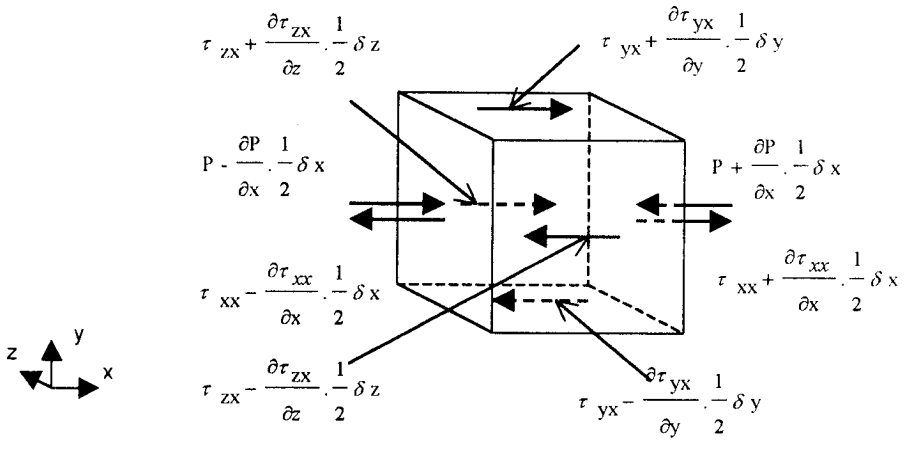

Figure 2.4 Stress components in the x-direction.

On the pair of faces (E, W), the following obtains:

$$\left[\left(P - \frac{\partial p}{\partial x}.\frac{1}{2}\delta x\right) - \left(\tau_{xx} - \frac{\partial \tau_{xx}}{\partial x}.\frac{1}{2}\right)\right]\delta y\,\delta z + \left[-\left(P + \frac{\partial p}{\partial x}.\frac{1}{2}\delta x\right) + \left(\tau_{xx} + \frac{\partial \tau_{xx}}{\partial x}.\frac{1}{2}\right)\right]\delta y\,\delta z$$
$$= \left(-\frac{\partial P}{\partial x} + \frac{\partial \tau_{xx}}{\partial x}\right)\delta x\,\delta y\,\delta z \qquad \text{Eq.2.7(a)}$$

The net force in the x-direction on the pair of faces (H, L) is:

$$-\left(\tau_{zx} - \frac{\partial \tau_{zx}}{\partial z}.\frac{1}{2}\delta z\right)\delta x\,\delta y + \left(\tau_{zx} + \frac{\partial \tau_{zx}}{\partial z}.\frac{1}{2}\delta z\right)\delta x\,\delta y = \frac{\partial \tau_{zx}}{\partial z}.\delta x\,\delta y\,\delta z \qquad \text{Eq.2.7(b)}$$

Finally the net force in the x-direction on faces N and S is:

$$-\left(\tau_{yx} - \frac{\partial \tau_{yx}}{\partial y}.\frac{1}{2}\delta y\right)\delta x\,\delta z + \left(\tau_{yx} + \frac{\partial \tau_{yx}}{\partial y}.\frac{1}{2}\delta y\right)\delta x\,\delta z = \frac{\partial \tau_{yx}}{\partial y}.\delta x\,\delta y\,\delta z \qquad \text{Eq.2.7(c)}$$

The total force per unit volume on the fluid due to these surface stresses is equal to the sum of Eqs. 2.7(a), 2.7(b) and 2.7(c) divided by the elemental volume $\delta x\delta y\delta z$:

$$\frac{\partial(-P + \tau_{xx})}{\partial x} + \frac{\partial \tau_{yx}}{\partial y} + \frac{\partial \tau_{zx}}{\partial z} \qquad \text{Eq.2.8}$$

Without further detailed considerations of the body forces, their overall effect can be included by defining a source term S_{mx} of the x-momentum per unit volume per unit time. To find the x-component of the momentum equation, the rate of change of x-momentum of the fluid particle (Eq. 2.6) is set equal to the total force in the x-direction on the element. The total force is due to surface stresses (Eq. 2.8) and rate of increase of x-momentum due to sources. The x-component of momentum equation can then be expressed as:

$$\rho\frac{Du}{Dt} = \frac{\partial(-P + \tau_{xx})}{\partial x} + \frac{\partial \tau_{yx}}{\partial y} + \frac{\partial \tau_{zx}}{\partial z} + S_{mx} \qquad \text{Eq.2.9(a)}$$

In a similar procedure, the y-component of the momentum equation is derived as:

$$\rho \frac{Dv}{Dt} = \frac{\partial \tau_{xy}}{\partial x} + \frac{\partial \left(-P + \tau_{yy}\right)}{\partial y} + \frac{\partial \tau_{zy}}{\partial z} + S_{my} \qquad \text{Eq.2.9(b)}$$

The z-component of the momentum equation is:

$$\rho \frac{Dw}{Dt} = \frac{\partial \tau_{xz}}{\partial x} + \frac{\partial \tau_{yz}}{\partial y} + \frac{\partial \left(-P + \tau_{zz}\right)}{\partial z} + S_{mz} \qquad \text{Eq.2.9(c)}$$

The Sign of the pressure is opposite to that of the normal viscous stress. This is because normal sign convention takes a tensile stress to be a positive normal stress so that pressure, which is a compressive normal stress, has a minus sign. The source terms S_{mx}, S_{my}, and S_{mz} in Eqs. 2.9(a)-(c) include contributions due to the body forces only. The body force due to gravity is modelled by $S_{my} = -\rho g$, while S_{mx} = zero, and S_{mz} = zero.

2.2.3 Chemical Species Conservation

For the conservation of chemical species, the rate of increase in mass of chemical species I equals the net inflow of species I into unit volume plus rate of reaction in unit volume by reaction. Chemical species conservation equation is a form of the continuity equation. For a chemical species I, let m_I denote mass fraction of a chemical species I. The m_I is defined as the ratio of the mass of the species I (contained in a given volume) to the total mass of the mixture (contained in the same volume). In the presence of a velocity field u, the conservation of m_I is expressed as:

$$\frac{\partial}{\partial t}\left(\rho m_1\right) + \operatorname{div}\left(\rho u m_1 + J_1\right) = R_1 \qquad \text{Eq.2.10}$$

Where the first term on the left hand side denotes the rate of change of mass of the chemical species per unit volume. The quantity $\rho u m_I$ is the convection flux of the species, i.e. the flux carried by the general flow field ρu. The symbol J_I stands for diffusion flux, which is normally caused by the gradients of m_I. The divergence of the two fluxes (convection and diffusion) forms the second term of the differential equation. The quantity R_I on the right hand side is the rate of generation of the chemical species per unit volume.

The generation is caused by the chemical reaction. R_I is positive for a reaction producing chemical species, otherwise R_I is zero for a non-reacting species.

2.2.4 Energy Conservation

The first law of thermodynamics states that the rate of change of energy of a fluid particle is equal to the rate of heat addition to the fluid particle plus rate of work done on the particle. In equation form the rate of increase of energy, E, of a fluid particle per unit volume is given by:

$$\rho \frac{DE}{Dt} \qquad \text{Eq.2.11}$$

Where:

$$\frac{DE}{Dt} = \frac{\partial E}{\partial t} + \frac{\partial E}{\partial x}\frac{dx}{dt} + \frac{\partial E}{\partial y}\frac{dy}{dt} + \frac{\partial E}{\partial z}\frac{dz}{dt}$$

The rate of work done on the fluid particle in the element by a surface force is equal to the product of the force and velocity component in the direction of the force.

$W = F\,v$

The work done by the forces given by Eq.2.7(a)-(c) is:

$$\left[\left(\rho u - \frac{\partial(\rho u)}{\partial x}\cdot\frac{1}{2}\delta x\right) - \left(\tau_{xx}\,u - \frac{\partial(\tau_{xx}\,u)}{\partial x}\cdot\frac{1}{2}\delta x\right) - \left(\rho u + \frac{\partial(\rho u)}{\partial x}\cdot\frac{1}{2}\delta x\right) + \left(\tau_{xx}\,u + \frac{\partial(\tau_{xx}\,u)}{\partial x}\cdot\frac{1}{2}\delta x\right)\right]\delta y\,\delta z$$
$$+\left[-\left(\tau_{yx}\,u - \frac{\partial(\tau_{yx}\,u)}{\partial y}\cdot\frac{1}{2}\delta y\right) + \left(\tau_{yx}\,u + \frac{\partial(\tau_{yx}\,u)}{\partial y}\cdot\frac{1}{2}\delta y\right)\right]\delta x\,\delta z$$
$$+\left[-\left(\tau_{zx}\,u - \frac{\partial(\tau_{zx}\,u)}{\partial z}\cdot\frac{1}{2}\delta z\right) + \left(\tau_{zx}\,u + \frac{\partial(\tau_{zx}\,u)}{\partial z}\cdot\frac{1}{2}\delta z\right)\right]\delta x\,\delta y$$

The rate of work done by these surface forces acting in the x-direction is given by:

$$\left[\frac{\partial[u(-P+\tau_{xx})]}{\partial x} + \frac{\partial(u\tau_{yx})}{\partial y} + \frac{\partial(u\tau_{zx})}{\partial z}\right]\delta x\,\delta y\,\delta z \qquad \text{Eq.2.12(a)}$$

Applying the same procedure in the y- and z-directions gives the additional rates of work done on the fluid particle due to the work done by these surface forces. In the y-direction we have:

$$\left[\frac{\partial(v\tau_{xy})}{\partial x}+\frac{\partial[v(-P+\tau_{yy})]}{\partial y}+\frac{\partial(v\tau_{zy})}{\partial z}\right]\delta x\,\delta y\,\delta z \qquad \text{Eq.2.12(b)}$$

Similarly in the z-direction we have:

$$\left[\frac{\partial(w\tau_{xz})}{\partial x}+\frac{\partial(w\tau_{yz})}{\partial y}+\frac{\partial[w(-P+\tau_{zz})]}{\partial z}\right]\delta x\,\delta y\,\delta z \qquad \text{Eq.2.12(c)}$$

The terms containing pressure are grouped together in compact vector form:

$$-\frac{\partial(up)}{\partial x}-\frac{\partial(vp)}{\partial y}-\frac{\partial(wp)}{\partial z}=-\mathrm{div}(p\,\mathbf{u})$$

Therefore the total rate of work done on the fluid particle by the surface stresses is:

$$[-\mathrm{div}\,(p\,\mathbf{u})]+\left[\frac{\partial(u\tau_{xx})}{\partial x}+\frac{\partial(u\tau_{yx})}{\partial y}+\frac{\partial(u\tau_{zx})}{\partial z}+\frac{\partial(v\tau_{xy})}{\partial x}+\frac{\partial(v\tau_{yy})}{\partial y}+\frac{\partial(v\tau_{zy})}{\partial z}\right.$$
$$\left.+\frac{\partial(w\tau_{xz})}{\partial x}+\frac{\partial(w\tau_{yz})}{\partial y}+\frac{\partial(u\tau_{zz})}{\partial z}\right] \qquad \text{Eq.2.13}$$

Heat conduction produces energy flux or heat flux in the three co-ordinate directions. They are represented by the heat flux vector **q**, broken into components q_x, q_y and q_z (Fig.2.5).

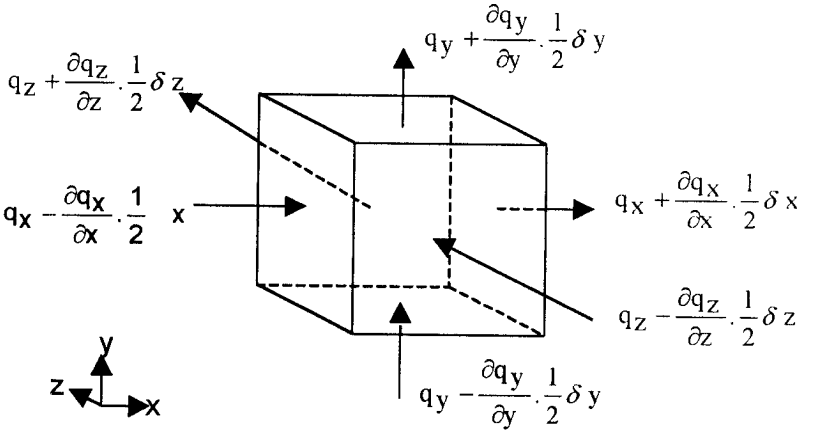

Figure 2.5 Heat Flux Vector Components.

The net rate of heat transfer to the fluid particle due to heat flow in the x-direction is given by the difference between the rate of heat input across face W and the rate of heat across face E:

$$\left[\left(q_x - \frac{\partial q_x}{\partial x} \cdot \frac{1}{2} \delta x\right) + \left(q_x + \frac{\partial q_x}{\partial x} \cdot \frac{1}{2} \delta x\right)\right] \delta y \delta z = -\frac{\partial q_x}{\partial x} \delta x \delta y \delta z \qquad \text{Eq.2.14}(a)$$

Similarly, the net rate of heat transfer to the fluid due to heat flow in the y- and z-directions is:

$$-\frac{\partial q_y}{\partial y} \delta x \delta y \delta z \quad \text{and} \quad -\frac{\partial qz}{\partial z} \delta x \delta y \delta z \qquad \text{Eq.2.14(b)-(c)}$$

The total rate of heat added to the fluid particles per unit volume due to heat flow across its boundaries is the sum of Eq.2.14 (a)-(c) divided by the elemental volume:

$$-\frac{\partial q_x}{\partial x} - \frac{\partial q_y}{\partial y} - \frac{\partial q_z}{\partial z} = -\text{div } q \qquad \text{Eq.2.15}$$

The energy of a fluid is defined as the sum of internal (thermal) energy (i), kinetic energy (k) and gravitational potential energy (z). The gravitational force is taken as a body force. Potential energy effects are treated as a source term. The source of energy is S_E per unit volume per unit time. Conservation of energy of the fluid particle is arrived at by equating the rate of change of energy of the fluid particle (Eq.2.11) to the sum of the net rate of work done on the fluid particle (Eq.2.13), the net rate of heat addition to the fluid, (Eq.2.15) and the rate of increase of energy due to sources. The energy equation is:

$$\rho\frac{DE}{Dt} = -d(pu) + \left[\frac{\partial(u\tau_{xx})}{\partial x} + \frac{\partial(u\tau_{yx})}{\partial y} + \frac{\partial(u\tau_{zx})}{\partial z} + \frac{\partial(v\tau_{xy})}{\partial x} + \frac{\partial(v\tau_{yy})}{\partial y} + \frac{\partial(v\tau_{zy})}{\partial z} + \frac{\partial(w\tau_{xz})}{\partial x} + \frac{\partial(w\tau_{yz})}{\partial y} + \frac{\partial(w\tau_{zz})}{\partial z}\right]$$

$$+\text{div}(k\,\text{grad}T) + S_E \qquad \text{Eq2.16}$$

Where $E = i + 0.5(u^2+v^2+w^2)$ and $-\text{div } q = \text{div } (k \text{ grad } T)$

2.2.5 Equation of State

The five partial differential equations of fluid motion in three-dimension have nine unknowns. The five partial differential equations are the mass conservation (Eq.2.4), momentum in x-, y- and z-direction [Eqs.2.9 (a)-(c)] and energy equations (Eq.2.16). The rest of the unknowns are the four thermodynamic variables of ρ, p, i and T, obtained by use of thermodynamic equilibrium. The state of a substance in thermodynamic equilibrium is described by only two state variables. Equations of state relate the other variables to the two state variables.

The equations for pressure (**P**) and specific internal energy (**i**) can be expressed as functions of ρ and T.

$$P = p(\rho, T) \text{ and } i = i(\rho, T) \qquad \text{Eq.2.17}$$

For a perfect gas the following equations of state apply:

$$P = \rho R T \text{ and } i = C_v T \qquad \text{Eq.2.18}$$

Where the density $\rho = 1/v$, v is the specific volume.

The specific gas constant, R, is given by:

$$R = Ru/MW \qquad \text{Eq.2.19}$$

R_u is the universal gas constant (8315 J/kmol-K) and MW is the gas Molecular Weight.

The assumption of the thermodynamic equilibrium eliminates all but the two thermodynamic state variables. Liquids at high speed behave as compressible fluids. Therefore, the equations of state provide the linkage between the energy equation on the one hand and the mass conservation and the momentum equations on the other. This linkage arises if the density varies due to pressure and temperature variations in the flow field. For low velocity flows there are no linkages and the conservation equations of mass and momentum are the only ones to be solved. The energy equation is solved only if the problem involves heat transfer

2.2.6 Navier-Stokes Equations for a Newtonian Fluid.

The Navier-Stokes equations of practical application for finite volume method are:

$$\rho\frac{Du}{Dt} = -\frac{\partial p}{\partial x} + \mathrm{div}(\mu\,\mathrm{grad}\,u) + S_{mx} \qquad \text{Eq.2.20(a)}$$

$$\rho\frac{Dv}{Dt} = -\frac{\partial p}{\partial y} + \mathrm{div}(\mu\,\mathrm{grad}\,v) + S_{my} \qquad \text{Eq.2.20(b)}$$

$$\rho\frac{Dw}{Dt} = -\frac{\partial p}{\partial z} + \mathrm{div}(\mu\,\mathrm{grad}\,w) + S_{mz} \qquad \text{Eq.2.20(c)}$$

The governing equations contain, as further unknowns, the viscous stress components (τ_{ij}). The most useful form of conservation equations is obtained by introducing a suitable model for the viscous stresses (τ_{ij}). In a Newtonian fluid, the viscous stresses are proportional to the rate of deformation. For a three-dimensional form of Newton's law of viscosity for compressible flows, two constants of proportionality are involved. These are the dynamic viscosity, μ, relating stresses to linear deformations, and the viscosity, λ, relating stresses to volumetric deformation. Not much is known about the second viscosity, λ, as its effects are practically negligible. For gases, a good working

approximation is obtained by taking λ = -2/3 μ [4]. Versteeg *et al* [3] discussed λ in details

Using the Newtonian model for viscous stresses in the energy equation in terms of internal energy, we obtain:

$$\rho \frac{Di}{Dt} = -p \text{ div } u + \text{div } (k \text{ grad } T) + \phi + S_i \qquad \text{Eq.2.21}$$

Where ϕ is the dissipation function for the effect due to viscous stresses in the internal energy equation.

So far derived are the conservative or divergence forms of the system of equations, which govern the time-dependent three-dimensional fluid flow and heat transfer of a compressible Newtonian fluid. Therefore, we have five flow partial differential equations (PDE's) and two algebraic equations (i.e. Eqs.2.4, 2.17, 2.18, 2.20(a)-(c) and 2.21). With a system of seven equations and seven unknown functions, the system is mathematically closed i.e. it can be solved provided that suitable auxiliary, initial and boundary conditions, are supplied. It is clear from the five flow equations (PDE's) that there are similarities between them. Introducing a general variable, φ, the conservative form of fluid flow equations, including equations for scalar quantities such as temperature and pollutant concentration etc can be written in the general useful form as:

$$\frac{\partial(\rho\varphi)}{\partial t} + \text{div}(\rho\varphi u) = \text{div}(\Gamma \text{ grad}\varphi) + S_\varphi \qquad \text{Eq.2.22}$$

In words, the sum of the rate of increase of φ of fluid element and net rate of flow of φ out of fluid element, is equal to the sum of the rate of increase of φ due to diffusion and the rate of increase of φ due to sources.

Equation 2.22 is known as the transport equation for property φ, highlighting the various transport processes. These are the rate of change term, and the convective term on the left hand side and the diffusion term (Γ=diffusion term) and the source term respectively on the right hand side. Equation 2.22 is used as the starting point for computational

procedures in the Finite Volume Method (FVM). The important step of the finite volume method is the integration of Eq.2.22 over a three-dimensional control volume CV yielding:

$$\int_{cv} \frac{\partial(\rho\,\varphi)}{\partial t} dV + \int_{cv} \text{div}\,(\rho\,\varphi\,u)\,dV = \int_{cv} \text{div}\,(\Gamma\,\text{grad}\;\varphi)\,dV + \int_{cv} S_{\varphi}\,dV \qquad \text{Eq. 2.23}$$

When the number of equations is equal to the number of variables, the system of equations is closed. The conservation equations described in Section 2.2 are closed by specifying laws, which describe the transport phenomena of flux laws and the source terms. Empirical laws of Newton, Fourier, and Fick are used Section 2.3 tackles the flux laws and source terms.

2.3 Flux Laws and Source Laws

2.3.1 Flux Laws

Molecular transport processes, i.e., diffusion, heat conduction and viscosity, have in common the transportation of corresponding physical properties by the movement of the molecules in the gas. Diffusion is the mass transport caused by concentration gradients. Viscosity is the transport of momentum caused by velocity gradients. Heat conduction is the transport of energy caused by temperature gradients. Additionally, there are other phenomena like mass transport caused by temperature gradients (*thermal diffusion* or *Sorret* effect) and energy transport caused by concentration gradients (*Dufour* effect). Dufour effect influence is usually very small and is often neglected in the simulation of combustion processes, although it may not be the case in other chemically reacting flows. A detailed discussion of the transport processes is found in the books of Hirschfelder *et al.* [5] or of Bird *et al.* [4]

Fourier's Law for Heat Conduction. For the transport of energy Q through area A, the empirically determined *Fourier law* of heat conduction states that the heat flux density j_q is proportional to the temperature gradient [4, 5]

$$j_q = \frac{\partial Q}{\partial t} = -k.\text{grad}(T) \qquad [W/m^2] \qquad \text{Eq.2.24}$$

This means that the heat flux occurs from a region of high temperature towards one with a lower temperature. The coefficient of proportionality k [W/m-K] is called *thermal*

Conductivity. The proportionality constant depends on the local properties of the components of the medium. In a turbulent fluid flow, the time-averaged fluctuations contribute to the energy transport in a much significant way than the heat conduction. This is caused by the effective heat conduction coefficient, which is the sum of the laminar and turbulent heat conduction coefficient. The dimensionless quantities like the Prandtl number (Pr) and the Lewis number (Le) relate the heat flux with other transport properties.

Ficks Law for Diffusion. For the mass transport caused by concentration gradients, *Fick's* law states that the mass flux j_m is proportional to the concentration gradient [4, 5].

$$j_m = \frac{\partial m}{\partial t.A} = -D.\mathrm{grad}(m) \qquad \left[\frac{kg}{cm^2 s}\right] \qquad \text{Eq.2.25}$$

The coefficient of proportionality D is called the *diffusion coefficient.* The proportionality constant depends on the local properties of the components of the medium. In turbulent premixed flows, the fluctuations take care of mass transfer components, more significantly than in diffusion, by using the effective exchange coefficient The exchange coefficient is the sum of the laminar and the turbulent exchange coefficient. The Schmidt and Lewis numbers relate diffusion to other transport properties.

Newton's Viscosity Law. For *Newton's law* of viscosity, it states that the transport of *momentum flux density* j_{mv} is proportional to the velocity gradient. [4, 5].

$$j_{mv} = \frac{\partial (m\ u)}{\partial t.A} = -\mu\ \mathrm{grad}(u) \qquad \text{Eq.2.26}$$

Thus, momentum is transported from regions of high velocity to regions of low velocity. The coefficient of proportionality μ is called *coefficient of viscosity.* The proportionality constant depends on the local properties of the components of the medium.

For ideal gases, the proportionality coefficients, *thermal conductivity* (k) and *coefficient of viscosity* (μ) are measured, while *diffusion coefficient* (D) is predicted. For details of the methods of their determination see chapter five in book of Warnatz *et al.* [6]

2.3.2 Source Laws

The source laws give expressions for the source term (i.e. S_φ) of the general differential equation. These expressions have a great variation in their equation form.

Chemical Reaction Kinetics studies the dynamical behaviour of mass and molar fractions. For an irreversible reaction:

$$A + B \longrightarrow C$$

The expression for the component A for chemical production velocity becomes:

$$R_A = m_A . m_B . B_K . T_k^{\alpha} . \exp\left(\frac{-E_K}{R_u . T}\right) \qquad \text{Eq.2.27}$$

Where:

m_A and m_B are the mass fractions of components A and B.

B_K and α are tabulated constants.

T is the temperature (K) and E_K is the activation energy.

R_u is the gas constant (J/kmol .K).

To solve Eq.2.27, it is necessary in numerical simulation to use a combustion model. This is required because of incomplete data, limited calculation times and lack of knowledge of the necessary chemical reaction velocities and reaction constants.

Momentum Source Terms. The momentum source terms arise from the flow of the fluid, and are several in number.

Pressure gradient: This is the second term of the viscous strain vector [7].

$$-\frac{\partial P}{\partial x_i} \qquad \text{Eq.2.28}$$

Where P is the hydrostatic pressure (N/m^2).

Viscous Terms: The most important viscous terms are expressed as:

div (μ.grad **u**) Eq.2.29

These terms were used as diffusion terms and the remaining part of the viscous strain vector is treated as source term.

Internal Resistance: This is the force per unit volume given by:

$f_i = F_j.\mathbf{u}$ Eq.2.30

Where F_j (kg/m^{3}s) is the resistance coefficient per unit length. Therefore, the resistance force per unit volume f_i is proportional to the local velocity.

Gravity: This is given as:

$$\rho.\bar{i}\,\bar{j}.\bar{g}_{grav} \qquad \text{Eq.2.31}$$

Where g_{grav} is the vector for gravity acceleration. Sometimes it is easier to define the gravity as:

$$(\rho - \rho_0)\bar{i}\,\bar{j}.\bar{g}_{grav} = \Delta\rho.\bar{i}\,\bar{j}.\bar{g}_{grav}$$

Where ρ_0 is the reference density given as $\rho = \rho_0/(1+\beta.\Delta T)$, and β is the cubic expansion coefficient.

Energy Source Terms. These are the viscous dissipation terms arising from heat developed as a result of slipping and is described by the shear stress vector:

$$-\mathrm{div}\,\overline{\overline{W}}_S \qquad \text{Eq.2.32}$$

Where:

$$\overline{\overline{W}}_S = \tau_1.\bar{u} + \tau_2.\bar{u} + \tau_3.\bar{u}$$

The other energy sources are: chemical reaction energy which appear implicitly through the diffusion fluxes of the chemical components, the turbulent energy which in most cases is negligible and the electric dissipation not applicable in the problem under study.

Radiative Transfer. This is the radiative energy flux $J_{\lambda\varphi}$ per unit area per unit wavelength, λ, per unit of space φ. The volumetric energy source term for radiative energy flux is:

$$S_{str} = \iint a(\lambda).J_{\lambda} \ .d\lambda.d \ - \int a(\lambda)(\lambda).d\lambda \qquad \text{Eq. 2.33}$$

Where **a** (m^{-1}) is the absorption coefficient and E_{λ} is the emissivity of medium. Therefore, the first term on the right hand side is that part of the entrance energy that is absorbed. The second term on the right hand side is the emitted part.

Mass Source Term. The mass source term, normally, cannot happen, however, it is useful to expand the continuity equation for two reasons. First, a homogeneous mixture of two media materials can move from one phase to the other phase. Secondly, in numerical work, during the first part of the calculations, often, the continuity equation is not satisfied. Therefore, the residue of the equation can easily be taken as a "mass source term". Hence:

$$\frac{\partial \rho}{\partial t} + \text{div} \left(\rho . \bar{u}\right) = S_{mass} \qquad \text{Eq. 2.34}$$

Where S_{mass} (kg/m^3s) is not always zero.

The flux laws and source terms can now be substituted in the conservation equations to get the basic differential equations, which are second order non-linear partial differential equations. The flux laws are less reliable than the conservation equations because some relations are not normally well known, for example the viscosity relations.

The basic differential equations for conservation of momentum, chemical species and energy are given as:

Momentum equation:

$$\frac{\partial}{\partial t}(\rho.\mathbf{u})+\operatorname{div}\left(\rho.\bar{u}.\mathbf{u}\right)=\operatorname{div}(\mu\ \operatorname{grad}\ \mathbf{u})-\frac{\partial P}{\partial x}+\rho.\bar{i}_j.\bar{g}_{grav} \qquad \text{Eq.2.35}$$

Chemical components equation:

$$\frac{\partial}{\partial t}\left(\rho.m_i\right)+\frac{\partial}{\partial x_i}\left(\rho.\mathbf{u}.m_i\right)=\frac{\partial}{\partial x_i}\left(\Gamma_i.\frac{\partial m_i}{\partial x_i}\right)+R_i \qquad \text{Eq.2.36}$$

Energy equation expressed in terms of enthalpy:

$$\frac{\partial}{\partial t}\left(\rho.\tilde{h}\right)+\operatorname{div}\left(\rho.\bar{u}.\tilde{h}\right)=\operatorname{div}\left(\Gamma_h.\operatorname{grad}\left(\tilde{h}\right)\right)+\frac{\partial P}{\partial t}+S_{str}-\operatorname{div}\left(\Gamma_h.\operatorname{grad}\left(\frac{-2}{\frac{u}{2}}\right)-\overline{Ws}\right)$$
$$+\operatorname{div}\left(\Sigma alli\left(\Gamma_h-\Gamma_i\right)\right)h_i.\operatorname{grad}\left(m_i\right) \qquad \text{Eq.2.37}$$

Governing equations only do not provide the complete specification of the mathematical problem; additional information is required. This information covers the turbulent nature of the flow necessary to solve the set of momentum equations in turbulent flow; generally, it forms turbulence models. This is tackled in Section 2.4. The second type of information is that associated with reactive flows; i.e. the specification of the rate of fuel consumption and probability of reaction. This is dealt with under combustion models in Section 2.5. The contributions, to the energy balance, normally vary according to the radiation and energy balance models adopted (Section 2.6). The closure model provide other information such as thermodynamic properties, boundary and inlet conditions, which should be specified in the model in order to solve the governing equations. Detailed analyses of the calculations are dealt with in Chapter Three.

2.4 Turbulence and its Modelling.

2.4.1 Turbulence

In most practical combusting equipment, e.g., reciprocating internal combustion engines, gas turbines, furnaces, boilers, and rocket engines, etc, turbulent flows are more

frequently encountered than laminar flows. The mathematical description of a turbulent flow and solution of the resulting governing conservation equations are much more difficult than for laminar flows. Analytical and numerical solutions to turbulent flows are engineering approximations even for the simplest geometries and can be subject to large errors. The main dilemma of solving a turbulent flow problem is that if all the information necessary for describing a flow is tracked, there is no computer in the world large enough to handle the work. On the other hand, even if the problem was simplified to reality using available computers, large errors may result, especially for flows that have not been studied experimentally. The improved understanding of turbulent combustion is still an active area of research where considerable progress is being made to develop descriptive and predictive methods that are useful in the design of practical devices.

Definition of Turbulence

Turbulence results when instabilities in a flow are not sufficiently damped by the viscous action and fluid velocity at each point in the flow. The flow exhibits random characteristics, which are fluctuating in nature. Velocity fluctuations can lead to fluctuations in the scalars such as density, temperature, and mixture composition. The fluctuations in velocity (and then the scalars) are a consequence of the vortices that are generated by shear within the flow. The growth of these vortices is the result of competition between the (non-linear) generation process and destruction process caused by viscous dissipation. The generation term exceeds the viscous damping term when a critical *Reynolds number* Re_{crit} is exceeded at which transition from a laminar to a turbulent flow takes place. Practically, for a pipe flow, transition to turbulent flow takes place between Re (=UD/ν) 2000 and 10^5. The Reynolds concept was first developed by Osborne Reynolds [8] in his famous experiment of transition from laminar to turbulent flow. The Reynolds number $Re = \rho vl/\mu$ is the ratio of a destabilising momentum to a stabilising (or damping) viscous effect. Here ρ denotes the density, v the velocity (or better a velocity difference), μ the viscosity of the fluid, and l a characteristic length of the system. The length l is geometry-dependent (for pipe flow, e.g., the diameter is used for l). The rapid intertwining of fluid elements is a characteristic that distinguishes turbulent flow from laminar flow. The turbulent motion of fluid elements allows momentum, species, and energy to be transported in the cross-stream direction much more rapidly than is possible by the molecular diffusion processes controlling transport in laminar flows. Because of this, most practical combustion devices use turbulence flows to enable rapid mixing and heat release in relatively small combustion chambers.

Length Scales in Turbulent Flows.

In the physical nature of turbulence, there are fluid blobs and filaments of fluid intertwining. This is the notion of a fluid eddy. An eddy is considered to be a macroscopic fluid element in which the microscopic elements comprising the eddies behave in some ways as a unit. An eddy is considered as a vortex imbedded in a flow. In turbulent flow, there can be many eddies with a multitude of sizes and vorticities, a measure of angular velocity. A number of smaller eddies may be imbedded in a larger eddy. A characteristic of the turbulence is the existence of a wide range of length scales i.e. eddy sizes. For a turbulent flow, the Reynolds number is a measure of the range of length scales present. The greater the Reynolds number, the greater the range of sizes from the smallest eddy to the largest. It is this large range of length scales that makes calculating turbulent flows from first principles unrealistic. Though there are many length scales defined in turbulence literature, only four scales of general relevance are frequently cited.

l_0, Characteristic Width of Flow or Macroscale. It is the largest length scale in the system and is upper bound for the largest possible eddies. Generally, this length scale is defined by the geometrical dimensions of the system or device being considered. This length scale is used to define a mean Reynolds number based on the mean flow velocity, but is not used to define a turbulence Reynolds number, as are the other three length scales.

l_T, Integral Scale or Taylor Macroscale. The integral scale physically represents the mean size of the largest eddies in a turbulent flow. Perturbations with long wavelengths (low frequency) are associated with large eddies. These eddies interact and fuse into smaller and smaller eddies (smaller wavelength means higher frequency). Thus, an energy cascade, from large eddies to many small eddies is observed. The major part of the kinetic energy is in the motion of the large eddies. The energy cascade terminates, as kinetic energy of the many small eddies (at or below the Kolmogorov scale l_K) is dissipated by viscosity into thermal energy (i.e., molecular motion). The distribution of the turbulent kinetic energy (TKE) among the spectrum of eddies with diameters l is described by the turbulent energy spectrum. The energy density e(k) describes the dependency of the turbulent kinetic energy (q) on the wave number k(k=1/l), i.e., the reciprocal value of the turbulent length scale. The energy spectrum begins at the integral length scale l_T (governed by the characteristic dimensions of the experiment) and ends at the Kolmogorov length-scale l_K. The integral scale l_T is always smaller than l_0 but is of same order of magnitude. In less precise terms, l_T represents the distance between two points in

a flow where there ceases to be correlation between the fluctuating velocities at the two locations.

l_λ, Taylor Microscale. The Taylor microscale is an intermediate length scale between l_T and l_K, but is weighted more towards the smaller scales. It is normally related to the mean rate of strain. In the steady state, the dissipation rate of the turbulent energy has to equal the rate of formation of turbulent energy (e.g. by shear processes causing turbulence in the boundary layers). An analysis of dimensions shows that the dissipation rate depends on the energy (q) of the spectrum and the integral length scale l_T [i.e. $\varepsilon = (2q)^{3/2}/l_T$]

l_K, Kolmogorov Microscale. The Kolmogorov microscale is the smallest length scale associated with a turbulent flow, and as such, is representative of the dimension at which the dissipation of turbulent kinetic energy to fluid internal energy occurs. Thus, the Kolmogorov scale is the scale at which molecular effects (kinematic viscosity) are significant. At l_K, the time for an eddy to rotate half revolution is equal to the diffusion time across the diameter l_K. Below l_K, diffusion (and in general molecular transport) is faster than turbulent transport; hence the turbulence does not extend below l_K. The Kolmogorov scale has two physical interpretations. In Tennekes' [9] model of a turbulent flow, l_K represents the thickness of the smallest vortex tubes or filaments that permeate a turbulent flow, while Ref. [10] suggest that l_K represents the thickness of vortex sheets imbedded in the flow.

Turbulent Reynolds Number

In an attempt to universally describe the degree of turbulence, three of the four length scales discussed above are used to define the *turbulent Reynolds number,* R_T. The turbulent Reynolds number is a measure for the ratio between integral length scale and Kolmogorov length scale. It is evident that turbulent Reynolds (R_T) number characterises turbulent flows better than the traditional Reynolds number (Re) which is explicitly geometry-dependent. In all the Reynolds numbers, the characteristic velocity is the root-mean-square fluctuating velocity, v'_{rms}. Thus we define $R_{TlT} \equiv v'_{rms}l_T/v$, $R_{Tl\lambda} \equiv v'_{rms}L_\lambda/v$, and $R_{TLK} \equiv v'_{rms}L_K/v$. The largest (the integral) and the smallest (Kolmogorov) turbulence length scales are related as follows [11] $l_T/l_K = (R_{TlT})^{3/4}$. The Taylor microscale, L_λ, is related to R_{TlT} as follows [12], i.e. $l_T/l_\lambda = (R_{TlT})^{1/2}$. The size of the scales of turbulence, in relation to the laminar flame thickness, determines the character of the turbulent flame.

2.4.2 Time-Averaged Conservation Equations for Turbulence

Rather than depend completely on empirical experimental methods, techniques have been developed that allow turbulent flows to be analysed to obtain useful information and to allow predictions. One fruitful method of analysing turbulent flows is to write the partial differential equations that embody the basic conservation principles (mass, momentum, energy, and species), then perform a Reynolds decomposition, and then average the equations over time. In turbulent flows, it is the time-mean behaviour that is usually of practical interest to engineers. Most engineering problems are related to non-homogeneous turbulence and hence time averaging is widely used. Therefore, the equations for unsteady laminar flow are converted into the time-averaged equations for turbulent flow by the averaging process in which it is assumed that there are rapid and random fluctuations about the mean value. The resulting governing equations are called the Reynolds-averaged equations. The averaging has two major consequences. The first is that it eliminates the fine details of the flow, e.g. the complex time-dependent velocity at a point can not be predicted using time-averaged equations of motion. The second consequence is the appearance of new terms in the time-averaged governing equations that have no counterpart in the original time-dependent equations. The additional terms arising from this operation are the Reynolds stresses, turbulent heat flux, turbulent flux etc. Finding a method to calculate or approximate the new terms is referred to as the closure problem of turbulence.

In turbulent flows, the time of averaging is longer as compared to the time of fluctuations and time of the phenomenon taking place. This time difference allows for the capture of the events taking place. However, the time of averaging is small as compared to the time of the phenomena-taking place. In turbulent flows, as discussed in the last section, there is appearance of eddying motions of a wide range of length scales. A typical flow domain of 0.1m by 0.1 m, with a high Reynolds number, turbulent flow might contain eddies of 10 to 100 μm size. This will require meshes of 10^9 up to 10^{12} grid points to be able to describe processes at all length scales. The fastest events take place with a frequency on the order of 10 kHz. This will require descritised time steps of the size of 100 μs. Speziale [13] states that the direct simulation of a turbulent pipe flow at a given Reynolds number of 500 000 requires a computer which is 10 million times faster than a current generation CRAY supercomputer. With today's computing power, it is only possible to track the dynamics of eddies in very simple flows at transitional Reynolds number (2000-10^5). Engineers need computational procedures which supply adequate information about

turbulent processes, but which avoid the need to predict the effect of each and every eddy in the flow.

Since turbulence is composed of random fluctuations, its mathematical description requires the use of a statistical approach [14]. Reynolds [15] was the first to use the concept of averaging. He considered various methods of averaging which include either an integral or summation. There are four most widely used methods of averaging. Time averaging is used for quasi-stationary turbulent flows i.e. turbulent flows whose average values do not change with time. Space averaging is used for homogeneous turbulence and is performed on all spatial co-ordinates by volume integral. Ensemble averaging is the most common type of averaging and can be used in all cases. The fourth method is the Favre or density-weighted mean, which takes account of the fact that the density is not uniform due to temperature and composition variations because of chemical reaction and heat transfer variations.

Reynolds Equations

One particularly useful way to characterise a turbulent flow field is to define *mean* and *fluctuating* quantities. Mean properties are defined by taking a time-average of the flow property over a sufficiently large time interval. For any flow property (φ), e.g., velocity, temperature, pressure, etc., let (Φ) be the mean value and therefore:

$$\Phi = \frac{1}{\Delta t}\int_{0}^{\Delta t} (t)\, dt \qquad \text{Eq.2.38}$$

Theoretically, the limit of time interval, Δt, is taken as approaching infinity. However, Δt is large enough if it exceeds the time scales of the slowest variations (due to the largest eddies) of property φ. The flow property φ is time dependent and can be thought of as the sum of a steady mean component Φ and a time-varying fluctuating component φ' with zero mean value.

The fluctuation, φ', is the difference between the instantaneous value of the property, φ, and the mean value, Φ. Fig.2.6.

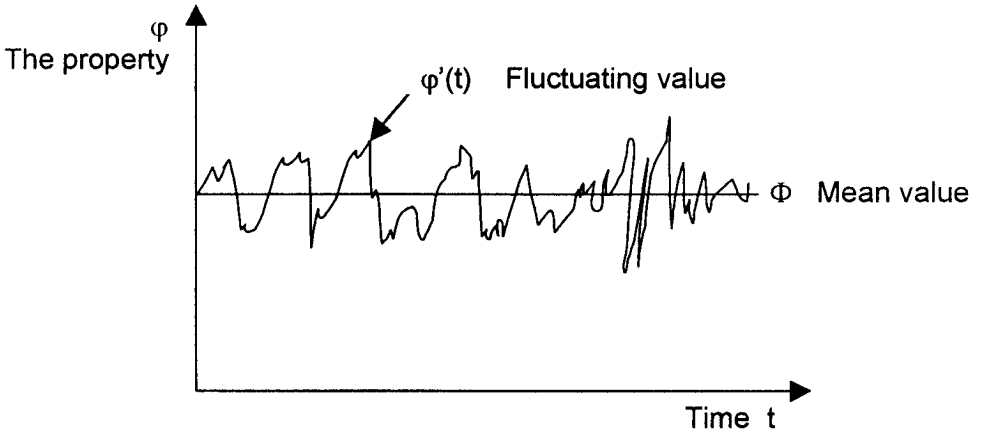

Figure 2.6 Typical point property measurement in a turbulent flow

Hence:

$\varphi(t) = \Phi + \varphi'(t)$

The time dependence of φ' is, by definition zero:

$$\overline{\varphi'} = \frac{1}{\Delta t}\int_0^{\Delta t} \varphi'(t)dt = 0 \qquad \text{Eq.2.39}$$

In turbulent flows with combustion, there are also frequently large random fluctuations in temperature, density, and species, as defined by

$T(t) = T + T'(t)$

$\rho(t) = \rho + \rho'(t)$

and

$m_i(t) = m_i + m_i'(t)$

This system of expressing variables as a mean and fluctuating component is referred to as the *Reynolds decomposition.* The following rules govern the time averages of the fluctuating properties $\varphi = \Phi + \varphi'$ and $\psi = \Psi + \psi'$ and there combinations, derivative and integrals:

$$\overline{\varphi'} = \overline{\psi'} = 0; \overline{\Phi} = \Phi; \overline{\frac{\partial \varphi}{\partial s}} = \frac{\partial \Phi}{\partial s}; \int \overline{\varphi} ds = \int \Phi ds; \overline{\varphi + \psi} = \Phi + \Psi; \overline{\varphi\psi} = \Phi\Psi + \overline{\varphi'\psi'}; \overline{\varphi}\,\overline{\psi} = \Phi\Psi; \overline{\varphi'\psi} = 0 \qquad \text{Eq.2.40}$$

These relationships are easily verified by application of Eqs.2.38 and 2.39. The above rules are extended to fluctuating vector quantities since **div** and **grad** are both differentiations. Combining the vector quantity **a = A + a'** and the fluctuating scalar

$\varphi = \Phi + \varphi'$.

We obtain:

$$\overline{\text{div a}} = \text{div A} : \overline{\text{div}(\varphi \text{a})} = \text{div}(\overline{\varphi}\,\overline{\text{a}}) = \text{du}(\Phi \text{A}) + \text{div}(\overline{\varphi' \text{a}'}), \overline{\text{div grad}\,\varphi} = \text{div grad}\,\Phi \qquad \text{Eq.2.41}$$

Consider the instantaneous continuity and Navier-Stokes equations for a compressible flow with constant viscosity. This considerably simplifies the algebra involved without detracting from the main tasks. Taking the cartesian co-ordinates so that the velocity vector **u** has x-component u, y-component v and z-components w:

$$\frac{\partial \rho}{\partial t} + \text{div}\,(\rho\,\mathbf{u}) = 0 \qquad \text{Eq.2.42}$$

To investigate effects of fluctuations, the flow variables **u** (u, v and w) and P in Eqs.2.42 and 2.43(a)-(c) are replaced by the sum of a mean and fluctuating component.
Thus:

$$\frac{\partial(\rho \text{u})}{\partial t} + \text{div}(\rho\ \text{u}\,\mathbf{u}) = -\frac{\partial \text{P}}{\partial \text{x}} + \text{div}(\mu\, grad\, \text{u}) + \text{S}_{\text{mx}} \qquad \text{Eq.2.43}(a)$$

$$\frac{\partial(\rho \text{v})}{\partial t} + \text{div}(\rho\ \text{v}\,\mathbf{u}) = -\frac{\partial \text{P}}{\partial \text{y}} + \text{div}(\mu\, grad\, \text{v}) + \text{S}_{\text{my}} \qquad \text{Eq.2.43}(b)$$

$$\frac{\partial(\rho\, w)}{\partial t} + \mathrm{div}(\rho\ w\,\mathbf{u}) = -\frac{\partial P}{\partial z} + \mathrm{div}(\mu\ grad\ w) + S_{mz} \qquad \text{Eq.2.43}(c)$$

u = U + u'; u =U + u'; v = V + v'; w = W + w'; p = P + p'

The time average is taken by applying the rules stated in Eq.2.41. The resulting time averaged Reynolds equations have the mean velocity components **U**, **V** and **W** and all terms on the right hand side are divided by the density, while the extra stress terms are written out in long hand to clarify their structure.

Time-mean averages have a clearer physical meaning than the density-weighted means, while many of the measured quantities do actually and acceptably represent the Favre mean [16, 17, 18]. The resulting equations are, however, much simpler when the Favre-mean is used. In practical flows, the mean density may vary and instantaneous density always exhibits turbulent fluctuations. Bradshaw *et al* [19] state that small density fluctuations do not appear to affect the flow significantly. In free turbulent flows, velocity fluctuations can easily reach values around Mach numbers of one. Therefore, in this study the Favre-averaged approach, [20] of the mean flow equations for compressible turbulent flow is used. The effects of density fluctuations are negligible but mean density variations are not. This is the form widely used in commercial CFD packages. The following are the density-weighted averaged form of the mean flow equations for compressible turbulent flows:

Continuity:

$$\frac{\partial \rho}{\partial t} + \mathrm{div}\,(\rho\, \mathbf{U}) = 0 \qquad \text{Eq.2.44}$$

Reynolds Equations:

$$\frac{\partial(\rho U)}{\partial t} + \text{div}(\rho UU) = -\frac{\partial P}{\partial x} + \text{div}(\mu \text{ grad } U) + \left[-\frac{\partial(\rho \overline{u'u'})}{\partial x} - \frac{\partial(\rho \overline{u'v'})}{\partial y} - \frac{\partial(\rho \overline{u'w'})}{\partial x} \right] + S_{mx} \qquad \text{Eq.2.45(a)}$$

$$\frac{\partial(\rho V)}{\partial t} + \text{div}(\rho VU) = -\frac{\partial P}{\partial y} + \text{div}(\mu \text{ grad } V) + \left[-\frac{\partial(\rho \overline{u'v'})}{\partial x} - \frac{\partial(\rho \overline{v'v'})}{\partial y} - \frac{\partial(\rho \overline{v'w'})}{\partial y} \right] + S_{my} \qquad \text{Eq.2.45(b)}$$

$$\frac{\partial(\rho W)}{\partial t} + \text{div}(\rho WU) = -\frac{\partial P}{\partial z} + \text{div}(\mu \text{ grad } W) + \left[-\frac{\partial(\rho \overline{u'w'})}{\partial x} - \frac{\partial(\rho \overline{v'w'})}{\partial y} - \frac{\partial(\rho \overline{w'w'})}{\partial z} \right] + S_{mz} \qquad \text{Eq.2.45(c)}$$

Scalar transport equation:

$$\frac{\partial(\rho \Phi)}{\partial t} + \text{div}(\rho \Phi \mathbf{U}) = \text{div}(\Gamma_{\Phi} \text{ grad } \Phi) + \left[-\frac{\partial(\rho \overline{u'\varphi'})}{\partial x} - \frac{\partial(\rho \overline{v'\varphi'})}{\partial y} - \frac{\partial(\rho \overline{v'\varphi'})}{\partial z} \right] + S_{m\Phi} \qquad \text{Eq.2.46}$$

Where the symbol ρ stands for the mean density.

The instantaneous continuity and Navier-Stokes Eqs.2.42 and 2.43(a)-(b) respectively form a closed set of four equations with four unknowns u, v, w and p. These equations cannot be solved directly. In performing the time averaging operation, on the momentum equations, six additional unknowns, the Reynolds stresses, in the time averaged momentum equations are obtained. Similarly, the time averaged scalar transport equations show extra terms containing the following:

$$\overline{u'\varphi'}, \quad \overline{v'\varphi'} \quad \text{and} \quad \overline{w'\varphi'}$$

The complexity of turbulence usually precludes simple formulae for the extra stresses and turbulent scalar transport terms. Therefore, Numerical simulation of turbulence models should have computation procedures of sufficient accuracy and generality for the predicting Reynolds stresses and scalar transport terms. These turbulence models employ concept of a turbulent viscosity or a turbulent diffusivity to express the turbulent stresses and fluxes. The result is that the time averaged equations for turbulent flow have the same appearance as the equations for laminar flow, but the exchange coefficient are

employ concept of a turbulent viscosity or a turbulent diffusivity to express the turbulent stresses and fluxes. The result is that the time averaged equations for turbulent flow have the same appearance as the equations for laminar flow, but the exchange coefficient are replaced by the effective (i.e. laminar plus turbulent) exchange coefficients. From a computational viewpoint, a turbulent flow within this framework is equivalent to a laminar flow with a rather complicated prescription of viscosity. Section 2.4.3 tackles the problem of modelling turbulence.

In addition to Eqs.2,45 and 2.46, which are of primary concern, other equations such as turbulent kinetic energy, turbulent kinetic energy dissipation and radiative heat transfer equations are to be solved to find the needed turbulent properties and source term species and-or energy equations. Since a large number of species are present in combustion processes, simplifications are necessary. Section 2.5 is concerned with simplifications of equations describing the combustion process. In the same section combustion rate for premixed and diffusion flames are discussed in some detail. The model problem to be investigated in this study is described in Section 3.4. The boundary conditions are also discussed in the same section.

2.4.3 Turbulence Modelling

A turbulent model is a set of equations, additional to the Navier-Stokes and "other conservation" equations which may express approximately, relationships between otherwise unknown terms in the latter equations. In short, it is a computational procedure to complete the system of mean flow Eqs.2.44, 2.45(a)-(c) and 2.46 so that a less wide variety of flow problems can be calculated. In particular, we always need expressions for the Reynolds stresses in Eq.2.45(a)-(c) and the turbulent scalar transport terms in Eq.2.46. For a turbulence model to be useful in a general purpose CFD code, it must have wide applicability, be accurate, simple and economical to run.

The above new Reynolds stress, Eq.2.45 corresponds to those of a laminar flow with a weird viscosity and weird conductivity. The turbulent transport of momentum and heat appears as large apparent (Reynolds) stresses and heat-flux rates. Model equations are required which give the unknown stresses and flux rates. Exact solutions of the Reynolds stresses can be derived from the Navier-Stokes equations. They are transport equations, giving only the rate of change of stress along a mean streamline. They contain further unknowns but they do provide useful hints. In particular they show that the stresses are

only loosely coupled to the local mean velocity field. The Navier-Stokes equations are closed when the empirical laws for the flux densities are used. The averaged conservation equations are not closed until analogous terms of the averaged form $\rho v'\varphi'$ are specified. These new terms generated in the averaging process are not explicitly known as functions of the dependent variables. Thus, there are more unknowns than equations (closure problem in turbulence theory). In order to solve the closure problem, models are proposed describing the Reynolds stresses $\rho v'\varphi'$ in terms of the dependent variables. There are many ways of relating these stresses to the mean quantities, either by algebraic expressions or by the more complicated partial differential equations. Only the relevant model to this study is briefly described here.

The eddy or turbulent viscosity concept was first introduced by Boussinsq, [21]. Eddy viscosity is the ratio of a stress to the corresponding rate of deformation or the ratio of a turbulence quantity to a mean flow quantity. He suggested that it is possible to replace the effective turbulent shear stress by $\mu_t \partial U/\partial y$. His proposal was simply that μ_t is proportional to l^2 and $\mu_t \partial U_i/\partial x_i$, where l is defined as the mixing length appropriate to each flow of the boundary layer type. For more complex flows, turbulence scales work better. Hence, progress in the field of evaluating μ_t, have advanced from merely formulating algebraic expressions to the more difficult task of solving the partial differential equations, for the kinetic energy of turbulence k as reported [22]. It was assumed that the local state of the fluid depends on one or more turbulence quantities, which can be, determined from the solution of their corresponding transport quantities. This concept allows the turbulent flows to be characterised by two turbulence quantities.

The facts discussed above necessitate, turbulence modelling. In the laminar flow regime, there are quite a number of programs, which can solve the three-dimensional time-dependence Navier-Stokes equations [23]. Moreover, turbulence is a three-dimensional time-dependent flow phenomenon. Therefore, one might simply deduce that one of the turbulence programs could be used directly to simulate turbulence. Turbulence is dissipated, and momentum, heat and matter are exchanged, by way of small-scale fluctuations. No existing or foreseen computer has the speed or memory to permit the small-scale features of flow to be predicted accurately within acceptable time and cost limits. In any turbulence model approach; there are three basic hypotheses to be considered. First, even if all details can not be represented, perhaps sufficient information about local effects of turbulence on dissipation and exchange can be deduced from

knowledge of a few statistical properties, e.g. energy, length scale. Secondly, perhaps equation systems can be devised which describe accurately enough how these statistical properties vary within the flow. Thirdly, possibly the equation systems have the form of those governing the "conservation" of mass, momentum and energy.

The most common turbulence models based on (time-averaged) Reynolds equations are:

1. Zero-equation model (mixing length model by Prandtl (1925))
2. Two-equation model (k-ε model, Kolmogorov (1942) energy frequency model, Harlow-Nakayama (1968) energy-dissipation rate model).
3. Reynolds stress equation model
4. Algebraic stress model

All the above models are classical models using the Reynolds equations developed in Section 2.4.2 and form the basis of turbulence calculations in currently available commercial CFD codes. Of the classical models the mixing length and the two-equation k-ε models are presently by far the most widely used and validated. They are based on the presumption that there exists an analogy between the action of viscous stresses and Reynolds stresses on the mean flow. In this study, the Harlow-Nakayama (two-equation) model is employed. It is the most popular two-equation model, but for historical rather than scientific reasons. Like the other two-equation models (k-f of Kolmogorov; k-kl of Ng-Spalding-Rodi; k-W of Saffmann-Spalding) the k-ε model is free from the need to prescribe the length scale distribution. The k-ε model is the simplest turbulence model for which only initial and-or boundary conditions need to be supplied. It also has excellent performance for many industrially relevant flows. The k-ε model is well established, and most widely validated. It costs more than the mixing length model because of the solution of the two similar form extra partial differential equations. For example the momentum equations, which are easily solved by the code used in this study. The systematic comparisons between experimental measurements and computer predictions have led to the establishment of values for C_1, C_2, σ_k Prandtl number for k and, σ_ε Schmidt number for ε having a fairly wide range of practical applicability. The k-ε model assumption that flow is locally isotropic is welcome especially in industrial combustors like furnaces where turbulence is not directional.

The k-ε Model Equations

In the mean flow closure, to satisfy dimensional requirements at least two scaling parameters are needed to relate the Reynolds stresses to the rate of strain. A feasible choice is the kinetic energy of turbulence (k) and its dissipation rate (ε). The standard k-ε model [24] has two equations one for k and the other for ε.

The k and ε define velocity scale ϑ and length scale ℓ representative of the large scale turbulence as:

$$\vartheta = k^{1/2} \qquad \ell = k^{3/2}/\varepsilon$$

Here, the use of the 'small eddy' variable ε to define the 'large eddy' scale ℓ is valid. This is because at high Reynolds numbers the rate at which large eddies extract energy from the mean flow is precisely matched to the rate of transfer of energy across the energy spectrum to small, dissipating, eddies. Specifying the eddy viscosity as follows:

$$\mu_t = C_\rho \vartheta \ell = \rho C_\mu k^2/\varepsilon$$

Where C_μ is a dimensionless constant.

The standard model uses the following transport equations for k and ε:

$$\frac{\partial(\rho k)}{\partial t} + \mathrm{div}(\rho k \mathbf{U}) = \mathrm{div}\left[\frac{\mu_t}{\sigma_k}\mathrm{grad}\,k\right] + 2\mu_t E_{ij} E_{ij} - \rho\varepsilon \qquad \text{Eq.2.47}$$

$$\frac{\partial(\rho \varepsilon)}{\partial t} + \mathrm{div}(\rho \varepsilon \mathbf{U}) = \mathrm{div}\left[\frac{\mu_t}{\sigma\varepsilon}\mathrm{grad}\,\varepsilon\right] + C_1\frac{\varepsilon}{k}2\mu_t E_{ij} E_{ij} - C_2\rho\frac{\varepsilon^2}{k} \qquad \text{Eq.2.48}$$

In words, the sum of the rate of change of k or ε and transport of k or ε by convection is equal to the sum of the transport of k or ε by diffusion and rate of production of k or ε minus rate of destruction of k or ε. The equations contain the five adjustable constants mentioned earlier in this section. The E_{ij} is the mean decomposition rate of deformation of a fluid element in a turbulent flow. The standard k-ε model employs values for the constants that are arrived at by comprehensive data fitting for a wide range of turbulent flows. Launder *et al.* [24], after extensive examination of free turbulent flows,

recommended that the constants of effective viscosity, kinematic energy equation k and its transport ε for steady state flows should take the following values respectively:

$$C_\mu = 0.09; \quad \sigma_k = 1.00; \quad \sigma_\varepsilon = 1.30; \quad C_1 = 1.44; \quad C_2 = 1.92$$

The constants can also be obtained from Ref. 25.

In spite of much research conducted on the most sophisticated Reynolds stress models, nothing has emerged to dislodge the k-ε model from its established position it has acquired. It has computational efficiency resulting from the solution of just two equations. The economy of computation represents an often underestimated top priority for furnace prediction procedures because of the number of partial differential equations, usually 11, which have to be solved [26]. As a compromise between the number of unknowns and computational time, the k-ε model for high Reynolds number flow is chosen, which is typical of an industrial combustion chamber. The k-ε model as originally proposed by Launder and Spalding [24] was for incompressible flow. However, the same model has been modified for compressible flows, [27] and has been tested by many researchers and found to yield reasonable results [28]. Therefore, without arguing its validity, this model is adopted for compressible flow in Favre-averaged form [17].

2.5 Combustion Analysis and its Modelling

2.5.1 Combustion Analysis

Combustion is the science of exothermal chemical reactions occurring in fluid flows accompanied by heat and mass transfer processes. Therefore, the development of the combustion theory is based on the achievements of the formal sciences, thermodynamics, kinetics of chemical reactions, fluid mechanics and heat and mass transfer. The system describing the equations of burning species in a gaseous phase, consists of the fluid mechanics, the energy conservation and the chemical species (element) conservation equations. The chemical species conservation involves the kinetics of chemical reactions. For mixtures of ideal gases, (in most industrial installations the combustion goes under conditions satisfying this hypothesis) these describing equations are the Navier-Stokes and the kinetics of chemical reaction equations. They are derived by the molecular-kinetic theory assuming that the length of the free path of molecules is negligibly small with regard to its characteristics dimensions and that the deviations from the thermodynamic, but not chemical, equilibrium at the given point of the mixture are insignificant. It is

assumed that the time of equilibrium of the transient and internal degrees of freedom of the molecules are negligibly short. This is with respect to the time dimension of the investigated process and with regard to the times for completing the chemical transitions. With this assumption, it is then possible to introduce correctly a characteristic temperature for each point of the system. It is also possible to represent the rates of chemical reactions as a function of this temperature and of species mass concentrations. This approximation is characterised by very high accuracy for most cases of modelling combustion process in industrial installations [29].

As shown in Fig.2.7, complex fluid motion mixes the fuel, air and recirculated hot vitiated products within the combustion chamber, and causes energetic products upstream to ignite the reactants mixture. Chemical kinetics determines the rate at which the reaction proceeds. Products not recirculated upstream are exhausted. In reality, chemical kinetics and recirculation of hot vitiated products in the combustor occur simultaneously on the micro scale. However, small micro zones of recirculation persist throughout the chamber, in addition to the large macro scale recirculation shown in Fig.2.7. The recirculation zones constitute well-mixed zones of combustion products. The size and strength of the recirculation zones influence flame stability, combustion efficiency and furnace residence time distribution.

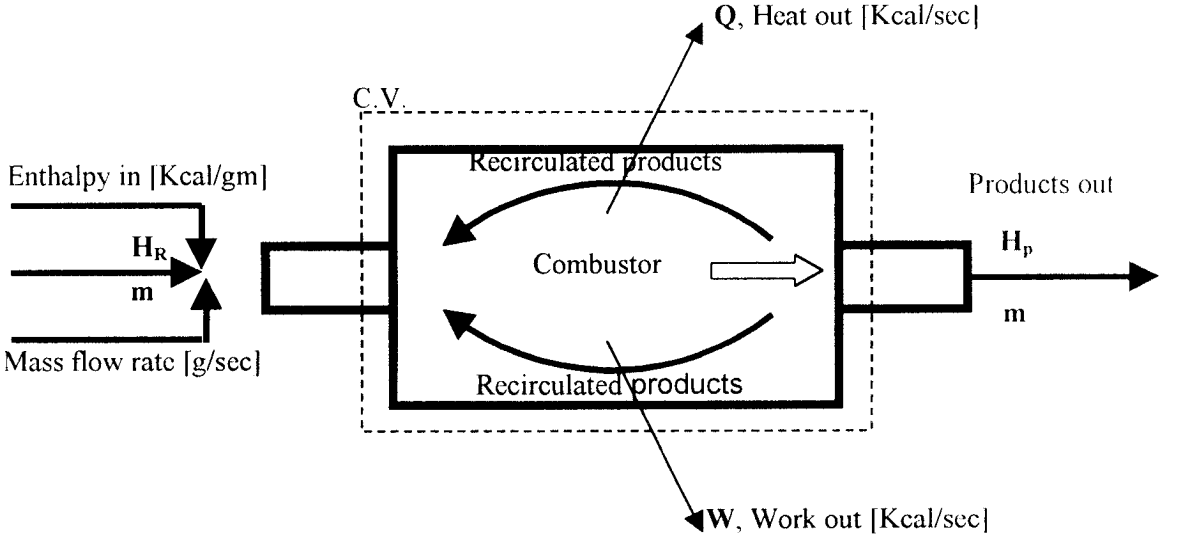

Figure 2.7 Control Volume

The coupling of the chemical kinetics and fluid mechanics on both macro and micro scale makes the combustion process very complex and difficult to analyse in details. These processes occurring in the combustor will be ignored, Fig.2.8, because fundamental concept and analyses of combustion are not concerned with the process occurring during combustion. Combustion is dealt with in chemical kinetics and fluid mechanics.

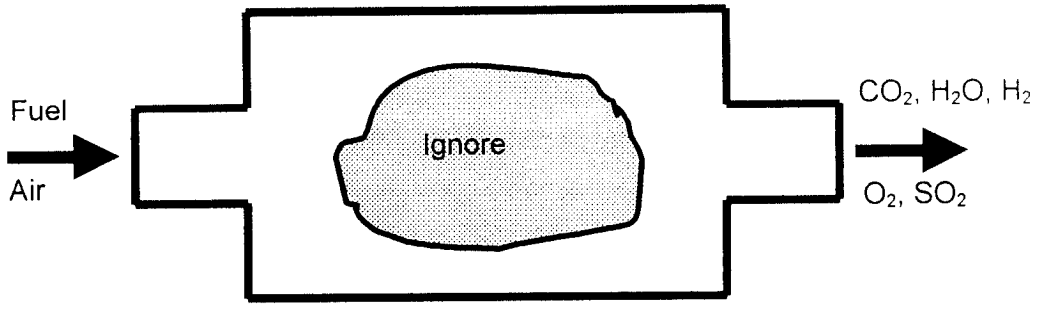

Figure 2.8 Classical Combustion Analysis

2.5.1.1 Classical Analysis of Combustion

Classical analysis of combustion is concerned with calculating mass of fuel required per unit mass of air, and resultant mass of products formed in the practical combustion devices. In describing classical analyses, our first obligation is to define two parameters fundamental to combustion; the stoichiometric fuel-air ratio and the equivalent ratio.

The stoichiometric fuel-air ratio also known as chemically correct fuel-air ratio is the ratio of air to fuel required to produce the products of complete combustion without excess air or oxygen.

Carbon	+	Oxygen	=	Carbondioxide	+	Heat
Hydrogen	+	Oxygen	=	Water	+	Heat
Sulphur	+	Oxygen	=	Sulphurdioxide	+	Heat

The equivalent ratio, is given by Φ and defined as the ratio of actual fuel-air ratio by mass or volume divided by the stoichiometric fuel-air ratio by mass or volume.

$$\Phi = \frac{\text{Fuel/Air}_{(\text{actual})}}{\text{Fuel/Air}_{(\text{stoichiometric})}}$$

$\Phi > 1$ fuel rich mixture i.e. excess fuel or air lean.

$\Phi = 1$ stoichiometric mixture.

$\Phi < 1$ air rich mixture i.e. excess air or fuel lean mixture.

Classical analysis of combustion is concerned with both volumetric and gravimetric analyses of combustion products. The main products are CO_2, H_2O, SO_2, ash, N_2 and O_2. Pollutant species are ignored (ignoring pollutant species is justified because the volume or weight of the pollutant species is small compared to that of the main products) as shown in Fig.2.7 of classical combustion analyses, the detailed process occurring within the combustor are ignored. Attention is only paid to the fuel-air mixture entering the combustor and products CO_2, H_2O, SO_2, ash, N_2 and O_2 exiting combustor.

Conceptionally, the adiabatic flame temperature is defined as the highest temperature that can be realised by the reaction mixture without adding heat to the combustion chamber. In the adiabatic chamber, all the energy released by the reactants goes into raising the temperature of the mixture. No energy is lost to the surrounding. However, for a practical system heat will be lost. Nonetheless, the adiabatic flame temperature may be realised early in the flame before time is available for the heat loss to occur. This concept of adiabatic flame temperature is useful because it identifies the maximum attainable temperature in a combustion process although the maximum temperature may be realised only locally as in the steam boiler. Analytically, the equation for the adiabatic flame temperature is developed upon the premise that the total enthalpy of the mixture is conserved.

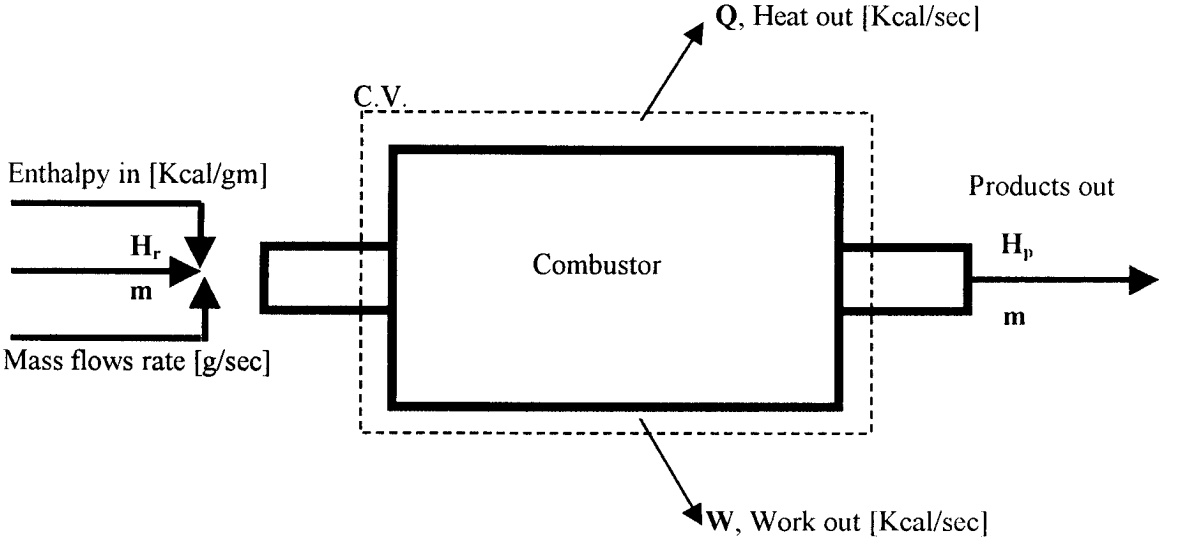

Figure 2.9 Control Volume Energy Balance

Specifically the products enthalpy is equal to the reactants enthalpy i.e. $H_p = H_r$ [kJ]. Where H_p is enthalpy of system products and H_r is enthalpy of the system reactants. In a flow system, enthalpy comprises the flow work as well as the internal energy. The energy balance on the volume is as shown in Fig.2.9 above.

In equation form the energy balance is:

$$h_p + \frac{\dot{Q}}{\dot{m}} + \frac{\dot{W}_s}{\dot{m}} = h_r \left[\frac{kJ}{kg}\right] \qquad \text{Eq.2.49}$$

For $Q = W_s = 0$ $h_p = h_r$ or $H_p = H_r$

h_p : Specific enthalpy of products
h_r : Specific enthalpy of reactants
Q : Heat loss
W_s : Work done
m : Mass flow rate of reactants

It is assumed that heat transfer from fluid to surrounding is neglected i.e. process is adiabatic. To apply $H_p = H_r$ to a combustion system the following abstract general reactions are introduced.

$$\Sigma_i b_j B_j = \Sigma_j a_i A_i \qquad \text{Eq.2.50}$$

Where a_i = number of moles of reactant species A_i
b_j = number of moles of product species B_j

Utilising Eq.2.49 when Q = W = 0

$$\Sigma\ b_j\ \overline{h}_{Bj} = \Sigma\ a_i\ \overline{h}_{Ai} \qquad \text{Eq.2.51}$$

Where h_{Bj} = enthalpy per unit mole of the species B_j [kJ/mole] and the over bar denotes molar quantity. It remains for us to obtain an expression for the enthalpy h_{Ai} and h_{Bj} in terms of temperature.

The definition of specific heat at constant pressure is

$$\overline{C}_p = \left(\frac{\partial h}{\partial T}\right)$$

For perfect gases, enthalpy is a function of temperature only. Hence:

$$d\,\overline{h}_{Ai} = \overline{C}_{pAi}\,[T]dT$$

Where: T = temperature in Kelvin [K]

C_{pAi} = specific heat per unit mole of species A_i [kJ/mole k]

Upon integration,

$$\overline{h}_{Ai} = h_{AiT_0} + \int_{T_O}^{T} \overline{C}_{pAi}\,[T]\,dT \qquad [\text{kJ/mole}] \qquad \text{Eq.2.52}$$

Where T_o is the reference temperature arbitrarily chosen to be 298K. The constant of integration h_{AiTo} is called heat of formation at 298K for the species A_i and usually replaced with a more austere symbol Δh_{f298Ai} [kJ/mole] the integration of $\int C_{pAi}\,[T]\,dT$ is called sensible enthalpy. With substitution of Δh_{f298Ai} for h_{AiTo} Eq.2.52 becomes:

$$\overline{h}_{Ai} = \Delta h_{f298Ai} + \int_{T_0}^{T} \overline{C}_{pAi}\,[T]dT \quad [\text{kJ/mole}] \qquad \text{Eq.2.53}$$

Equation 2.53 is the expression for the enthalpy of species A_i at temperature T. The values for the heat of formation and sensible heat are tabulated in JANAF and Ihsan Barin Tables.

Having known the expression for the enthalpy in terms of temperature Eq.2.53 is combined with Eq.2.50 to establish the desired adiabatic flame temperature.

Thus:

$$\Sigma_j\, b_j\left(\Delta H_{f298Bj} + \int_{T_0}^{T_{adia}} \overline{C}_{pBj}[T]dT\right) = \Sigma_i\, a_i\left(\Delta H_{f298Ai} + \int_{T_0}^{T_i} \overline{C}_{pAi}[T]dT\right) \qquad \text{Eq.2.54}$$

Where T_i is the initial temperature or temperature of reactants and T_{adia} is the adiabatic temperature to be determined.

If we arbitrarily define a new variable ΔH_{R298} as the difference between the products and the reactants heat of formation

$$\Delta H_{R298} = \Sigma_j b_j \Delta H_{f298Bj} - \Sigma_i a_i \Delta H_{f298Ai} \qquad [kJ] \qquad \text{Eq.2.5}$$

Equation 2.54 is simplified to:

$$\Sigma_j b_j \int_{298}^{T_{adia}} C_{pBj}[T]dT = -\Delta H_{R298} + \Sigma_i a_i \int_{298}^{T_i} \overline{C}_{pAi}[T]dT \qquad \text{Eq.2.56}$$

ΔH_{R298} is called the heat of the reaction at 298K. It should be noted that the equality $H_p = H_r$ determines the adiabatic flame temperature. To use Eq.2.56 to establish the peak temperature in an adiabatic device, the information to be known prio are a_i`s (moles of reactants) and initial temperature of reactants $T_i$. The $b_j$`s (moles of products) are functional dependent upon the adiabatic temperature and are calculated from equilibrium kinetics chemistry depending on a_i and may change according to temperature. Higher temperatures may promote dissociation of species into additional species that could not be otherwise present at lower temperatures. Adiabatic flame temperature can be obtained from the simple iterative calculation of Eq.2.56 [30].

2.5.2 Simplification of Species Conservation Equations.

The three major features of flow are the turbulence characteristics, combustion characteristics and heat transfer characteristics. The mathematical modelling of turbulent combustion process is the problem of the interaction between the turbulent flow and the chemical reaction. The whole process takes place under condition of continuos changes in the temperatures, concentration of chemical components, velocity and chemical state of the reacting species. Under these conditions the process can be presented

mathematically by formulating a complex system of non-linear differential equations. The analytical solution of these equations is impossible such that numerical methods are used. The system of equations consists of two parts: balance equations for u, v, w, h and ρ describing turbulent flow and balance equations for number of reacting species N_i, describing the change in the chemical composition of the components. Since in the combustion chamber there are considerable temperature differences, density is a highly variable quantity, therefore, it is better to use averaged equations according to Favre. The determination of the chemical reaction rate is the basic problem in modelling of combustion process. The difficult arises from the non-linear character of the chemical reaction rate. The reaction rate is a function of the temperature, pressure and mass fraction of species, but the mean value of reaction rate is not a function of its averaged value [19].

Naturally then, the whole aim of combustion modelling is to arrive at the calculation of the temperature (T), density (ρ), mass fraction of species (m_i) and the rate of reaction (R_i), all being time-averaged quantities. Practical combustion systems in general are full of complex features. Formation of soot and pollutants, and significant heat transfer by radiation are common. Therefore, the closure of the species conservation equations is indeed a formidable task. Many researchers such as Spalding [31], Khalil [28], Hutchinson et al.[32], Pope [33], Khalil [34] etc. have suggested that in some circumstances the overall features of turbulent flames are independent of the detailed chemistry involved.

There is reason to believe, therefore, that a theory of turbulent combustion, based on the instantaneous equations, which contain some uncertainty, may be successful. Such a simple approach was applied to furnace and combustor flows. The effect of turbulence on reaction is of prime importance in that it is the most serious obstacle to the formation of a closed set of time- averaged equations that describes reacting flows. The effect of reaction on turbulence is due to changes in the viscosity and more especially in the local density due to reaction. This aspect has been considered by Favre [17], Bilger [35], Bray [36], Pope [33] and Khalil [37, 38].

2.5.2.1 The Simple Chemical Reacting System (SCRS)

During combustion of a fuel reacting with oxidant, the products are formed in a series of reactions. In addition to all flow equations, the transport equations for mass fraction m_i of each species must be solved. In the SCRS the task is to resolve Eq.2.22

$$\frac{\partial(\rho\, m_l)}{\partial t} + \text{div}\,(\rho\, m_l \mathbf{u}) = \text{div}\,(\Gamma_l \text{grad}\ m_l) + S_l \qquad \text{Eq.2.57}$$

Where S_l is the source (sink) term for the volumetric rate of generation (or destruction) of a species due to chemical reaction.

Then total of the mass fractions of fuel, oxidant and inert species is one, so

$$\sum_{\text{all species } l} m_l = 1 \qquad \text{Eq.2.58}$$

Chemical energy is released as heat during combustion and the resulting enthalpy is obtained by solving its equation

$$\frac{\partial(\rho h)}{\partial t} + \text{div}(\rho h \mathbf{u}) = \text{div}(\Gamma_l \text{grad}\, h) + S_h \qquad \text{Eq.2.59}$$

Where S_h is the source term for enthalpy including radiation loss or gain, pressure work as well as the chemical energy. The viscous energy dissipation is normally assumed to be negligibly in low Mach combusting number flows. The temperature is calculated from the enthalpy by means of:

$$T = \frac{h - m_{fu} H_{fu}}{\overline{C}_p} \qquad \text{Eq.2.60}$$

Where H_{fu} is the calorific value of fuel,

$$\overline{C}_p = \frac{1}{(T - T_{ref})} \int_{T_{ref}}^{T} C_p\, dT$$

and $$C_p \equiv \sum_{\text{all species } l} m_l C_l$$

Where C_l is the specific heat capacity of species l.

The local density of the mixture is dependent on the reactant and product concentrations and on the mixture temperature. Its value can be calculated from

$$\rho = \frac{P}{RT \sum_{all\ l} \frac{m_l}{M_l}}$$

Since the flow field is in turn affected by changes in temperature and density, all the flow equations must be solved in addition to the species and enthalpy equations. The resultant set of partial differential equations is very large and requires vast amount of computing resource to consider all the intermediate reactions. Simple models incorporating only a few reactions are often preferred in numerical combustion procedures used in CFD. The simplest known procedure is the Simple Chemical Reacting System (SCRS) of Pun and Spalding [39]. By simulating combustion using the SCRS, reality is simplified but realities of major practical importance are retained (taken care of). The SCRS assumes a global-one-step infinitely fast chemical reaction, where the oxidant combines with the fuel in stoichiometric proportions to form products:

1 kg of fuel + S kg of oxidant = (1+ S) kg of products Eq.2.61

For the combustion of methane the Eq.2.61 becomes:

CH_4	+	$2O_2$	=	CO_2	+	$2H_2O$
1 mole of CH_4		2 moles of O_2		1 mole of CO_2		2 moles of H_2O

i.e. I kg of CH_4 + 64/16 kg of O_2 = (1 + 64/16) kg of products Eq.2.62

The transport equations for the fuel and oxygen mass fraction are

$$\frac{\partial(\rho m_{fu})}{\partial t} + \mathrm{div}(\rho m_{fu}\,\mathbf{u}) = \mathrm{div}(\Gamma_{fu}\,\mathrm{grad}\,m_{fu}) + S_{fu} \qquad \text{Eq.2.6}$$

$$\frac{\partial(\rho m_{ox})}{\partial t} + \mathrm{div}(\rho m_{ox}\,\mathbf{u}) = \mathrm{div}(\Gamma_{ox}\,\mathrm{grad}\,m_{ox}) + S_{ox} \qquad \text{Eq.2.6}$$

The mixture fraction f is linearly related to the mass fractions of fuel m_{fu} and oxygen m_{ox} [3] The mixture fraction, being a passive scalar, obeys the following transport equation:

$$\frac{\partial(\rho f)}{\partial t} + \mathrm{div}(\rho f \mathbf{u}) = \mathrm{div}(\Gamma_f \mathrm{grad}\, f) + S_f \qquad \text{Eq.2.65}$$

For the reaction of Eq.2.62 is irreversible, i.e. rate of the reverse reaction is presumed to be very slow. The energy released, called the " heat of combustion" is taken as independent of temperature; this results in equality (even constancy) of the specific heats of reactants and products. Therefore, the enthalpy of a mixture of fuel, oxidant and products can be found from Eq.2.60. In addition, the ratio of the masses of fuel, oxygen and products engaged in the reaction obey Eq.2.58. Taking into account experimental data, it is reasonable to assume that the exchange coefficients or diffusion coefficients of fuel Γ_{fu}, oxygen Γ_{ox} and products Γ_{pr} are all equal to each other and the diffusivity of heat. Therefore, the Prandtl-Schmidt numbers are equal. This results in unity Lewis number where it is assumed that energy diffuses at the same rate for all species and the flame is stable. This is not far from the truth for laminar gaseous flow: and it is very close to the truth for turbulent fluids. An important consequence is that it is possible to describe the composition of a reacting mixture by just two variables. These are m_{fu}, the mass fraction of fuel and f, the mixture fraction of material originating from fuel, per unit mass of mixture, regardless of whether it is burned or not.

The reactants may be accompanied by inert species, such as N_2, that do not take part in the reaction. The mass of the inert species can be obtained by the linear relationship for inert mixing illustrated in Fig.2.10.

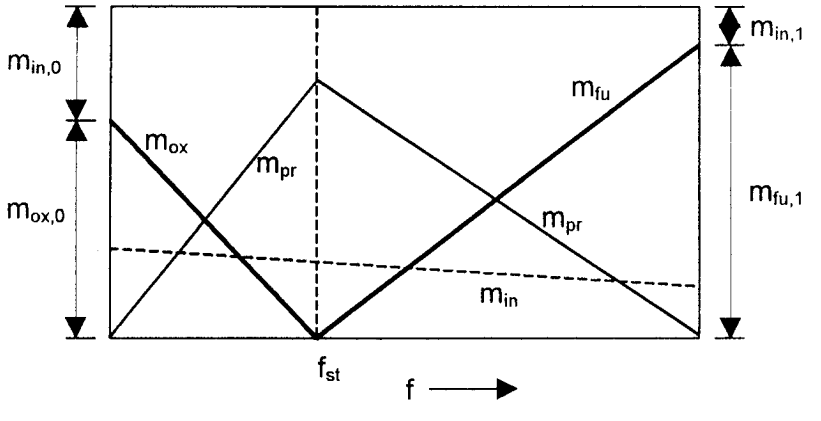

Figure 2.10 Mixing and Fast Reaction between Fuel and Oxidant Streams.

Simple geometry gives the total mass fraction of the inert species m_{in} after combustion at any value of f as:

$$m_{in} = m_{in,o}(1-f) + m_{in,1}.f \qquad \text{Eq.2.66}$$

The mass fraction of the products of combustion may be obtained from:

$$m_{pr} = 1 - (m_{fu} + m_{ox} + m_{in}) \qquad \text{Eq.2.67}$$

The above equations represent the SCRS model as shown graphically in Fig. 10.

The SCRS has made simplifications or assumptions, which fix algebraic relationships between the mixture fraction f and all the mass fractions m_{fu}, m_{ox} and m_{pr}. Consequence it is only necessary to solve one extra PDE (for f) to calculate combusting flows rather than individual PDE's for each mass fraction. In the SCRS approach, fluctuations of temperature are often taken into account by incorporating a probability density function (pdf) to calculate mean properties. In the pdf method (which originates from the turbulence modelling) the average value of a scalar variable (m_{fu}, m_{ox}, etc) is obtained by weighting the instantaneous value with a probability density function for mixture fraction f.
The mean value of a property φ is given by:

$$\overline{\varphi} = \int_0^1 \varphi(f)\, p(f)\, df$$

Where φ is any variable which is a function of f alone, and p(f) is the probability function. The clipped Gaussian and Beta functions give the best results amongst the various different pdf's. The interested reader is referred to [40, 41, 42 and 43].

2.5.3 Combustion Rate in Premixed Flames and the Eddy-Break-Up Model

Two factors complicate the determination of the reaction rate in engineering equipment. Firstly, some 200 intermediate species have been identified in the combustion of the typical hydrocarbon fuel. For example, over 40 elementary reactions are involved in the combustion of methane (CH_4), the simplest hydrocarbon fuel. Any attempt to simulate anything like all of the corresponding intermediate reactions would precipitate a computational problem. Secondly, because of the non-linear dependence of reaction rate

on temperature, the determination of the time-averaged value is far from straightforward. For the first difficult, it is solved by applying the one-step global reaction to carbon dioxide and water for all important heat release for practical purposes. An effective way to circumvent the second difficult is contained in the fact that the time scale of the turbulence decay, which may be characterised by the integral length scale divided by the mean flow velocity; is typically much larger than the chemical kinetic time scale. Since practically all of the combustion occurs after mixing between the small scale dissipative eddies, we cannot go too far wrong by ignoring the kinetics rate of the overall reaction altogether and linking the combustion rate to the turbulence decay rate, for which we can make simple order of magnitude estimates. Magnussen and Hiertager have just done this [44].

The premixed flame situation flow has fuel and oxidant mixed prio to be delivered to the combustion chamber. A source term is required in the conservation equation of species to account for the disappearance of species at finite rate. The reaction mechanism between fuel and oxygen can take place in intermediate steps; producing radicals in the initiation reactions to consequently yield carbon dioxide, water and hydrocarbon fuels. Each step is governed by a particular equation to account for the rate of formation or disappearance of the species. It is expressed in the Arrhenius form, and is strongly temperature dependent as indicated by the exponential term: it is also dependent, albeit to a lesser degree, on the local concentration of reactants. Spalding [31] proposed the eddy-break-up model (EBU). which accounts for the time scale of turbulence and combustion. The EBU model presents the chemical reaction as eddy dissipation in a turbulent flow. The rate of consumption of fuel is specified as a function of local flow properties. The Mixing-controlled rate of reaction is expressed in terms of the turbulence time scale k/ε. The model considers the dissipation rates of fuel, oxygen and products, and takes the slowest rate as the reaction rate of fuel. The idea to present the chemical reaction by "eddy dissipation" is based on some assumptions that the reaction rate is finite, single step and irreversible. The probability distribution of fuel mass fraction is a clipped Gaussian function. The fuel conservation equation is solved with the appropriate reaction rate term. This yields the fuel mass fraction, which together with the value of m_{fu}^2 obtained from its conservation equations, are used to obtain pdf for p (m_{fu}). Consequently, other scalar properties are obtained.

Considering the model formulation, in the mixing zone of fuel and oxidant, the rate of single-step chemical reaction can be expressed as:

$$R_{fu} = A_0 \rho^2 M_{fu} M_{ox} \exp\left(-\frac{E}{RT}\right) \qquad \text{Eq.2.68}$$

Time-averaging Eq.2.68 (also known Arrhenius expression) and neglecting turbulent fluctuations yields:

$$\overline{R}_{fu} = A_0 \overline{\rho}^2 \overline{M}_{fu} \overline{M}_{ox} \exp\left(-\frac{E}{R\overline{T}}\right) \qquad \text{Eq.2.69}$$

The difficulty with using above expression to calculate the reaction rate is that, it is necessary to solve additional equations of conservation, thus large computer storage is required. To avoid solving the additional equations, Spalding [31] proposed a reaction rate based on the species concentration fluctuations and the rate of break-up of eddies. The EBU reaction rate is:

$$\overline{R}_{EBU} = C_R \, \overline{\rho} \frac{\varepsilon}{k} \left(\overline{m_{fu}^{\,2}}\right)^{\frac{1}{2}}$$

Where C_R is a constant of the model. The term ε/k has the dimensions of s^{-1}, and the diffusion scale $\tau_{so} = k/\varepsilon$ (s) should be compared to the chemical time scale τ_k given by Borghi [45] as:

$$\tau_k = \left[A_0 \, \overline{\rho} \left(\overline{m}_{ox} + i \, \overline{m}_{fu}\right) \exp\left(-\frac{E}{R\overline{T}}\right) \right]^{-1}$$

This is done to determine the flame type. In the computational solution procedure, the two reaction rates are compared and the smaller one is taken to be the effective controlling rate. Evidently, the smaller rate of reaction corresponds to the larger of the time scales (τ_{so} and τ_k). It is natural that the process that takes the larger time controls the reaction. When τ_{so} is very small, which corresponds to a large dissipation rate of eddies and rapid mixing, the reaction is kinetically influenced. This implies that the reactants are in intimate contact

but their temperature and concentrations are not suitable for the reaction to proceed: the smaller rate in this case is given by Eq.2.69. In the region where τ_{so} is larger than τ_k the mixing of the reactants is slow and the reactants are at a suitable temperature and concentrations to react as soon as they intimately mix. Therefore, the reaction then is diffusion controlled; i.e. it is controlled by the rate given by the eddy break-up reaction rate. To determine the eddy break-up rate of reaction, it is necessary to evaluate the averaged m_{fu}^2 The EBU model is appropriate for premixed flame situations where the rate of reaction is both finite and very high. In other words, the model is restricted to situations where the Damkholer number $N_D = \tau_{so}/\tau_k$ is very small. This model applies successfully to controlled flames and axisymmetric furnaces. Good predictions of the temperature field in furnace configurations were obtained with the eddy break-up model by Magnussen and Hjertage [44]. Further application of the scalar fluctuations were done by Gosman *et al.* [46]. Both predictions compare very well with experimental data.

2.6 Radiation and its Modelling

2.6.1 Introduction

It is important to realise that all matter, solids, liquids and gases, can radiate heat; invisible hot furnace gases, for example, radiate heat to their surroundings. Although radiation is more striking within high temperature ranges, it is actually a factor in heat transfer even at relatively low temperatures. Hot gases radiate heat even when no combustion is taking place. Good radiating gases include carbon dioxide, water vapour and hydrocarbons; carbon monoxide is a relatively poor radiator of heat. For combustor geometries of dimensions 1 m or more, heat transfer is substantial and should therefore be taken into consideration.

The concept of radiation intensity (radiosity, or radiance) is of great theoretical and practical importance. Theoretically, the intensity of radiation is defined as the quantity of radiant energy emitted in a direction of angle Ψ per unit time from an elementary area within the limits of a unit elementary solid angle. The solid angle is reduced to the projection of this area on the plane which is orthogonal to the direction of radiation. The directional distribution of radiation intensity may differ greatly and distribution may be uniform in a special case. The concept of radiation intensity considered in this study is the volumetric radiation. Volumetric radiation is characteristic of a medium filling some volume (space) of a system and which is capable of emitting, absorbing and scattering radiation. It is also characterised by irradiance given in J/m^3.

While turbulent flow and turbulent combustion have been studied quite extensively and fairly satisfactory methods are available for their prediction, more complete understanding of radiation heat transfer in an industrial furnace is needed. The radiation-related problem is the interaction of radiation with turbulence or turbulent combustion.

Song [47] showed that the flow field and turbulent quantities results obtained by accounting for the interaction and by neglecting the turbulence-radiation interaction is not discernible. This is because temperature only affects the flow field by changing the local density. Therefore, the small difference in the predicted temperature between the two models has little influence on the flow field. Song further showed that the mass fraction of the fuel, the flame shape and the mean temperature distributions show slight difference from the calculation accounting for the turbulence-radiation interaction. These observations by Song clearly showed that the effect of turbulence-radiation interaction is significant when the flame is large in size compared to the volume of the furnace especially when the temperature of the fresh mixture is low, say 300 K, resulting in a long flame.

One of the important parameters in accessing the performance of a furnace is the heat flux distribution to the material being processed. Methods based on fundamental principles are now available using numerical techniques and the digital computer; that permit predictions to be made. These prediction procedures require empirical inputs to describe turbulent transport, chemical kinetics and thermodynamic properties. The quality of the prediction essentially depends on the validity and relative importance of these factors as elaborated in Sections 2.4 and 2.5. Decoupled models are required to solve problems of radiation heat transfer. The problems associated with the prediction of radiation heat transfer within a combustion chamber are three fold: Firstly, evaluation of radiation exchange to all points within an enclosure if the temperature, absorption, emission, scattering, emissivity and reflectivity characteristics are known. Secondly, evaluation of the absorption, emission and scattering characteristics from knowledge of temperature and radiating species. Thirdly, evaluation of temperature and radiating species concentration. In the development of a radiation exchange model only the first and second points need be considered as the temperature and concentration of radiating species can be obtained by the methods described in Sections 2.4 and 2.5 or from a flow physical model and chemical heat release pattern [48]. Therefore, a rigorous calculation of radiative heat transfer from a flame to heat sinks in an enclosure requires the

simultaneous solution of partial differential equations of fluid flow with chemical reaction and energy transfer. The interdependence of these processes makes the problem highly complex.

Radiation normally presents two difficulties, one physical and the other mathematical. The latter is dealt with in subsequent sections in detail, but for now the physical model will be tackled. The radiative properties of materials are highly diverse. If attention is restricted to a particle-free gas, then its local absorptivity is a complex function of composition, temperature and wavelength. If particles are present, the distribution of the scattering angle should be known. Additionally, surfaces have different properties according to their roughness, the presence of oxides films etc. This information about properties is far from having been fully collected and documented. Consequently, often times assumptions have to be made about them. The majority of combustion chambers contain both a mixture of gases, which will only absorb and emit in certain wavebands and suspended particulate material such as soot, pulverised coal or fly ash, which have a continuos radiative contribution (not necessarily gray) over the infrared spectrum. The mathematical difficulty of radiation is brought about by its six- dimensional nature. The angle has two dimensions, wavelength has one co-ordinate and position has three co-ordinates. Therefore, the description of a radiant flux field is much more voluminous than that of other fields like temperature or velocity. The other thing is the nature of radiation to penetrate; so by its agency, all points in the field that can 'see' each other participate in interactions, no matter how far away they are. The mathematical expression of this fact is by way of the class of equations called "integro-differential" which are especially difficult to solve. An example of such equations is Eq.2.70. All practical flames lie between two extremes. The first is the thin-gas situation, in which, perhaps because of small dimensions or low gas pressure, almost all radiation emitted by gas escapes to the wall without re-absorption. The second is the thick-gas layer, where radiation reduces to the same form as thermal conduction. The thin and thick gas approaches make it easy to deal with "integro-diffferentials." Ideally, the accurate solution of radiation exchange within an enclosure at equilibrium is obtained by the spectral summation of the multiple reflection, absorption and scattering of a semi-infinite number of limited monochromatic radiation beams. Due to the difficulties alluded to above plus physical and computational limitations, several techniques for the evaluation of radiation exchange have been developed [49]. These techniques are commonly referred to as "Monte Carlo method", "Zone method" and "Flux method". All these methods are fundamental by nature and in their limits they lead to the ideal solution.

Before looking at these methods the following section first deals with the basis (i.e. equation of radiation energy transfer) of all methods for the solution of radiation problems.

2.6.2 Radiation Energy Balance

The equation of radiant energy transfer is derived by formulating a balance on the monochromatic radiant energy, passing in a specified direction, through a small volume element in an emitting-absorbing-scattering medium.

This equation can be written in the form [50]:

$$(\hat{n}.\nabla)I_{\lambda} = -(K_{\lambda a} + K_{\lambda s})I_{\lambda} + K_{\lambda a}.I_{b\lambda} + \frac{K_{\lambda s}}{4\pi}.\int_{\omega=0}^{4\pi} I_{\lambda}(\omega).d\omega \qquad \text{Eq.2.70}$$

(1) (2) (3) (4)

Where n is the unit vector; λ is the wavelength; I_{λ} is the intensity of the radiation energy at wavelength λ; $K_{\lambda a}$ is the monochromatic absorption coefficient; $K_{\lambda s}$ is the monochromatic scattering coefficient and $I_{b\lambda}$ is the intensity of the radiation of a black body at wavelength λ. For the terms:

Term (1) represents the gradient of intensity in the specified direction.
Term (2) represents the attenuation of the beam due to absorption and scattering.
Term (3) represents the increase in intensity due to emission according to Planck's Law.
Term (4) represents the increase in intensity due to radiation incident on the differential volume, which is scattered in the direction of the unit vector [51].

In Fig.2.11, radiation energy is going out of the small volume gas. The emitted energy is dependent on the gas concentration and temperature. The incoming energy is difficult to calculate due to the radiation rays originating from a 4π space radians and each bundle originating from a surface temperature and reflected radiation. The intensity is dependent on the absorption and the scattering of the medium.

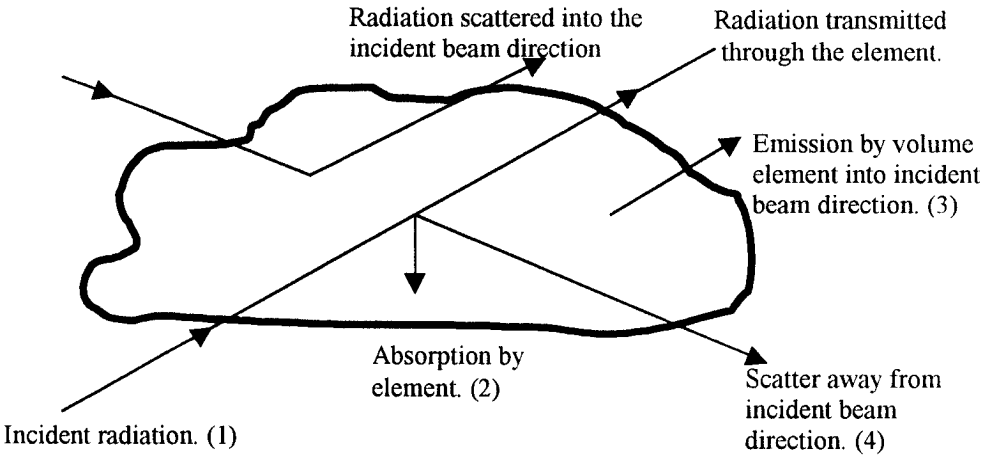

Figure 2.11 Radiant energy balance on a monochromatic beam passing in a specified direction through an element in an absorbing-emitting-scattering medium

The total received radiation is determined by integrating the radiation energy balance Eq.2.70 twice over the 4π space radians from $\omega = 0$ to 4π (steradians) and over the whole wave length area from $\lambda = 0$ to ∞. The resulting equations are integro-differential. Since the incoming and outgoing fluxes are not known, an iterative solution method is necessary. The numerical calculations of these integro differential equations are very expensive and therefore use is made of radiation models with a number of simplifications [7]. The techniques applied to the solution of Eq.2.70 differ widely but fall into three main categories: Flux models, statistical methods based on Monte Carlo simulation and Zonal analysis. These methods are the subject of the next Section 2.6.3.

2.6.3 Radiation Models

In this study, the composite flux model of radiation is used. The reason is that its mathematical expression, by way of the finite-difference equations, leads to a sparse matrix coefficients; and its method can easily be integrated into computational fluid dynamic models. The solution of the radiation field can be carried out using the same numerical techniques used to solve the conservation equations for the flow, temperature and composition fields. The composite flux model is more appropriate in principle but perhaps not so in practise. Since it considers radiation intensities in all co-ordinate directions it is more accurate. In CFD models, calculation of the radiative transfer is typically handled using a six-flux model, or, more recently, the discrete method developed

by Lockwood and Shah [52]. Therefore, the Zone method and Monte Carlo methods are only briefly described here.

2.6.3.1 Zone Method

The method was originally developed by Hottel and Cohen [53] and latter further developed by Hottel and Sarofim [54]. The starting point for the zone method of analysis is an assumed knowledge of the patterns of fluid flow, chemical heat release and radiating gas concentration within a furnace. From this point equations describing the conservation of energy within the furnace are drawn up. This is carried out by dividing the furnace into a large number of zones, both surface zones and gas zones, which are small enough for each zone to be assumed to be isothermal and to have constant properties. These considered volumes are usually bigger than the control volume for the flow equation elements. The radiative interchange in the enclosure is first obtained by determining the radiation exchange factors for each zone pair combination in the furnace. While doing so, account is taken of the attenuation by intervening gas, and including the effects of reflection within the enclosure. These exchange factors and the " total exchange areas" are the constants of proportionality in equations relating the exchange of radiative energy to the difference of the fourth power of the temperature of each respective zone pair, and give a solution for the radiation exchange within the furnace. Total energy balance equations for each zone can then be drawn up, taking account of all forms of energy transfer in the furnace, such as convection of heat due to gas mass flow, chemical heat release and net radiative transfer with other zones. This leads to a set of simultaneous non-linear, algebraic equations in terms of the temperature field within the furnace, and this then enables heat flux to be evaluated [49].

2.6.3.2 Monte Carlo Method

The Monte Carlo methods provide a statistical approach to the problem of solving Eq.2.70, by simulating the paths of a large number of randomly directed bundles of energy through the radiating medium. The overall radiation behaviour is then determined from the average behaviour of these bundles. The technique relies on the generation of random numbers to select each beam and significant errors are possible if satisfactory tests are not applied to ensure randomness. Steward and Cannon describe the application of the Monte Carlo technique to furnaces in detail [55].

The Monte Carlo method is potentially the most rigorous and flexible, it is simple in concept, easy to formulate and able to simulate both complex geometry and spatial variation in radiative properties. However, it has a statistical uncertainty unless excessive computing times are used. The results fluctuate around a real solution and many radiation bundles must be considered. With a reasonable use of computing time, the Monte Carlo method has little merit over the zone method in terms of accuracy. The zone method has successfully been applied to the prediction of radiation heat transfer in enclosures. Acceptable predictions of radiation heat transfer to the walls of the combustion chamber and heat sink have been obtained; but the prediction of temperature profiles has not been good. Though the zone method is regarded as a finite-difference representation of the integro-differential equations, it leads to a full matrix of coefficients in the equations, and so entails much computational work. Both methods are numerical exact. Unfortunately, both methods use another numerical algorithm to solve the flow equations, which makes it difficult to combine with most CFD codes.

2.6.3.3 Flux Method

The mathematical formulation of the radiant energy balance in a specified direction, on a small radiating volume element in thermodynamic equilibrium within an enclosure results, in an integro-differential equation for the unknown intensity of radiation [56]. Solution of this equation is complicated by the fact that the intensity is a function of both direction and position. The basis of all flux methods is to simplify the problem. This is achieved by making an approximate allowance for the variation of intensity with direction. The variation is achieved by subdividing the total solid angle at any point into a number of smaller solid angles. In each of the smaller solid angles the intensity is assumed to be independent of direction. The integro-differential equation is then averaged over each of the smaller solid angles in turn, leading to a set of differential equations for the unknown intensities. The simultaneous equations are solved by applying a total energy balance and appropriate boundary conditions. This leads to obtaining values of intensity for each solid angle at all points within the enclosure. The accuracy of the solution of any problem can be improved at the expense of increased computational effort by using finer sub-divisions of the angle range. Further description of the flux models are found in excellent reviews by Siddall [57] and Siegel [58]. The details of the axial symmetric six flux model used in this study are now dealt with as outlined by Lamers [7].

The differential equations are:

$$\frac{1}{r}.\frac{d}{dr}(r.I) = -(a+s).I + a.E + \frac{s}{6}.(I+J+K+L+M+N) + \frac{J}{r} \qquad \text{Eq.2.71.(a)}$$

$$\frac{1}{r}.\frac{d}{dr}(r.J) = (a+s).J - a.E - \frac{s}{6}.(I+J+K+L+M+N) + \frac{J}{r} \qquad \text{Eq.2.71.(b)}$$

$$\frac{d}{dz}(K) = -(a+s).K + a.E + \frac{s}{6}.(I+J+K+L+M+N) \qquad \text{Eq.2.72.(a)}$$

$$\frac{d}{dz}(L) = (a+s).L - a.E - \frac{s}{6}.(I+J+K+L+M+N) \qquad \text{Eq.2.72.(b)}$$

$$\frac{1}{r}.\frac{dM}{d\theta} = -(a+s).M + a.E + \frac{s}{6}.(I+J+K+L+M+N) \qquad \text{Eq.2.73.(a)}$$

$$\frac{1}{r}.\frac{dN}{d\theta} = (a+s).N - a.E - \frac{s}{6}.(I+J+K+L+M+N) \qquad \text{Eq.2.73.(b)}$$

Where; r is the radial distance, **a** and **s** are the absorption and scattering coefficients per unit of length, and **E** is the emitted radiation intensity of a black body in a certain wavelength interval.

Further; J and I, K and L, and M and N are the radiation intensities in the positive and negative y-, z-, and θ-directions respectively.

For an axisymmetric chamber, the y-direction is the radial distance, the z-direction is the axial distance and the θ-direction is the angular distance, also considered as x-direction. The intensities are the total scattered radiation division that goes through a surface in the positive and negative direction respectively.

By carrying out additions, differentiations, subtractions, combinations and substitutions operations on the three pairs of first order differential Eqs.2.71 to 2.73 we obtain the three second-order differential equations given below:

In the positive and negative radial directions:

$$\frac{1}{r}.\frac{d}{dr}\left(\frac{r}{\left(a+s+\frac{1}{r}\right)}.\frac{d(I+J)}{dr}\right)=a.(I+J-2.E)+\frac{s}{3}[2.(I+J)-(K+L)-(M+N)] \qquad \text{Eq.2.74}$$

In the positive and negative axial directions:

$$\frac{d}{dz}\left(\frac{1}{(a+s)}.\frac{d(K+L)}{dz}\right)=a.(K+L-2.E)+\frac{s}{3}[2.(K+L)-(I+J)-(M+N)] \qquad \text{Eq.2.75}$$

In the positive and negative angular directions:

$$\frac{1}{r}.\frac{d}{d\theta}\left(\frac{1}{(a+s).r}.\frac{d(M+N)}{d\theta}\right)=a.(M+N-2.E)+\frac{s}{3}[2.(M+N)-(I+J)-(K+L)] \qquad \text{Eq2.76}$$

Finally, the radiation is transferred by scattering between the three fluxes given above. The Eqs.2.74-2.76 can now be solved numerically in a simple way, as they are linear except for the terms with the emitted radiation intensity **E**.

It may be shown that the model equations for the flux methods can be manipulated to the form of the following anisotropic conduction equation [58], [59]:

$$0=\frac{\partial}{\partial x_i}\left(\Gamma_{\varphi}.\frac{\partial \varphi}{\partial x_i}\right)+S_{\varphi} \qquad \text{Eq.2.77}$$

Where φ can be (I+J), (K+L) and (M+N) as the radiation intensities according to the direction; Γ_{φ} is the exchange coefficient in the form 1/(a+s) etc and S_{φ} is the source term according to the direction of flux. Equation 2.77 compares well with Eq.2.22 (the general conservation equation) when the unsteady and convective terms are equal to zero like in this case of radiative heat transfer. This type of equation is the most compatible with the other transport equations for the solution scheme discussed in Chapter Three.

3.0 METHOD OF SOLUTION

3.1 Introduction

The first step, in the development of a numerical procedure for solving the governing differential equations, is to superimpose a grid distribution on the flow domain. This is done to discretise the differential equations on all the grid points of the flow field, and to obtain equivalent algebraic expressions called the *Finite Difference Equations* (FDE's). The accuracy of the set of FDE's, which approximate the *Partial Differential Equations* (PDE's), is totally dependent on the formulation of these difference equations and on the number of grid nodes which represent the flow field. To solve the governing equations numerically, there are three options to choose from. These are the finite difference method, the finite element method, and the Taylor series expansion method. The first and second methods were examined critically by Antonopoulos [1]. He showed that in most cases the two methods lead to the same resultant equations. However, the third method is less general than either the finite difference or the finite element method. This is because, apart from offering less physical insight in the derivation of the FDE's, the reciprocity requirement for the fluxes, at locations midway between grid nodes, usually leads to the central difference formulation. This formulation is an inaccurate representation of the fluxes at high Peclet numbers; this method, therefore, was discarded. Of the two other alternatives, the finite element was discarded because of the difficulty in prescribing the boundary conditions. Hence, in this study, the finite difference method is used in its special form of the *Finite Volume Method* (FVM). This is due to the fact that FVM is the most advanced in terms of fluid mechanics applications today.

Numerical schemes are designated as *explicit* or *implicit*. This terminology is appropriate to parabolic and hyperbolic equations, which posses an irreversible time or time-like co-ordinate, and in which the solution can be obtained by forward matching [2]. The steady laminar boundary layer equations form a parabolic system, with the streamwise direction as the matching co-ordinate [3]. Elliptic-type problems, such as those encountered in this study, are solved as steady state solutions of transient or pseudo-transient systems. As such it is then possible to use the parabolic or hyperbolic algorithms to solve the transient systems. Consequently, the terminology of explicit and implicit is meaningful when applied to this iterative (relaxation) approach to solving elliptic-type problems.

3.2 Summary of the Solution Scheme

3.2.1 Numerical Procedure for the Three-Dimensional Flow

All the differential equations for the model are of one of the two following forms:

$$\frac{\partial}{\partial t}(\rho \varphi) + \frac{\partial}{\partial x_i}(\rho u_i \varphi) = \frac{\partial}{\partial x_i}\left(\Gamma_\varphi \frac{\partial \varphi}{\partial x_i}\right) + S_\varphi \qquad \text{Eq.3.1}$$

$$0 = \frac{\partial}{\partial x_i}\left(\Gamma_\varphi \frac{\partial \varphi}{\partial x_i}\right) + S_\varphi \qquad \text{Eq.3.2}$$

Equation 3.2 is for the radiation transfer and is simpler than Eq.3.1 in that the unsteady and the convective terms are absent. Solution of the convective transport equation poses a number of computational problems, due to the numerical algorithm and computer capacity requirements. Successful numerical schemes for solving the convective transport equation have only become available recently [4, 5, 6]. Many algorithms are available to solve for the primitive variables of the flow field. Therefore, for a particular problem, a suitable choice of an algorithm has to be made.

Grid Arrangement

For the three-dimensional flow, the arrangement of a staggered grid is employed. The numerical grid consists of a set of orthogonal intersecting lines in the co-ordinate directions, with no restriction on the distribution of the grid lines in the solution domain. The intersection of these lines forms the grid nodes at which all the flow properties, except the velocities U, V, and W, are stored. The swirl velocity, U, is located midway between grid nodes in the angular direction. The radial velocity, V, is located midway between grid nodes in the radial direction, while the axial velocity, W, is located midway between the grid nodes in the axial direction. Figure 3.1 below shows the grid arrangement in the y-z plane.

The grid distribution was adaptively adjusted according to each case being simulated, i.e. furnace only, furnace with PCC and furnace with optimised PCC. The grid distribution was such that in the regions of large gradients, the grid points had high density. Large gradient regions correspond to the flame sheet region. Flame sheet regions are normally found around inlet ports and near the wall boundaries.

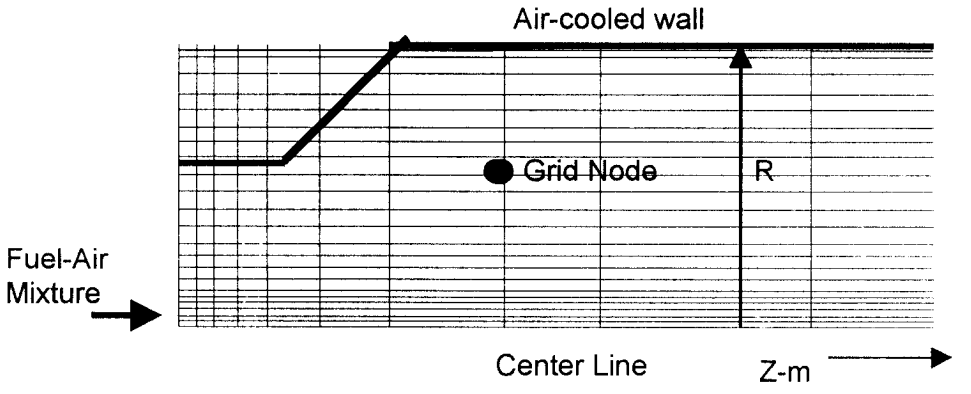

Figure 3.1 Numerical Grid Arrangement in the Axisymmetric Furnace.

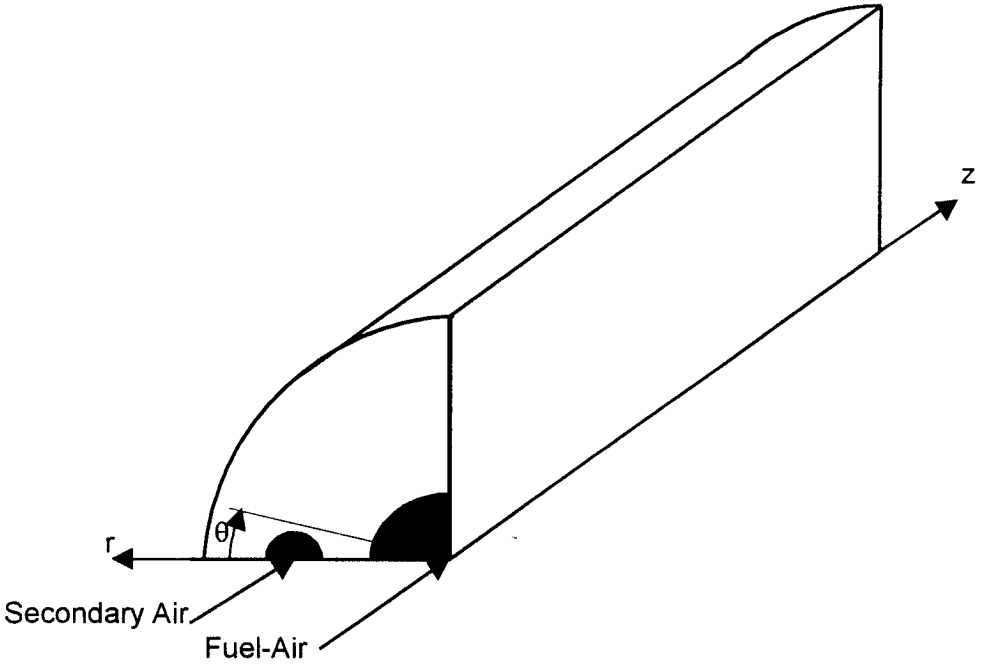

Figure 3.2 Integration Domain

Finite Difference Equations

The PDE's, dealt with in chapter two, can be represented by the general form:

$$\frac{\partial}{\partial z}\bar{\rho}\,\overline{W}\,\overline{\varphi}+\frac{1}{r}\frac{\partial}{\partial r}\bar{\rho}\,r\overline{V}\,\overline{\varphi}=\frac{\partial}{\partial z}\Gamma_{\varphi}\frac{\partial\bar{\varphi}}{\partial z}+\frac{1}{r}\frac{\partial}{\partial r}r\Gamma_{\varphi}\frac{\partial\bar{\varphi}}{\partial r}+\bar{S}_{\varphi} \qquad \text{Eq.3.3}$$

The finite difference counterpart of the general partial differential Eq.3.3 is derived by assuming that each variable is enclosed in its own control volume of cell as shown in Fig.3.3.

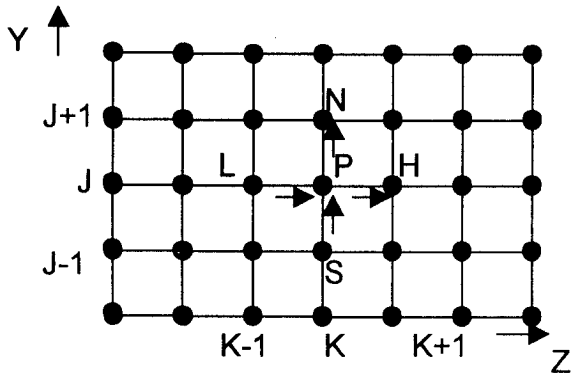

Figure 3.3 Three-Dimensional Finite Difference Grid (Y-Z) Plane)

The grid node P is surrounded by two neighbouring nodes L and H in the low and high z-directions respectively and two nodes N and S in the north and south y-directions respectively. Three indices are used for the notation of the grid surfaces and grid-node locations as shown in Fig.3.3 above. The index I pertains to the θ = constant surfaces, J to the r = constant surfaces, and K to the z = constant surfaces. The location of any grid node is therefore specified by the values of I, J, and K. The PDE is integrated over the control volume, with the aid of assumptions that relate the nodal value of Φ to the rates of generation-destruction of this entity within the cell, and to its transport by convection and diffusion across the cell boundaries. The former relation is represented, in a linearised form, as

$$S_\Phi = \int_v S_\Phi \, dv = S_W + S_P \, \Phi_P \qquad \text{Eq.3.4}$$

The resultant FDE for any dependent variable Φ, is derived at any grid node P by integrating the pertinent differential Eq.3.3 over a control volume surrounding P. The resulting equation is in the form:

$$a_P = (a_{\Phi,z+} . \Phi_{z+} + a_{\Phi,z-} . \Phi_{z-} + a_{\Phi,r+} . \Phi_{r+} + a_{\Phi,r-} . \Phi_{r-} + a_{\Phi,\theta+} . \Phi_{\theta+} + a_{\Phi,\theta-} . \Phi_{\theta-} + S_{\Phi,P}) / a_{\Phi,P} \qquad \text{Eq.3.5}$$

Where

$$a_{\Phi,P} \equiv a_{\Phi,z+} + a_{\Phi,z-} + a_{\Phi,r+} + a_{\Phi,r-} + a_{\Phi,\theta+} + a_{\Phi,\theta-} \qquad \text{Eq.3.6}$$

Variable Φ_P is the value of Φ at the grid node 'P', the **a**'s are the finite difference coefficients evaluated at the control surfaces, and the subscripts (z+, z-, ...,θ-) to the Φ's refer to the locations of the immediate neighbouring grid nodes relative to the considered node P; whereas the same subscript to **a**'s refer to the locations of the coefficient evaluation point with respect to P, as displayed in Fig 3.4. In Fig 3.4(a) and (b) the convention for neighbouring nodes in cylindrical-polar and cartesian co-ordinates are shown for a general variable. Figure 3.4(c)-(e) shows the neighbouring nodes for the axial, radial and swirl velocities respectively. The coefficient **'a'** express the contributions of the convection and diffusion crossing the control surfaces.[7]. Equations 3.4 and 3.5 are formulated for each of the variables U, V, W, and Φ. An equation for the remaining unknown, which is pressure, is obtained by combining the continuity and momentum equations in the manner explained by Caretto *et al.* [8] and Patankar *et al.* [9]. This entails connecting changes in pressure, denoted by P', with the velocities U, V, and W by approximate formulae, which are derived from the momentum FDE's as described below.

Pressure Correction and Velocity Correction

The presence of the pressure gradient as a source term in the momentum equations requires the evaluation of the local pressures. The continuity equation coupled with the momentum equations yields the pressure correction equation.

The incorporation of the p' equation in the solution procedure proceeds in the following sequence:

1. Initially the momentum equations are solved with an assumed pressure field, thus yielding the first estimate of the velocity fields u*, v*, and w*. These in general will not satisfy the continuity equation, because the initially assumed pressure field is incorrect.
2. In the next step, simultaneous corrections are made to both the velocity and pressure fields, such that the newly corrected velocity components u, v, and w, satisfy mass conservation and are connected to the pressure corrections through the following linearised expressions of the momentum equations:

$$w_P = w_P^* + \frac{A_{z,p}}{a_{w,P}}\left(p'_{z-} - p'_P\right) \qquad \text{Eq.3.7(a)}$$

$$v_P = v_P^* + \frac{A_{r,P}}{a_{v,P,P}}\left(p'_{r-} - p'_P\right) \qquad \text{Eq.3.7(b)}$$

$$u_P = u_P^* + \frac{A_{\theta,P}}{a_{u,P}}\left(p'_{\theta} - p'_P\right) \qquad \text{Eq.3.7(c)}$$

Where p' is the local pressure correction and the subscripts denote the position of the pressure grid nodes relative to the pertinent velocity component, according to the notation displayed in Fig.3.4. $A_{z,p}$, $A_{r,P}$ and $A_{\theta,P}$ are the main-grid-node control surface areas perpendicular to w_P, v_P, and u_P respectively. Whereas $a_{w,P}$, $a_{v,P}$, and $a_{u,P}$ are the coefficients given by Eq.3.5 for w, v, and u respectively. The PDE for pressure correction is obtained in the form

$$a_P p' = a_{\Phi,z+}.p'_{z+} + a_{\Phi,z-}.p'_{z-} + a_{\Phi,r+}.p'_{r+} + a_{\Phi,r-}.p'_{,r-} + a_{\Phi,\theta+}.p'_{\theta+} + a_{\Phi,\theta-}.p'_{\theta-} + S_{U,P}) \qquad \text{Eq.3.8}$$

$S_{U,P}$ is the mass imbalance resulting from the initial starred velocity field and is expressed as

$$S_{U,P} = (\rho w^*_{z-} a_{\Phi,z-}) - (\rho w^*_{z+} a_{\Phi z+}) + (\rho v^*_{r-} a_{\Phi,r-}) - (\rho v^*_{r+} a_{\Phi r+}) + (\rho u^*_{\theta-} a_{\Phi,\theta-}) - (\rho u^*_{\theta+} a_{\Phi\theta+}) \qquad \text{Eq.3.9}$$

The values of p' are calculated from the solution of FDE's for p', which have the same form as Eq.3.5. The FDE for p' at any given main grid P, is derived by substituting the right hand side of Eq.3.7(a)-(c) for the velocity components appearing in the expression for the conservation of mass over the control volume surrounding P. Consequently, the values of u_p, v_p, and w_p derived from Eq.3.7(a)-(c), for the calculated values of p', satisfy mass conservation over each of the main grid node control volumes. The effect of the pressure, temperature and concentration on the density need not be included in the pressure correction equation as they are accounted for by the thermodynamic functions. Therefore omission of these effects does not affect the correctness of the final solution as the pressure correction equation is only used to obtain the final pressure distribution.

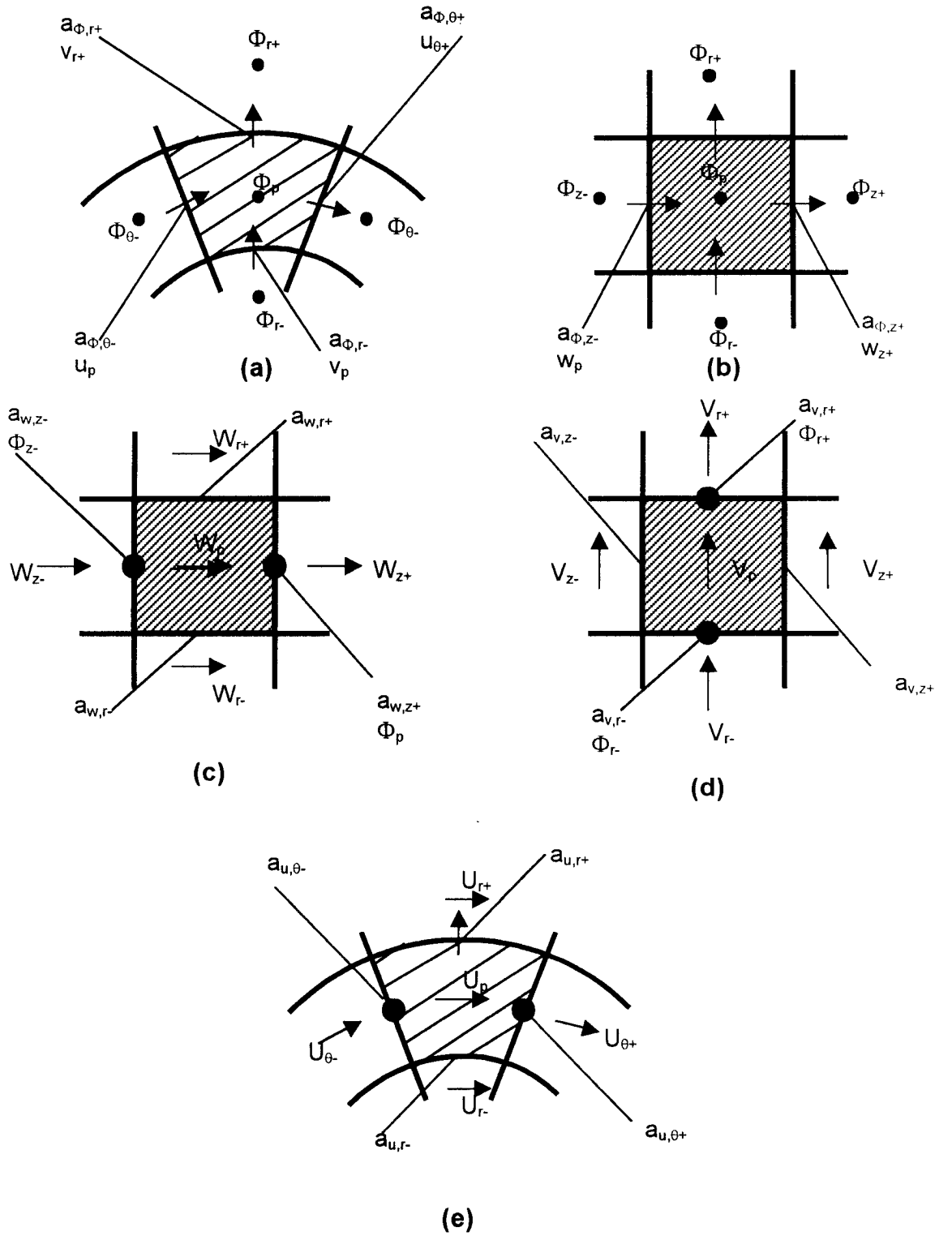

Figure 3.4 Convention for Neighbouring Nodes and Coefficients

Solution Algorithm

The FDE's have the problems of non-linearities and pressure-velocity coupling. Their solution is only obtained by using the iterative finite difference strategy of the SIMPLE algorithm proposed by Caretto *et al.* [8] and Patankar *et al.* [9]. SIMPLE is an acronym for Semi-Implicit Method for Pressure-Linked Equations. The algorithm is frequently applied to recirculating and reacting flows. It involves a series of guess and correct operations for the coupling of the pressure with velocities. However, the SIMPLE algorithm requires more memory space and the pressure correction method used gives poor adaptation for the pressure field. Therefore, another family of the SIMPLE algorithm, SIMPLEST, is used to overcome these shortcomings in order to obtain an optimal solution. SIMPLEST is an acronym for SIMPLE-Shortened. This scheme is described in detail in [10].

For the SIMPLEST algorithm used in this study, two iteration sequences are employed: an inner sequence and an outer one. The outer iteration sequence involves the cyclic application of the following steps:

1. A field of intermediate swirl, radial, and axial velocities denoted by ur*, v*, and w* is obtained by solving the associated momentum equations using the prevailing pressure field p*. The Jacobi point by point iteration method is used to solve for these velocities. The Gauss-Seidal method can also be used, but it is not used inside the computer code used to avoid resulting asymmetry.
2. Continuity is then enforced, by solving the pressure correction equation for p' by using the SNIP algorithm (Start with New Integration for Pressure) [11]. This determines the required adjustments to the velocities and pressures.
3. The sets of FDE's for the remaining variables are then solved successively. The sequence of solution among these variables is chosen according to their relative influence on each other. The auxiliary variables like density, turbulent viscosity, and difussivity are calculated from the dependent variables.

At the end of each iteration, a check is made on the degree of convergence of the solution, and if this is not satisfactory, a new iteration is initiated and the procedure is repeated until a satisfactory solution is obtained. This means that the residual (imbalance) in any of the FDE's is less than 10^{-4} of a specified inlet value of the entity in question.

In the SIMPLEST algorithm, the coefficients of the momentum equations ($a_{\Phi,z+}$, $a_{\Phi,z-}$, $a_{\Phi,r+}$, $a_{\Phi,r-}$, $a_{\Phi,\theta+}$, and $a_{\Phi,\theta-}$) contain only diffusion contributions. The convective terms are added as supplement to the source term ($S_{\Phi,P}$)

The inner iteration sequences is employed to solve the equation sets of the individual variables. From Eq.3.4, for any variable, the FDE at a given grid node P links the value of the variable at P to its values at the neighbouring grid nodes, z+, z-,r+,.....,thus the set of FDE's at the different grid nodes constitutes a system of simultaneous algebraic equations. Their solution is obtained by performing successive line iterations in the three co-ordinate directions. In the procedure, the FDE's at all the grid nodes along a given grid line are solved simultaneously for the values along that line, whilst the neighbouring values along the other grid lines are fixed at their previous iteration values.

Along the grid lines in the z- and r-directions, the set of FDE's yields a tridiagonal matrix of coefficients whose solution is obtained rapidly by means of the Tri-Diagonal Matrix Algorithm, (TDMA), in the line by line counterpart of the point Gauss-Seidal iteration. Solution is by a form of block iteration and correction, in which a simple recurrence formula, described in Ref. [11] is used to solve simultaneously for the variables along each grid line,

In this problem, there are no cyclic θ-boundary conditions. Hence, the TDMA is employed by fixing the θ-boundary values. The procedure is as follows. First attention is given to one Z-Y plane, the coefficients are calculated, and the equations are solved by double sweep: then one proceeds to the next Z-Y plane. Due to the iterative nature of the solution procedure, the θ-boundary values may be fixed from the previous iteration solution and updated at each iteration. This leads to very poor accounting of the interactions in the θ-direction. Investigations with this practise [12] revealed that the solution converged very slowly than when the θ-boundary values are introduced implicitly by way of the algorithm.

Complete convergence of the inner sequence is not necessary, and usually one to three applications of the block procedure suffices. All the quantities are relaxed for numerical stability as soon as they are calculated. At the end of each solution, the source term constants are reset to zero for future use to calculate the next variable.

3.2.2. The Computer Code Used

The SIMPLEST algorithm used in this study is embodied in the PHOENICS code. PHOENICS is an acronym for Parabolic Hyperbolic Or Elliptic Numerical Integration Code Series. The PHOENICS computer code was developed by Spalding, D. B. and Rosten, H. I. It is software version 1.4, Document Revision 04 code. Table 3.1 summarises the most important features of PHOENICS. Figure 3.5 shows the block diagram of PHOENICS highlighting its structure.

Table 3.1 Summary of Important Features of PHOENICS.

Basic Features	Three-dimension Steady and Unsteady Parabolic, Hyperbolic and Elliptic Solver.
Co-ordinate System	x-y-z Cartesian r-θ Cylindrical-polar z-r Cylindrical BFC (Body Fitted Co-ordinates)
Differencing Scheme	"Fully-Implicit upwind" by default (but user selection of other schemes is available)
Linear Equation Solver	SIMPLEST Alternating direction TDMA with block correction.
Grid	Uniform Non-uniform

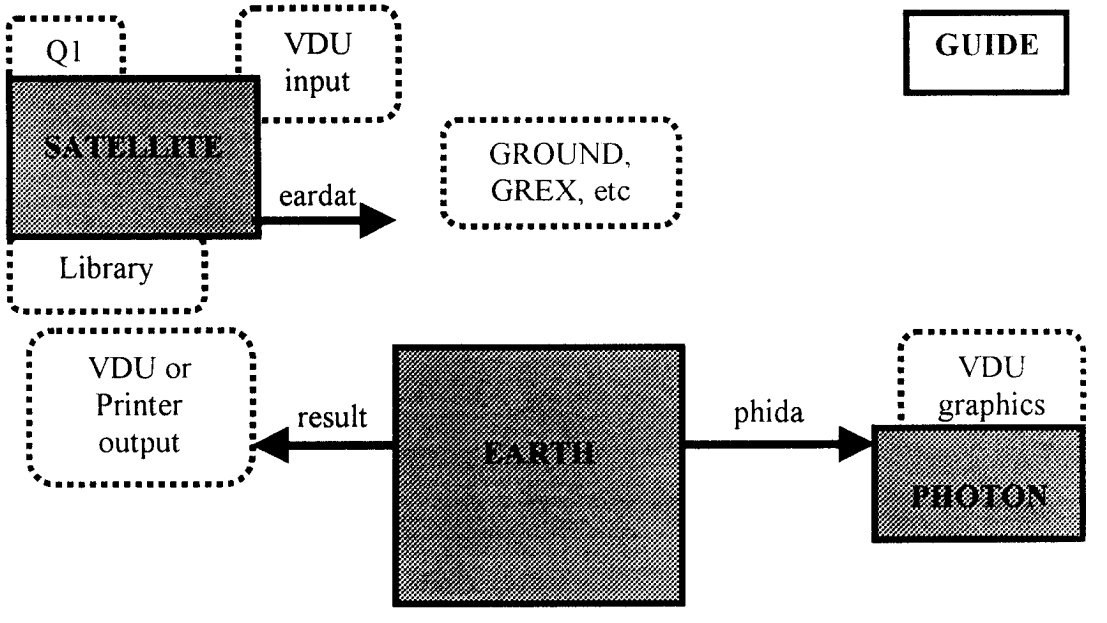

Figure 3.5 Structure of PHOENICS

PHOENICS has a 'planetary' arrangement, with a central core of subroutines called EARTH, and a satellite program, accepting inputs, which correspond to a particular flow simulation. EARTH and the satellite are distinct programs. The satellite is a data-preparation program; it writes a data file which EARTH reads. PHOENICS users work mainly with the satellite, but they can access EARTH also in controlled ways.

GROUND is the EARTH subroutine which users access when incorporating special features of their own. The satellite reads a pre-existing "quick-input file", which may be drawn from a library containing hundreds of examples. The user can then modify the data interactively via the VDU keyboard. A Fortran sub-routine, SATLIT, also accepts user's inputs if these are supplied. A MAIN program is accessible for rarely needed operations, e.g. re-dimensioning. GROUND is a subroutine which is called by EARTH at pre-set points of the solution cycle. If the user inserts appropriate FORTRAN statements at the entry points in GROUND, EARTH absorbs these into the solution process.

Special communication subroutines allow the user to extract information from EARTH, manipulate it in GROUND and then return new information or instructions to EARTH. Many "service" sub-routines are attached, performing commonly needed arithmetic operations. These greatly reduce the user's need to write Fortran-coding sequences. EARTH starts with a MAIN program, open to users for re-dimensioning operations. The other user-accessible source subroutines are GROUND, GREX1 and GREX2 (GROUND examples 1 and 2) and others of the same kind. EARTH contains sequences for:

(i) Storage allocation.
(ii) Formulation of finite-volume equations.
(iii) Iterative solution of finite-volume equations.
(iv) Calling GROUND when required.
(v) Termination of iteration sequences.
(vi) Output of results.

The program EARTH of PHOENICS controls and executes the solution procedure as follows:

1. Obtain information about co-ordinate system, domain lengths and variable definitions to solve and establish number of algebraic equations per dependent variable.
2. The coefficients and sources are regarded as temporarily constant so that the linear-equation solver can be used to solve the equation sets.

3. On the next cycle, the coefficients and sources are updated from the latest values of the auxiliary and independent variables, and the linear equations re-assembled and solved.
4. Many sweeps are made in succession, and the process should be continued, ideally, until all equations are in such perfect balance that further adjustments are unnecessary.
5. Output necessary data, iterative or final.

PHOTON is a service routine which allows the picking up of PHIDA file written by EARTH and then, in response to instructions entered by user through VDU keyboard, represents the computed grid and flow pattern graphically on the screen. In EARTH, the coefficients of the discretised equations are calculated and the finite difference equations are solved iteratively employing the SIMPLEST method of Patankar and Spalding [2].

3.3 Miscellaneous Details

The numerical solution is required to pass two acceptance tests. Firstly it must satisfy the FDE 's (typically, the imbalance must be 0.01% or less), and secondly, it must be invariant with further increase in the number of grid nodes.

Convergence and Stability

The simultaneous and non-linear nature of the FDE's necessitates the use of under-relaxation factors relating the old and new values of the general dependent variable Φ. This matter is dealt with in Appendix E.

Grid Independent Results

It is important to test the grid dependence of the solution, in order to economise on computer time by using the minimum number of nodes which can give a grid independent solution. In this study, a series of tests were performed for each flow configuration to determine the influence of the number and distribution of grid nodes. A coarse grid was used initially giving physically plausible results revealing the main features of the flow. The grid was refined gradually until there was no significant change in the results. In this study, for sudden axisymmetric enlargement flow at d/D = 0.375, grid size distribution tested were (10 x 10 x 15), (10 x 15 x 20), (10 x 15 x 25), (15 x 20 x 25) and (30 x 30 x 30). The distributions obtained with (10 x 15 x 25), (15 x 20 x 25) and (30 x 30 x 30) nodes were, for all intents and purposes the same, and the local flow properties were found to be grid independent.

The domain of 10 x 15 x 25 non-uniform control volumes was used. This is a reasonable compromise between numerical accuracy and computing time. Currently, three-dimensional calculations for furnaces commonly do not exceed 30 x 30 x 30 finite difference nodes [13]. The grid size, however, is not fine enough to accurately calculate the large changes of the turbulent quantities and the diffusion coefficients in the boundary layer region near the wall. To overcome this difficulty, the wall functions embodied in the code used are applied. They are input in the SATELLITE program.

Numerical Accuracy

Three different schemes are used to represent the convective and diffusive flux expressions in the FDE. These are the central, upwind and hybrid difference formulae. The central difference expressions give unrealistic results for |Pel > 2. In the upwind scheme, the diffusive flux is present irrespective of the cell Peclet number. Therefore at large |Pel the upwind difference is preferable as reported by Gosman *et al.* [14]. The computer code used, PHOENICS, employs by user's choice, a combination of the two expressions, namely the hybrid formula. The hybrid formula cuts out the combined diffusive fluxes for Pe > 2, therefore it is used in the calculation of furnace flows. False diffusion gives numerical errors with the finite difference representation of the conservation equations. False diffusion occurs when the flow is oblique to the grid lines and when there is nonzero gradients of the dependent variable in the direction normal to the flow. False diffusion effects diminish at high Reynolds number i.e. in turbulent flows, due to the large value of the effective viscosity, μ_{eff}.

Thermodynamic Properties

The thermodynamical properties of gas need not be modelled as already explained in the combustion modelling of SCRS assumptions. The specific heats of the fuel, oxidant and products species in the combustion space are temperature independent and hence constant The gas constant in the ideal gas law does not change since the combustion of methane causes no change in the total number of moles.

For the purpose of this study, the density of the mixtures of air, the combusting gases and the combustion products are represented with adequate precision by the equation of state for perfect gases already dealt with in Section 2.2.5, (ρ =P/(RT/MW). Here, MW and P are determined from the appropriate mass fractions and Dalton's Law of partial pressures.

The molecular weight MW is obtained from $MW = MW_i/\sum M_i$. M_i is the mass fraction of component I gas. The heat of reaction of the fuel is represented by $H_{fu} = \sum M_i H_i$, with the values of H_i, determined from JANAF Chemical Tables [15]. The specific heat capacity the mixture was obtained from the equation

$$C_p = \sum M_i Cp_i \qquad \text{Eq.3.10}$$

Where

$$C_{pi} = a_0 + a_1 z + a_2 z^2 + a_3 z^3 \qquad \text{Eq.3.11}$$

With $z = (T - 1400)/200$ and T being the temperature of the gas in Kelvin (K) and values of the coefficients computed for each gas. The use of third or higher order polynomials is found to be significantly more satisfactory. [16]. Ref. [17] gives values for the coefficients.

3.4 Formulations and Boundary Conditions for a Three-dimensional Furnace

The selection of acceptable boundary conditions for aerodynamic flow problems is a major topic in itself [18]. Very few studies on combusting flows, like those by Gosman *et al.* [19] and by Khalil [20], emphasise the importance of boundary conditions and associated problems. To economise on the grid nodes, conditions adjacent to solid wall are matched to some assumed boundary layer profiles of velocity, temperature and species. This practice is known as employing wall functions [21]. In addition to the wall functions, boundary layer pressure approximation of zero pressure gradient normal to the wall is often invoked. As in most of the combusting flows, regions of interest are far from the wall, considerable lassitude in the wall boundary conditions is often tolerated. Wall regions are represented by first ensuring that the near wall region is adequately resolved by the computational mesh. The following assumptions are realistically made:

1. No slip at wall.
2. Zero turbulent fluctuations.
3. Specified wall temperature or an adiabatic wall.
4. Zero normal gradient of species mass fraction.
5. The normal pressure gradient is computed from the momentum equation applied to the wall.

The inlet boundary conditions are generally not well defined, and unfortunately the predicted solution can exhibit a considerable sensitivity to poorly defined, but computationally required inlet information [16, 22, 20]. The sensitivity of the predictions to the streamline direction entering the computational domain is not known very precisely at the exit plane of the furnace or combustor. The inlet conditions have the problems of shape of the inlet profiles and magnitude of the variable at inlet. The influence of various inlet profiles investigated showed significant effect on the mean flow pattern [20]. However, in this study, the inlet conditions were taken from real furnace values. Measurements of inlet velocity and turbulence intensity profiles in combustor flows are scarce, but some detailed measurements were recently reported and were obtained with the aid of a Laser Doppler Anemometer. [23, 24, 25, 26].

Exit boundary conditions have not been proved to be troublesome in practical applications. Linear extrapolation from the internal nodes is employed by specifying that the axial gradient is zero, that $\partial\Phi/\partial z$ equals zero, and that the overall conservation of mass and species is satisfied. The location of the exit plane was taken far down stream so as not to influence the upstream properties. Along the axis of symmetry the gradients in the radial direction of all variables are equal to zero.

The mathematical formulations developed in chapter two are generally applicable to gas-fired industrial furnaces. This study considers a three-dimensional cylindrical rotary furnace as a model problem to be investigated. Figure 3.6. (a) and (b) illustrates the model furnace for no post combustor chamber situation and one with a post combustor chamber incorporated in the exhaust system of the furnace. The furnace is composed of refractory, inlet of premixed fresh mixture and outlet of waste gas. A premixed fresh mixture of air and natural gas enters the combustion chamber and is burned. Since natural gas is mostly composed of 95 percent methane, the fuel is safely regarded as methane in this study. Heat is transferred to the refractory surface by radiation and convection. The inlet is composed of three ports, the centre port for the premixed fuel-primary air and the two side ports for the secondary air. The primary air is for igniting the mixture while secondary air sustains the combustion in the chamber. The refractory on the outside is exposed to ambient air and the net heat loss coefficient from the inside of the refractory to the ambient is prescribed as α_{out}. All the variables are solved in dimensional form since there are many system parameters for the problem at hand. Even when non-dimensionalised, the number of dimensionless parameters

is so large that one is not likely to find many different furnaces operating with the same set of dimensionless parameters. Therefore, the solution for a specific problem on one furnace is rarely applicable to another furnace by matching the dimensionless parameters. This fact makes it not sufficiently worthwhile to non-dimensionalise the model equations. The most important mathematical models that are used in this study are summarised as follows:

(i) k-ε turbulence model.

(ii) SCRS combustion model.

(iii) Eddy-Break-Up combustion rate model.

(iv) Six-flux radiation transfer model.

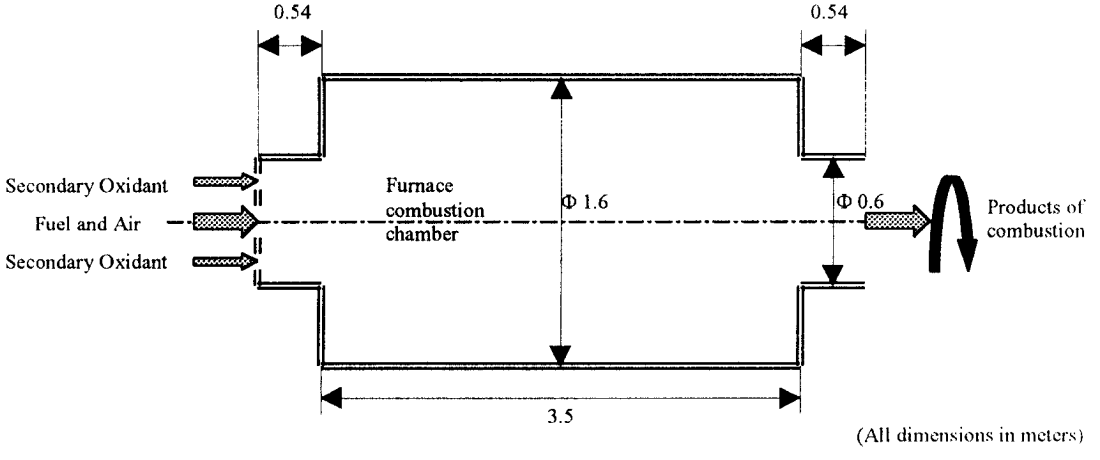

(a)

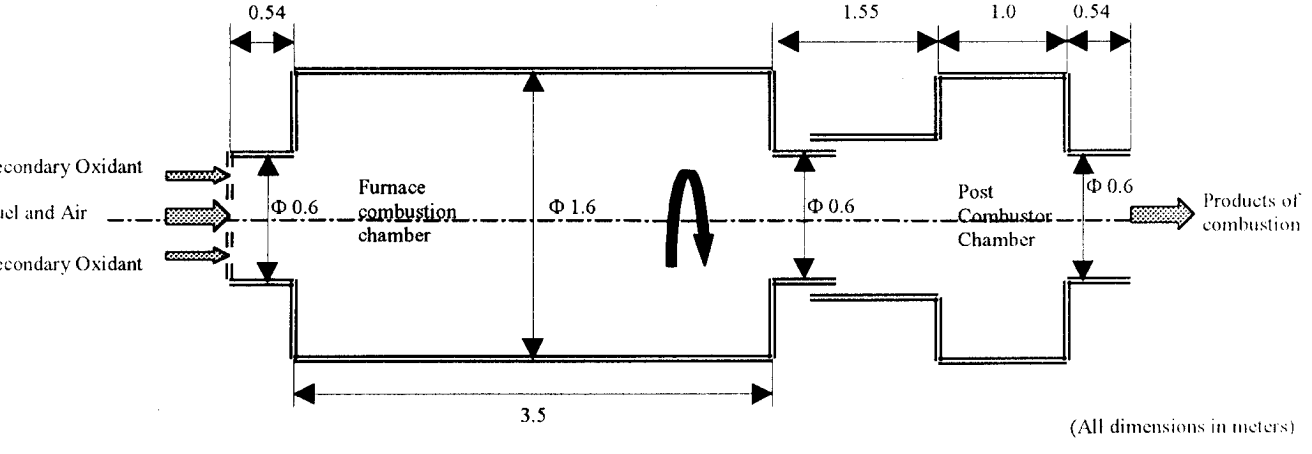

(b)

Figure 3.6 Schematic of the Rotary Furnace (a) Without PCC and (b) with PCC.

Table 3.2 List of Variables for the Model Analysis

Symbol	Type [1]	Eqn.[2]	Γ_Φ [3]	S_Φ or Algebraic Expression
U	FM	T	μ_{eff}	Equation 2.45 (a)
V	FM	T	μ_{eff}	Equation 2.45 (b)
W	FM	T	μ_{eff}	Equation 2.45 (c)
T	FM	A	-	From h= (T, m_l)
K	FM	T	μ_{eff}/σ_k [3]	2 μ_t $E_{ij}.E_{ij}$ - $\rho\varepsilon$
ε	FM	T	$\mu_{eff}/\sigma_\varepsilon$ [3]	C_1 ε/k 2 μ_t $E_{ij}.E_{ij}$ - $C_2\rho\varepsilon^2/k$ [3]
H	FM	T	μ_{eff}/σ_h [3]	Equation 2.46
F	FM	T	μ_{eff}/σ_f [3]	-
(I+J)	TM	AC	r/(a+s+1/r) [4]	a.(I+J-2.E) + s/3[(2.(I+J)) - (K+L) - (M+N)]
(K+L)	TM	AC	1/(a+s) [5]	a.(K+L-2.E) + s/3[(2.(K+L)) - (I+J) - (M+N)]
(M+N)	TM	AC	1/(a+s).r [6]	a.(M+N-2.E) + s/3[(2.(M+N)) - (I+J) - (K+L)]
m_{fu}	FM	T	μ_{eff}/σ_{fu} [3]	Equation 2.46
m_{ox}	FM	A	μ_{eff}/σ_{ox} [3]	Equation 2.46

Footnotes:

(1) FM: Favre mean quantity (Eq.2.39).
TM: Time mean quantity (Eq.2.45).

(2) T: Convective transport equation (Eq.2.22). A algebraic expression.
AC: Anisotropic conduction form (Eq.2.77).

(3) C_μ=0.09; σ_ε=1.3; σ_k=1.0; $\sigma_{fu}=\sigma_{ox}=\sigma_f=\sigma_h$ 0.9; C_1=1.44; C_2=1.92

(4) For the negative and positive radial directions.

(5) For the negative and positive axial directions.

(6) For the negative and positive angular directions.

Table 3.3 Boundary Conditions

Symbol	Inlet	Outlet	Sink	Refractory
U	0.0	0.0	Not considered	No slip
V	0.0	0.0	Not considered	No slip
W	WINF	Mass conservation	Not considered	No slip
T_1	Tin	Adiabatic	Not considered	Adiabatic
K	0.005 $WINF^2$	Adiabatic	Not considered	0. 0
ε	$C_\mu k^{3/2}/0.005y_a$ (1)	Adiabatic	Not considered	0.0
H	Adiabatic	Adiabatic	Not considered	Adiabatic
m_{fu}	M_{fu}	Adiabatic	Not considered	Adiabatic
R_{ij} (2)	Adiabatic	Adiabatic	Not considered	Adiabatic

Footnotes:

(1) y_a is the characteristic length, i.e. jet radius of burner.

(2) R_{ij} is the energy flux sum in any of the three directions i.e. θ, r or z.

The numerical scheme discussed in the previous sections is used to solve the model problem described in Section 4.1. Some of the quantities are expressed in steady transport, Eq.2.22, and anisotropic heat conduction equations, Eq.2.77, and still some others are algebraic in form. Table 3.2 lists the unknown variables to be determined. The mass conservation equation is not shown. The equations together with the diffusion coefficient Γ_Φ are summarised in Table 3.2. The sources S_Φ for the PDE's and the algebraic expressions are also listed. Table 3.3 lists the boundary conditions for the variables governed by differential equations.

The values of k and ε at the inlet depend on the port configuration. The values of k and ε are taken from Ref. [27] and are a generally acceptable turbulence level. The turbulence is low at inlet, while most of the turbulence in the flow is generated inside the furnace. Thus, the absolute value of k and ε at the inlet is not very critical for low turbulence inlet condition. Finally, it is necessary to express the convective and radiative heat fluxes at the wall. The convective heat flux q_{conv} from the gas to the wall is given by:

$$q_{conv} = \left(C_p \Gamma_h \frac{\partial T}{\partial x_n} \right)_w \qquad \text{Eq.3.12}$$

Since the walls are impermeable to the species diffusion, Eq.3.12 can be rewritten as:

$$q_{conv} = \left(\Gamma_H \frac{\partial h}{\partial x_n} \right)_w \qquad \text{Eq.3.13}$$

The radiative heat flux q_{rad} from the gas to the wall in the radial direction is obtained from the axial symmetrical six-flux radial-directed second order differential equation:

$$\frac{1}{r}\frac{d}{dr}\left(\frac{r}{\left(a+s+\frac{1}{r}\right)} \cdot \frac{d(I+J)}{dr} \right) = a.(I+J-2.E) + \frac{S}{3}[2.(I+J)-(K+L)-(M+N)] \qquad \text{Eq.3.14}$$

3.5 Simultaneous Predictions of Flow Patterns and Radiation for Three-Dimensional Flames

From Chapter Two and the preceding sections, a procedure for the simultaneous prediction of the convective, diffusive and radiative transfer equations in three-dimension is summarised below in block form:

The Problem

Given: Geometry of combustor and Post Combustion Chamber.
(i) Fuel and air input conditions.
(ii) Thermal boundary conditions.
(iii) Thermal, transport, radiation and chemical kinetics properties.
Calculate: velocity, temperature, composition etc through out chamber with and without Post Combustion Chamber.

Figure 3.7 The Problem: Statement

Interconnections Between Phenomenon

Variable	Depends on	Which depends on
q, T_{wall},	λ_{eff} emissivity T	μ_{eff}, σ_{eff} T, composition λ_{eff}, emissivity, u, v, w
u, v, w k, ε Composition	μ_{eff} u, v, w, μ_{eff}	k, ε see above see above reaction rate
Reaction rate	T, composition	See above

Figure 3.8 The Problem: Why Simultaneous Prediction is needed.

The Problem of Calculating Turbulent Flow

Turbulence
(i) Scale disparities entail use of turbulence model (TM).
(ii) TM selected to give optimum balance of universality and simplicity.
(iii) Fluctuation of concentration and temperature must be computed, not just time average values.
(iv) Influence of turbulence on reaction rate must be accounted for.

Figure 3.9 The Problem: Physical Aspects, 1.

The Problem of Calculating the Rate of Chemical Reaction

Chemical Kinetics
(i) Fuel-air combustion proceeds by many intermediate steps.
(ii) For separate fuel, air injection, main flame features can be predicted without knowledge of these steps.
(iii) Chemical-kinetic knowledge is needed for prediction of carbon-content distribution.

Figure 3.10 The Problem: Physical Aspects, 2.

The Problem of Calculating Radiative Heat Transfer

Radiation

(i) Properties (emission, and scattering coefficient) depend on composition, temperature, wavelength and angle.
(ii) Properties are not yet fully documented.
(iii) Most important composition features is solid-carbon content, which is hard to predict.

Figure 3.11 The Problem: Physical Aspects, 3.

The Problem of Solving the Convection Equations

Flow Patterns

(i) Momentum and continuity equations are non-linear, simultaneous.
(ii) TM's introduce additional non-linear simultaneous differential equations.
(iii) In the flow, density varies depending on the temperature and concentration.
(iv) The non-uniform density links momentum, continuity with energy, concentration equations.
(v) The practical flame considered is three-dimensional.

Figure 3.12 The Problem: Mathematical Aspects, 1.

The Problem of Solving the Radiation Equation

Radiation

(i) Radiative flux is six-dimensional (3 position, 2 angle, 1 wavelength co-ordinate.
(ii) Classical equations are integro-differential.
(iii) Mathematical problem simplifies for very transparent media and very opaque media.
(iv) Neither of the last two simplifications often applies to practical flames.

Figure 3.13 The Problem: Mathematical Aspects, 2.

The Turbulence Model

k-ε model

(i) The k-ε (energy-dissipation-rate) TM is used.
(ii) The empirical constants and functions fit experimental data on two-dimensional flames.
(iii) Concentration fluctuations are taken as very small.
(iv) It would however be easy to calculate the fluctuation.

Figure 3.14 The Solution Procedure: 1, Turbulence.

Thermodynamic and Chemical-Kinetic Assumptions

(i)	For simplicity, specific heat has been supposed not to depend on composition or temperature.
(ii)	Reaction is presumed to be: Fuel + O_2 = products. Therefore, Simple Chemical Reacting Scheme combustion model is used.
(iii)	For the premixed flame, eddy-break-up model for rate of combustion is employed.
(iv)	Equilibrium prevails at all points (neither chemical kinetics nor turbulence delays reaction.

Figure 3.15 The Solution Procedure: 2, Chemistry

The Method adopted for Radiation Transfer

(i)	Six-flux model is employed (leading to three-second order ordinary differential equations).
(ii)	Gas emissivity is taken as uniform.
(iii)	No division into wavelength bands is made.
(iv)	Neither of the last two simplifications is essential.

Figure 3.16 The Solution Procedure: 3, Radiation.

The Method of Solving the Equations

(i)	For the thermal gas dynamics the SIMPLEST algorithm is used.
(ii)	For radiation, variables employed are (I+J), (K+I) and (M+N) energy fluxes.
(iii)	The thermal gas dynamics, energy, concentration and radiation equations are solved by program PHOENICS.

Figure 3.17 The Solution Procedure: 4, Mathematics.

4.0 NUMERICAL RESULTS AND DISCUSSIONS

4.1 Overview and Problem Description

The purpose of this chapter is to gain improved understanding of the complex flow physical and chemical processes in a combustion furnace. This is done by examining the effect of installing the post combustion chamber in the exhaust system of the old combustor. Of great importance is the intensity of turbulence especially at the inlet because if it is too high it can lead to flame extinction. To this end, the model problem described in Section 3.4 with typical furnace parameters is considered as a reference problem. The solution is obtained using the three-dimensional mathematical description of the system (Tables 3.2 and 3.3). The reference (baseline) problem employs all the mathematical models (Table 3.2) that have been developed. To examine the effects of the post combustion chamber, the following was done. The post combustion chamber was incorporated in the exhaust system of the old combustor and simulations done. The results obtained are compared with those based on the reference problem. See Table 4.1 below for details of the reference problem and Table 4.2 for details of the post combustion chamber. The computational details are shown in Table 4.3.

Table 4.1 System Parameters of the Reference Problem.

Item	Parameter	Description
1. 1	Dimension	1.6 m (Dia) x 3.5 m (L)
2.	Inlet and outlet size	0.6 m (Dia)
3.	Incoming mixture	CH_4 + 0% excess air
4.	Inlet temperature	773 K
5.	Inlet velocity: Fuel-Air mixture Oxidant	251.29 m/s 325.7 m/s
6.	Energy input	2.46 MW
7.	Ambient temperature	300 K
8.	Refractory emissivity	0.85 (gray)

Table 4.2 System Parameters of the Post Combustion Chamber

Item	Parameter	Description
1	Dimension of PCC	1.6 m (Dia) x 1.0 m (L)
2	Inlet and outlet size	0.6 m (Dia)
3	Ambient temperature	300 K
4	Refractory emissivity	0.85 (gray)

NB: The dimensions of the furnace in this case are same as the reference problem.

Table 4.3 Some Computational details of the Simulation for reference and real case

Item	Parameter	Furnace Only	Furnace With PCC
1	Grid Employed	10 x 215 x 25	10 x 215 x 25
2	Memory Storage	20 KB	18 KB
3	Computer used	Tulip 486 dx 50	Tulip 486 dx 50
4	Number of iterations	700	700
5	Typical Computer Time	13.3 Hours	14.8 Hours

The characteristics under study are discussed as needed for the explanation of the results. One important furnace parameter was studied before hand using the reference case only to establish the optimum combustion conditions or fuel-air ratio. This is the excess air percentage.

Effect of Excess Air

Complete combustion cannot be attained in a practical combustor unless more air than is required is used. The necessity for extra air is due to the difficulty of obtaining intimate contact between the air and the combustible gases or finely divided particles of fuel. For example the fuel itself may constitute in cases of gaseous fuel, combustible gases or vapours, and solids leaving the fuel bed in case of solid fuel may constitute particles Extra air is required in order to complete combustion within the combustion space available. The concentration of oxygen and of combustibles decreases towards the end of the combustion zone. However, chemical reaction speed is proportional to the reactants concentration. It is then necessary to use excess of air in order to speed up the reaction and complete it before the gases leave the furnace.

For maximum efficiency, it is necessary that the correct percentage of excess air (i.e. the proportion in excess of the theoretically necessary) should be used. Using too much air will waste the fuel because the extra air will become heated, additional heat will thus pass out of the system as sensible heat in the chimney gases. If too little air is used combustion will not be complete. This will result in the chimney gases carrying away unused potential heat in the form of unburned combustible gases. These gases are carbon monoxide, hydrogen and methane, which might have been usefully burnt in the combustion chamber.

The correct or desirable (optimum) percentage of excess air will depend on the type of fuel used, the construction of the plant and operating conditions. For a given fuel, the adiabatic flame temperature will decrease as the equivalence ratio digresses from the

stoichiometric. The variation of the adiabatic flame temperature for methane-air combustion at ambient pressure of 0.15 Mpa was simulated in this study and shown in Fig.4.1. The reference furnace was simulated for the range of equivalence ratio from 0.52 to 1.67. In the rich region, the excess fuel acts as the diluent, absorbing energy. In the lean region, the excess air acts as the inert diluent and absorbs energy.

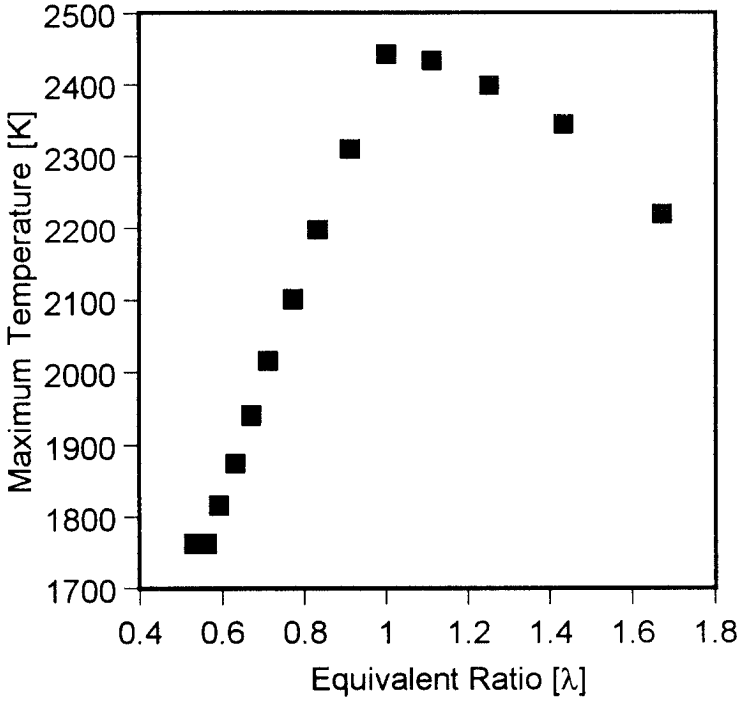

Figure 4.1 Adiabatic Flame Temperature Dependency on Equivalent Ratio [λ] at pressure of 0.15 MPa

The fuel-air ratio should be maintained as close as possible to the stoichiometric so that the combustion of fuel is complete. Song [1] has shown that the thermal efficiency and the local heat flux increases with reduction of the excess air percentage in a furnace. The thermal effectiveness also increases because of the longer residence time (or lower mass flow rate) for smaller excess air. Hence, for maximum thermal efficiency, the fuel-air ratio must be controlled accurately to achieve near stoichiometric combustion. For this case, the simulation with equivalent ratio λ=1 gave the highest possible temperature, 2444 K, in the combustor.

4.2 Effect of Post Combustion Chamber: Results and Discussions

In the plots, Figs.4.2 to 4.5, it was noted that the velocity contour plots in the Y-Z plane at plane angle from the vertical of $\theta = 0°$, 45° and 90° showed no significant variation of the results and hence only planes $\theta = 0°$ are shown here. An exception is only in the case of vector plots which have been plotted in two planes to show the recirculation zones in the plane ($\theta = 90°$) with all the three inlet ports. Since the contour plots are done in black and white, scatter plots have been included for each respective contour plot to bring to the fore the numerical values.

4.2.1 Flow Field

Velocity

The flow field and turbulence quantities are depicted in Figs. 4.2 to 4.11 for the cases of the furnace only and furnace with post combustion chamber. Figures 4.2 and 4.3 show the velocity vectors and recirculation flow zones (r.f.z). The r.f.z were located in the primary and secondary combustion zones. The r.f.z in the primary combustion zone was small in size compared to the r.f.z located in the secondary combustion zone. The primary combustion zone is shown in magnified form in Figs. 4.3 and 4.4 for furnace only and furnace with the post combustion chamber respectively. The second r.f.z is located down stream within the large confines of the combustor. This region constitutes the secondary combustion zone. The mixture discharging from the primary zone into the large confines of the combustor is typical of a fuel jet. That is the mixture bulk velocity, from the primary zone, is higher compared to the entire mixture. However, the jet like bulk velocity of the mixture decay as it progresses down stream. This phenomenon can be attributed to the rapid mix of the oxidant, reactant and hot vitiated products taking place in the primary combustion zone. This r.f.z are desirable features for the kind of combustor being studied in this thesis. The mixture from the primary zone is catapulted into the secondary combustion zone with accelerated velocity, approximately four times the velocity of the mixture when not combusted. As the jet leaves the primary combustion zone and discharges into the main combustion chamber it suddenly expands and tries to fill up the entire secondary combustion space. The sudden expansion causes the jet to assume a conical shape. This behaviour is typical of a fuel jet discharging in an enclosed combustor. Chisale *et al.* [2] using LDV in swirling cold flows and Tangirala *et al.* [3] observed a similar phenomenon.

Figures 4.2 to 4.7 show that in these regions the flow pattern is fairly axisymmetric. It is observed that there is intense recirculation in the inlet section for the furnace incorporating the post combustion chamber (Fig 4.4) than the case of the furnace only (Fig 4.3). This observation is further depicted by the polar plot in Fig. 4.7 in the lower values of r/R from 0 to 0.4.

Comparing, Fig. 4.8, the sizes for the r.f.z it was noticed that case of furnace only had a bigger r.f.z followed by the case of normal PCC and the case of optimised PCC had the smallest r.f.z. The distinctions in sizes of the r.f.z, in the case of furnace without and with PCC are not that noticeable. However, the case of optimised PCC (Fig. 4.18), when compared with the other two cases, shows high recirculation intensity in the combustor when the PCC was optimised. Chisale *et al.* [2] analysed and observed that for a furnace of fixed size, small r.f.z had high swirling intensity, which enhanced the mixing process. Based on the works of Chisale *et al.* [2] it can be deduced that, for the case of optimised PCC, intensive swirl enhanced mixing resulting in a stable and shorter flame with less emission levels.

Chisale *et al* [2] confirmed, experimentally in cold flow, that the elongation of the r.f.z is associated with swirling intensity. The elongation of the r.f.z in the case of the PCC is as a result of the residence time of the fluid mass being increased.

Figures 4.6 and 4.7 show velocity vectors for the chamber cross-sections in the plane orthogonal to the flow direction. These are at z/L = 0.01, 0.2, 0.4, and 1 for furnace only and at z/L = 0.01, 0.095, 0.196, and 1 for furnace with PCC. These cases show some penetration either into the main stream at inlet plane or out of it at exit plane. The nature of the penetration for fuel injection in a confined combustion chamber is that though combustion is premixed, the preparation of combustion gases from primary combustion zone is typically a diffusion jet. Namely, fuel jet momentum and velocity decay with axial distance.

The effect of buoyancy is taken to be negligible because the buoyancy force is much smaller than the inertia force. The existence of recirculation is confirmed by many experiments [4, 5, 6], and the flow field is similar to the flow over a backward facing step. As in laminar flow, the extent of recirculation is greater if the effective viscosity is smaller.

The Reynolds number is therefore defined in terms of the effective viscosity as

$$Re_t = \frac{\rho U D}{\mu_{eff}} \qquad \text{Eq.4.1}$$

and is an indication of the flow structure. In the above equation, U is the bulk velocity and D is a typical dimension of the furnace, namely the diameter. The Reynolds number defined by Eq.4.1 is not constant in the flow field but is typically of the order of 100. Recirculation near the furnace exit is indiscernible, and it is consistent with experimental observations [7]. This is due to very high turbulent viscosity near the exit.

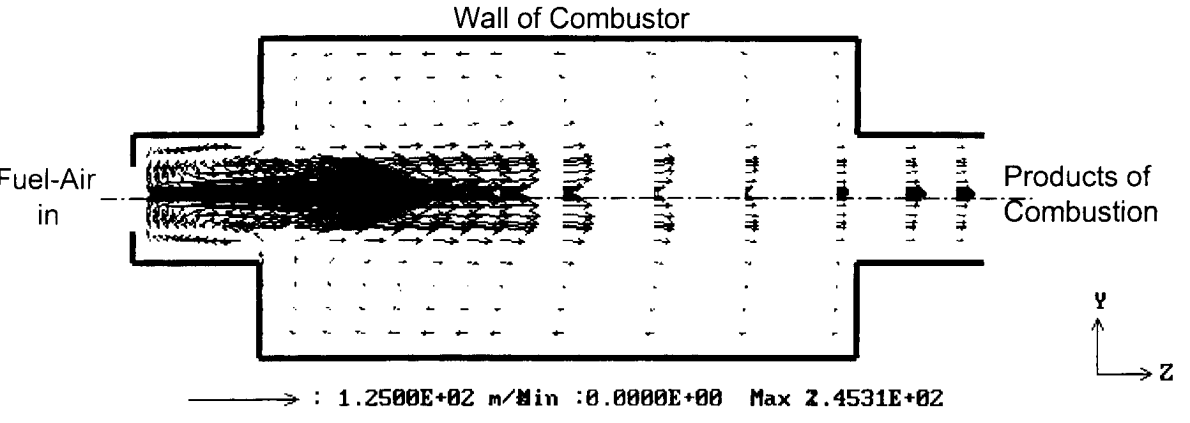

(a)

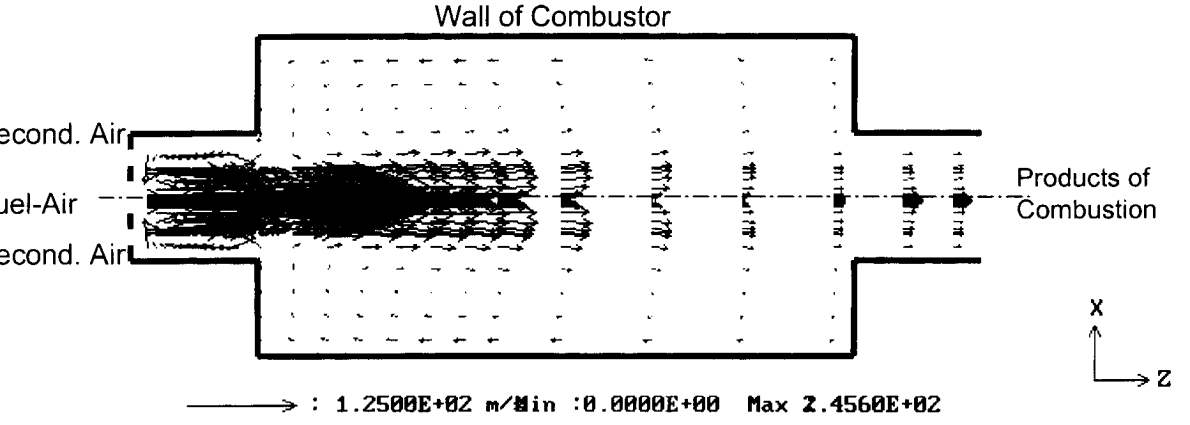

(b)

Figure 4.2 Velocity vector plots for furnace only in Z-Y plane:
(a) At θ=0° and 180 ° (b) At θ=90° and 270 °

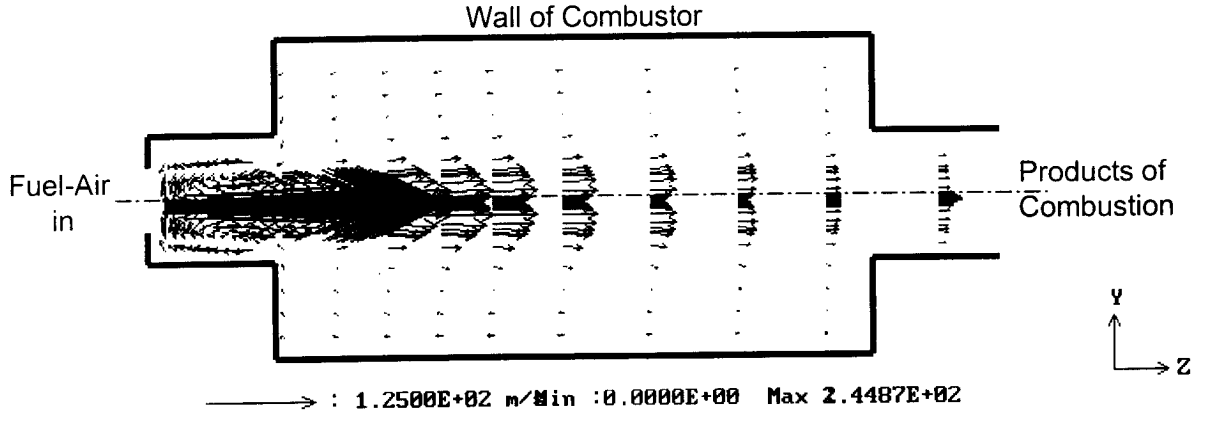

(a)

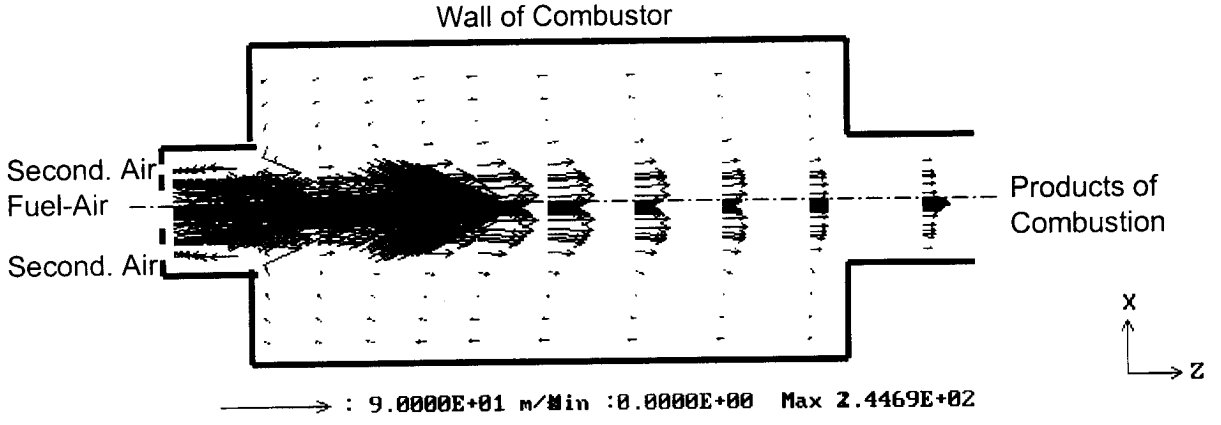

(b)

Figure 4.3 Velocity vector plots for furnace with PCC in Z-Y plane:
(a) At θ=0° and 180 ° (b) At θ=90° and 270 °

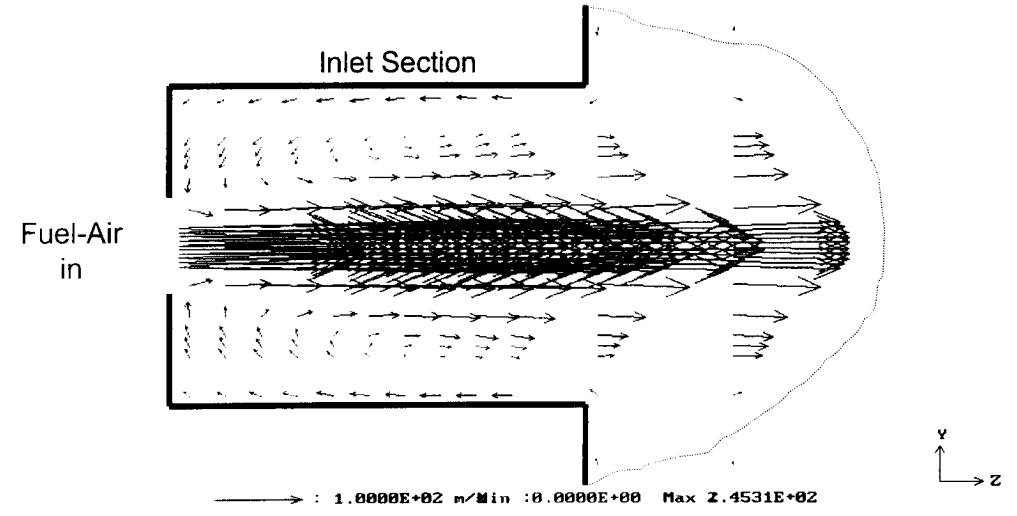

(a)

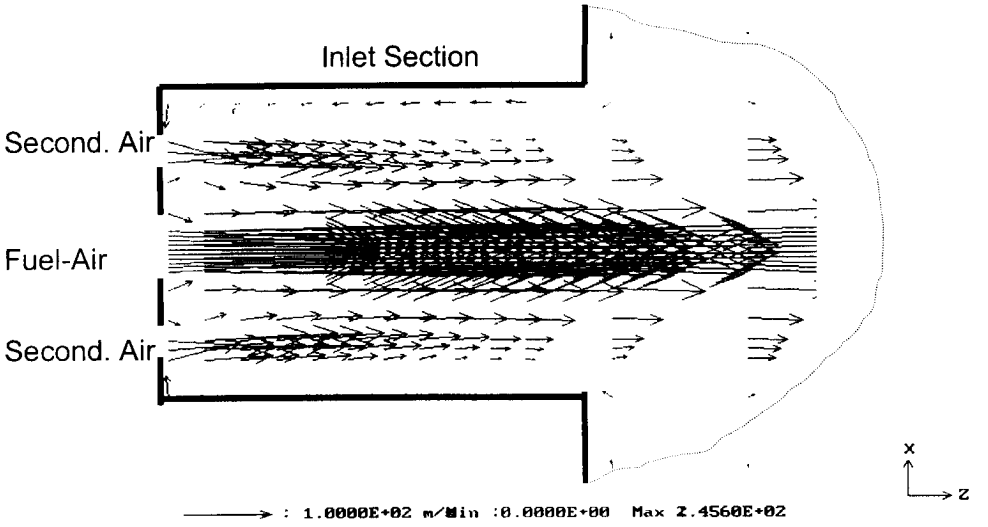

(b)

Figure 4.4 Velocity vector plots for inlet section of furnace only in Z-Y plane: (a) At θ=0° and 180 ° (b) At θ=90° and 270 °

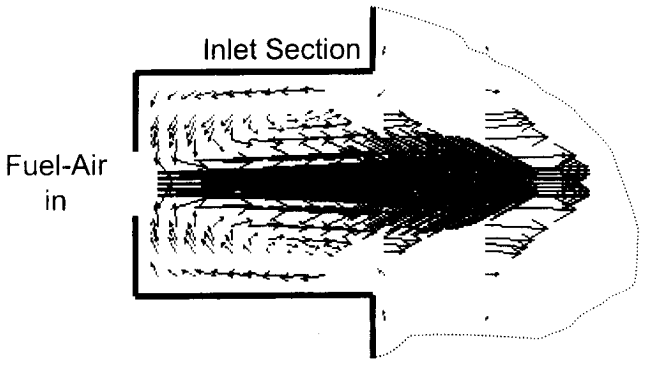

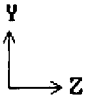

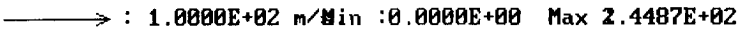

(a)

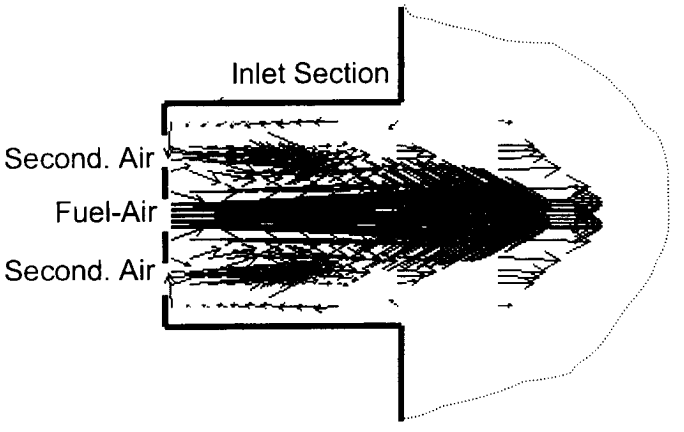

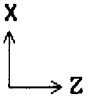

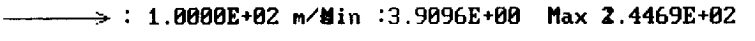

(b)

Figure 4.5 Velocity vector plots for inlet section of furnace with PCC in Z-Y plane: (a) At θ=0° and 180 ° (b) At θ=90° and 270 °

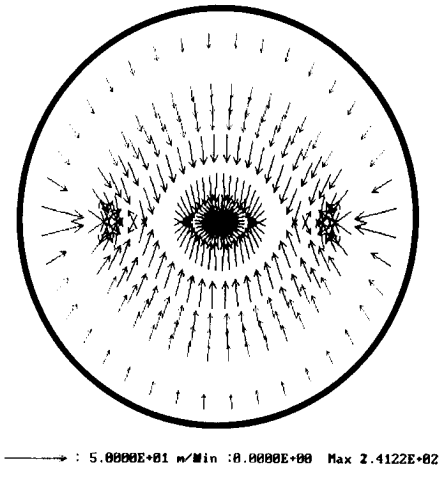

(a)

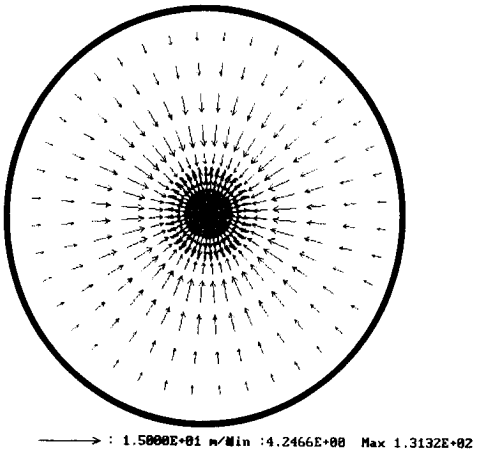

(b)

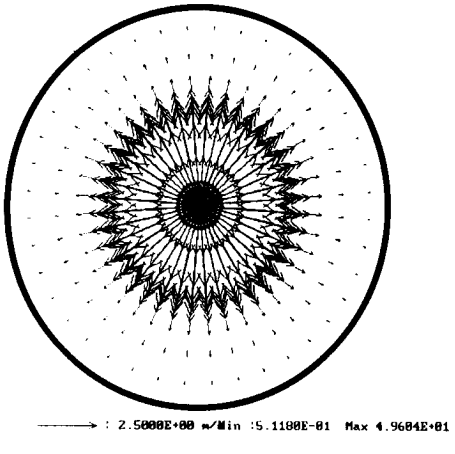

(c)

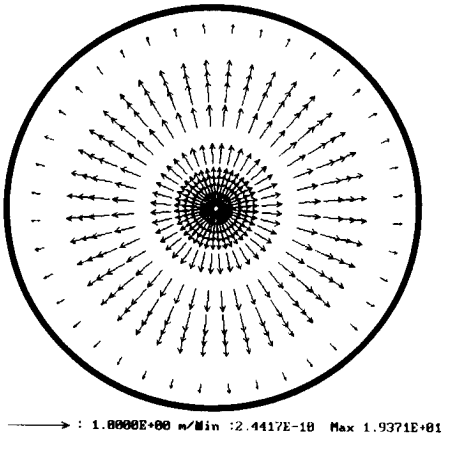

(d)

Figure 4.6 Velocity Vector plots in cross-stream of Furnace only in Y-Z plane (a) At z/L = 0.01 (b) At z/L = 0.2 (c) At z/L = 0.4 (d) At z/L = 1

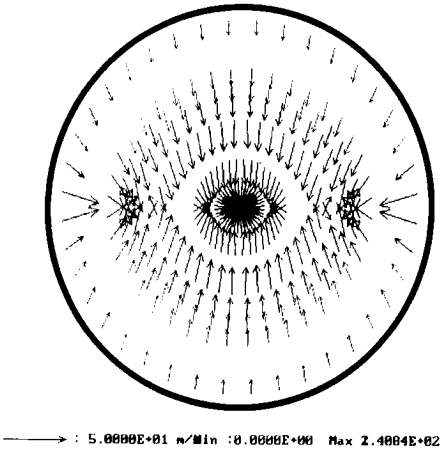

(a)

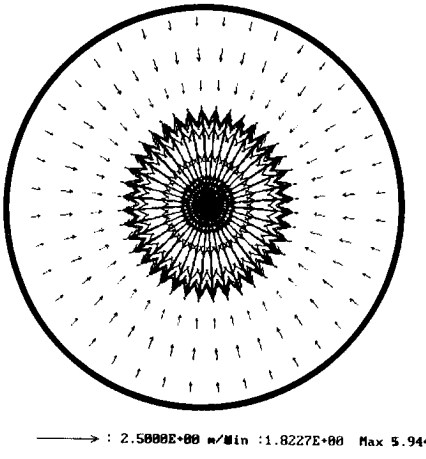

(b)

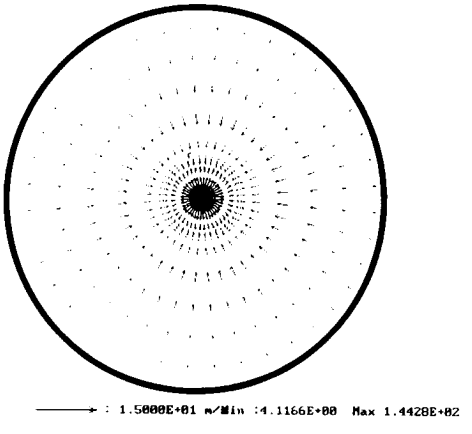

(c)

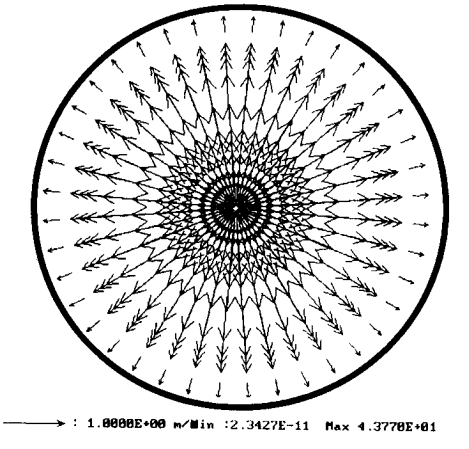

(d)

Figure 4.7 Velocity Vector plots in cross-stream of Furnace with PCC in Y-Z plane (a) At z/L = 0.01 (b) At z/L = 0.095 (c) At z/L = 0.196 (d) At z/L = 1

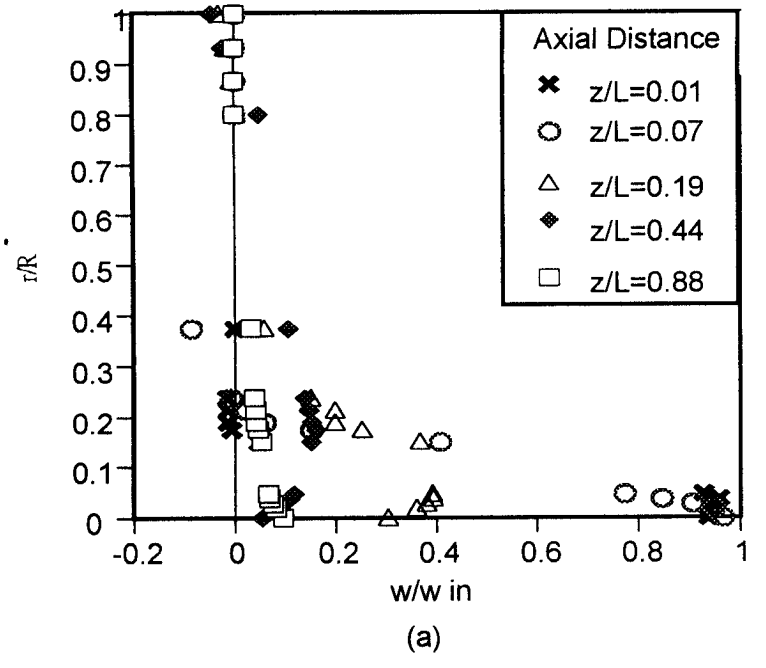

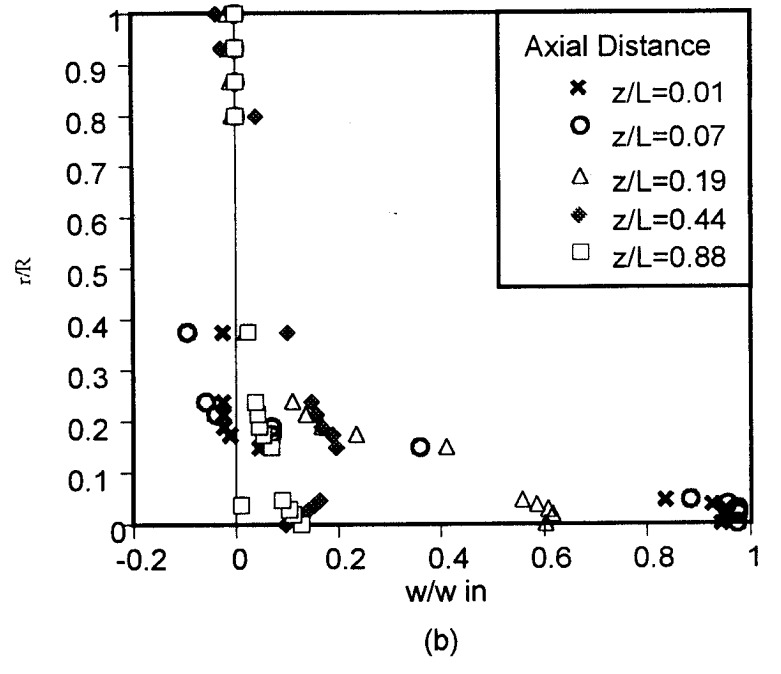

Figure 4.8 Axial Velocity Distribution at various r/R and λ=1 in Y-Z plane atθ =0° and 180°: (a) Furnace only (b) Furnace with PCC

Turbulent Kinetic Energy

Generation of turbulent kinetic energy, k, occurs where the velocity gradient is sharp and-or the gradient of pressure is in the opposite direction of the density gradient. For the case of furnace only, turbulent kinetic energy (TKE) intensity is highest at z/L = 0.2 downstream along axis of the furnace. The case with PCC has the highest intensity at z/L = 1.0 downstream along the axis of furnace. In the wall region, the TKE intensity is much lower than in the axial region. Consequently, the production of TKE is intense near the flame (z/L = 0 to 0.2) where large velocity gradients exists for case of furnace only. In this region typical value of TKE, is 1.75 MJ. For furnace with PCC, the highest value of TKE occur at z/L = 1.0, namely 1.80 MJ. The TKE intensities are high in the axial region due to the fact that r.f.z rotates like a solid body and at the interface of the r.f.z with the rest of the flow in the combustor a lot of energy is released. Chisale *et al* [2] confirmed this experimentally in swirling cold flow measurement.

False diffusion is significant near the inlet when the velocity is at an oblique angle to the grids. The following equation expresses the false diffusion coefficient Γ_{false} [8],

$$\Gamma_{false} = \frac{\rho\, U\Delta x\Delta y \sin 2\theta}{4\left(\Delta y \sin^3\theta + \Delta x \cos^3\theta\right)} \qquad \text{Eq.4.2}$$

A calculation of the false diffusion has shown that it is in the order of 0.001 kg/m-s in the shear layer between the centre line and the wall. False diffusion is negligible along the centre line and near wall regions. It is sufficiently small and is neglected in the calculations. However, a higher false diffusion, Γ_{false} = 0.01 kg/m-s, occurs very close to the inlet and outlet. The region where this false diffusion occurs is very small, and hence has negligible effects on the overall flow and other scalar fields.

The following expression is used to calculate the turbulence macroscale for the k-ε model [9],

$$l_c = C_D \frac{k^{\frac{3}{2}}}{\varepsilon} \qquad \text{Eq.4.3}$$

The value obtained is of the order of few centimetres. The macroscale increases from the centre of the jet to the shear layer and from the wall to the inner flow region. The magnitude of the macroscale length justifies the assumption that the optical depth of an eddy (macroscale here may be understood as the largest eddy size) is very small since the highest absorption coefficient is of the order of 1 m^{-1}. It is also noteworthy, in this study that this scale decreases with down stream distance because the turbulence decreases as the gas flows along the furnace.

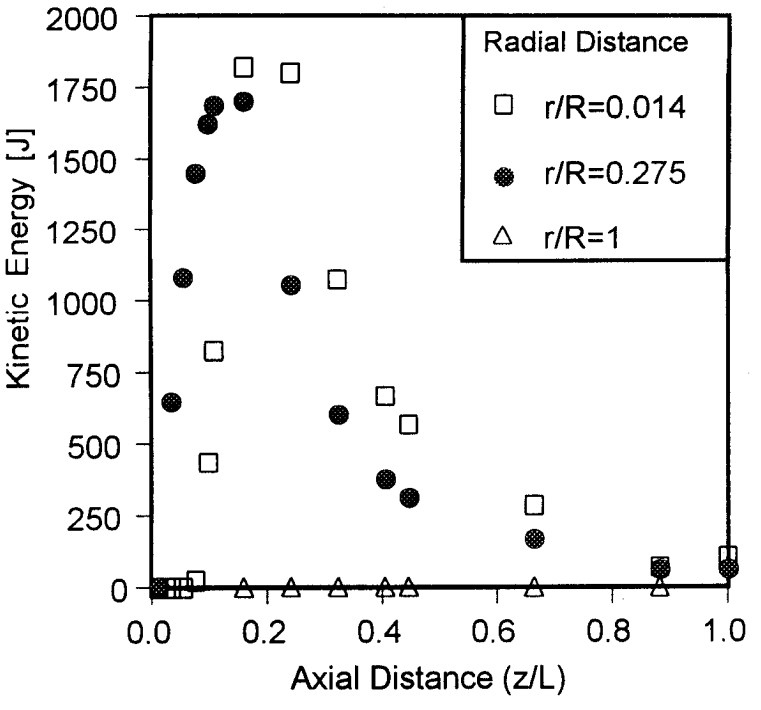

(a)

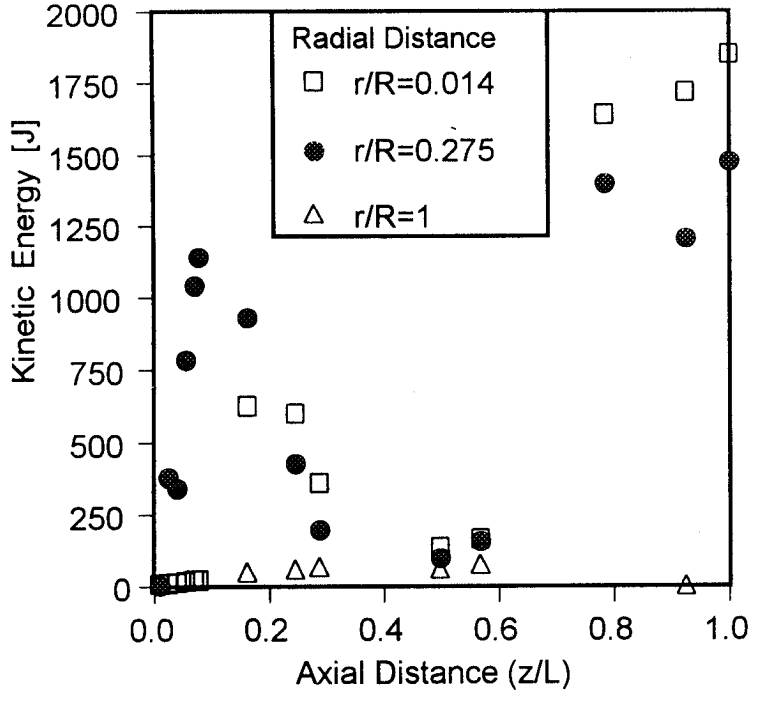

(b)

Figure 4.9 Turbulent Kinetic Energy (J) in Y-Z plane at λ=1
(a) Furnace only (b) Furnace with PCC

Turbulent Dissipation

The turbulent kinetic energy dissipation, ε, is a very complicated function. Production and destruction of turbulent kinetic energy are always closely linked. The dissipation rate of ε is large where production of k is large. The model equation (Eq.2.48) for ε assumes that its production and destruction terms are proportional to the production and destruction terms of the k-equation (Eq.2.47). Adoption of such forms ensures that ε increases rapidly if k increases rapidly and that it decreases sufficiently fast to avoid (non-physical) negative values of turbulent kinetic energy if k decreases.

As observed in Figs.4.10 and 4.11, the dissipation is almost proportional to the turbulent kinetic energy as can be ascertained from. The absolute values of k and ε are greater near the flame than near the exit this is because of advection of the quantities from upstream and intense production of turbulence by high velocity gradient near the flame. As a result, the turbulent viscosity is smaller near the flame than near the exit. This explains why the recirculation near the exit is insignificant in the exit region.

Considering the case for furnace incorporating a post combustion chamber, it is observed that there is a reduction in the dissipation of the average kinetic energy by 9.63 percent compared to the case of furnace without a post combustion chamber, Figs.4.10 and 4.11.

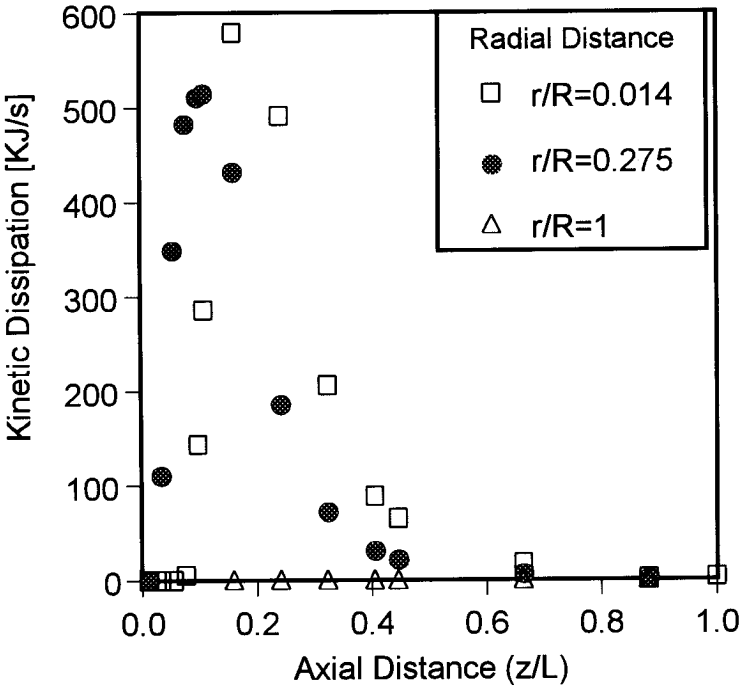

(a)

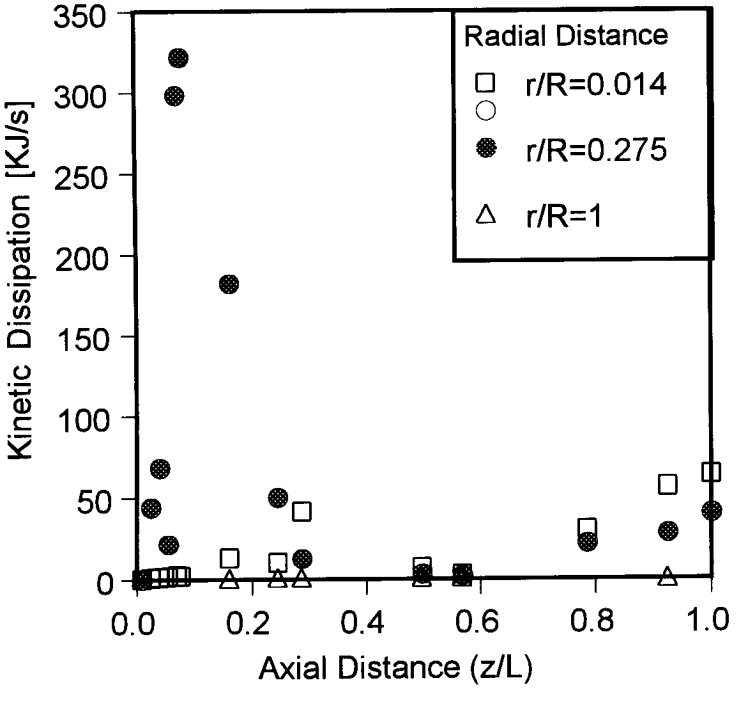

(b)

Figure 4.10 Turbulent Dissipation (KJ/s) Y-Z plane at λ=1
(a) Furnace only (b) Furnace with PCC

4.2.2 Combustion and Temperature field

The mixture fraction, fuel concentration, and the temperature distributions along the axis of the combustor are shown in Figs.4.11 to 4.14. The mixture, f, is appropriately defined as the mass of material from the fuel stream in unit mass of mixture, and can be viewed as a tracer for fuel mixing with air. The fuel concentration and temperature distribution profiles show that combustion is intense close to the inlet due to high turbulence in the region. (Figs. 4.11 to 4.12). Damkohler [10] and later Karlovitz *et al.* [11] proposed the following expression for turbulent flame speed for a weakly turbulent flame,

$$S_T = S_L + u' \qquad \text{Eq.4.4}$$

The laminar speed S_L may be found from Dugger`s experimental expression [12] for stoichiometric mixture of methane and air,

$$S_L = 8 + 0.00016\ T^{2.11} \quad \text{cm/s} \qquad (T \text{ in } K) \qquad \text{Eq.4.5}$$

This equation is only valid for a fresh mixture up to the temperature of 615 K, however, it is extensively used also for higher temperatures. The heat transfer rate is not very sensitive to the precise location of the flame. Assuming 90 percent of the stoichiometric flame speed for the stoichiometric mixture and adding u' = 0.6 to 0.8 m/s, one obtains a turbulent flame speed S_T in the range between 3.7 to 3.9 m/s. However, the present combustion model assumes 100 percent final reactedness by neglecting dissociation of CO_2, otherwise if dissociation rate is required the reactedness will not be 100 percent. It is important to note that autoignition does not take place before the fresh mixture reaches the flame temperature. According to Lefebvre and Lowell [13], the ignition delay for the mixture under consideration is found to be as long as 0.4 s.

Figures 4.14(a)-(b) show the predicted mean axial temperature distributions at $\theta = 0°$ and 180° for r/R = 0, 0.24, 0.69 and 1. The mean axial temperature distributions at r/R = 0.24, 0.69 and 1 were more or less uniform namely, 2500 K. This can be attributed to the fact that the secondary r.f.z were more or less, for all cases, located at r/R = 0.24, 0.69 and 1. Recirculation Flow Zones are also considered to be the regions of equilibrium with the entire r.f.z mass flow rotating as a solid disc. Therefore, temperatures in the r.f.z should

remain more or less uniform as confirmed by Chisale *et al* [2]. However, at r/R=0 the axial temperature is observed to rise very quickly and increases almost linearly in the case of furnace only, from z/L = 0 to 0.20, Fig 4.14(a), and exponentially in the case of furnace with existing PCC, Fig 4.14(b), and optimised PCC, Fig 4.22. This indicates that the flame position had shifted up stream The region, from z/L = 0 to 0.20, represents a primary combustion zone. In this region, a lot of combustion chemical reactions, accompanied by heat release take place until a stable flame is established. This increases the temperature to 2500 K.

In this study the mean gas temperature increases abruptly after passing through the flame and then is uniformly maintained up to exhaust, (Figs.4.13 and 4.14). The temperature variations in the combustor is greatest near the flame and it reaches values as high as 2447 K, Fig.4.13. This large temperature fluctuation occurs because the turbulent flame zone is alternatively occupied by the cold fresh mixture and by the products.

Figures 4.11 and 4.12 shows the axial variation of mixture fraction along the centre line and the wall and the unburned fuel-concentration in the combustion space at θ = 0°and 180° planes. In the primary combustion zone, the species concentration of unburned fuel exhibits a maximum near the point of injection. A sharp reduction of fuel concentration distribution in radial direction was observed in Fig. 4.11. This concentration distribution depend on the mode of fuel injection and burner design feature Chisale [14], Chisale *et al* [2] and Levebre [15] From the figures, it can be seen that nearly all the combustion occurs in the primary zone because, within the secondary zone, very little unburned fuel remains. In the present case fuel and air enter the primary zone in a stoichiometric proportion whereas in practise the mixture is likely to be a little fuel rich. Beyond the combustion zones, i.e. downstream, the ratio of minimum fuel to maximum amount worked out to be to be 9 1%. Therefore 90.9% of the fuel has been consumed. Since the fuel being used is methane, only 5% is required, as minimum, to ignite the mixture. This fuel will escape with the exhaust gases. In the case of no PCC it will rather burn on the exhaust duct and in the case with PCC this fuel will remain comparatively longer in the furnace and consequently burn. A very small amount of fuel is present near the outer casing, which gradually diminishes in magnitude with downstream distance.

It can be clearly inferred that highest temperatures occur in the primary combustion zone due to the presence of high concentrations of fuel and turbulence. The temperature level of the gases at exit is about 2441 K for the reference case and 2444 K for the case with post chamber, Fig.4.13. In general, axial temperature increases with axial distance. For the case with the post combustion chamber, the axial mean temperature of the gas increases rather slowly owing to the fact that the flame position in the case of PCC has shifted downstream, Fig.4.14(b). This type of flame has delayed and slow diffusion mixing rate. This is due to the absence of the recirculation flow in the combustor in the wake of the fuel jet velocity being greater than the bulky flow velocity in the combustor. This is only correct on the macro level. Chisale *et al* [15] showed that this mixing is such that, the mixture velocity, close to the burner tip, exceed the flame velocity due to the relative higher amount of chemical heat released behind the flame. The post combustion chamber introduces pressure downstream at the combustor exit thereby inducing stagnation within the flow in the combustor. Stagnation of the combustion mixture downstream in the combustor improved the combustion by causing high rates of entrainment of ambient fluid into the flame. Therefore, quick mixing took place in the vicinity of the inlet ports and in the primary recirculation flow zones. This is desirable in that it increases the residence time of the combusting gases in the furnace space. Temperature fluctuations varied from 773 to 2447 K and were generally high over the entire combustion space in the furnace with a post combustion chamber.

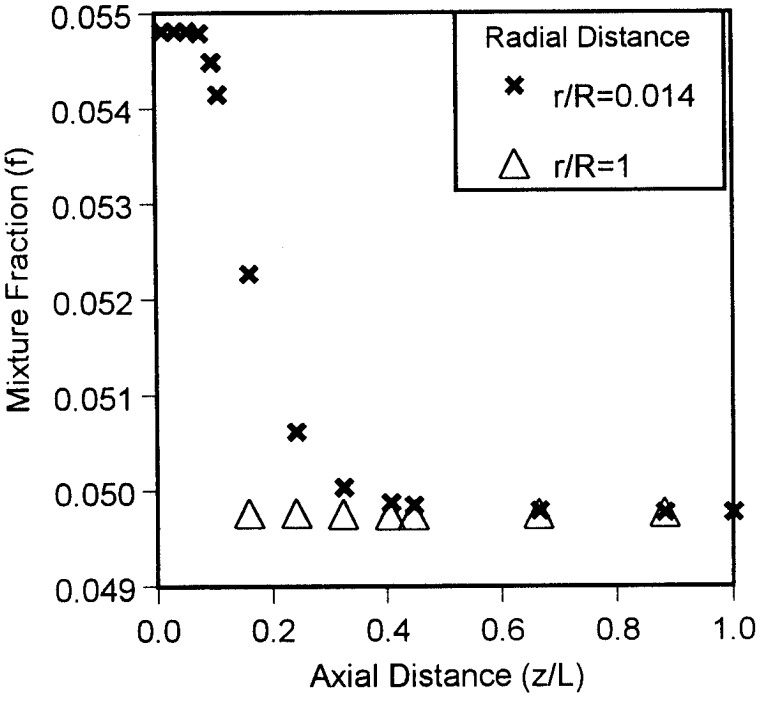

(a)

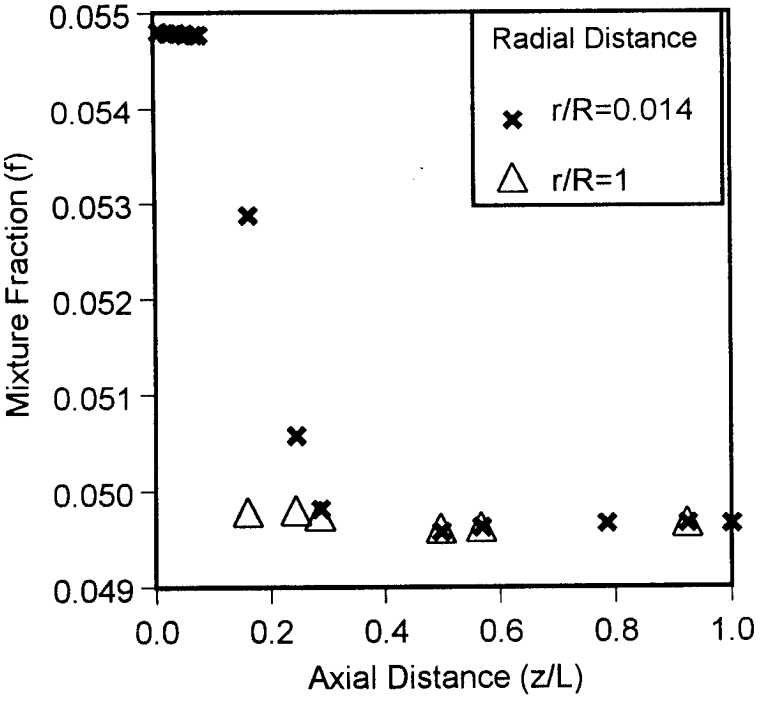

(b)

Figure 4.11 Mixture Fraction Distribution in Y-Z plane at λ=1
(a) Furnace only (b) Furnace with PCC

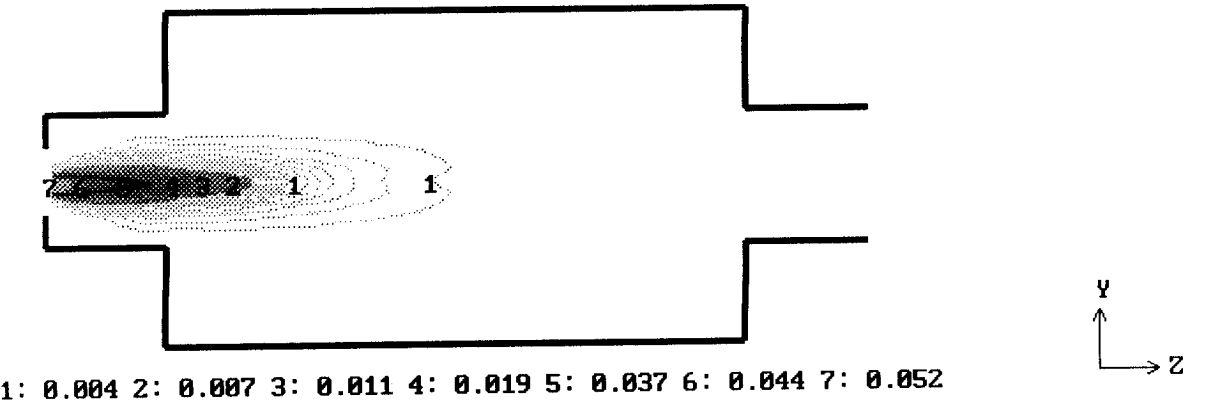

(a)

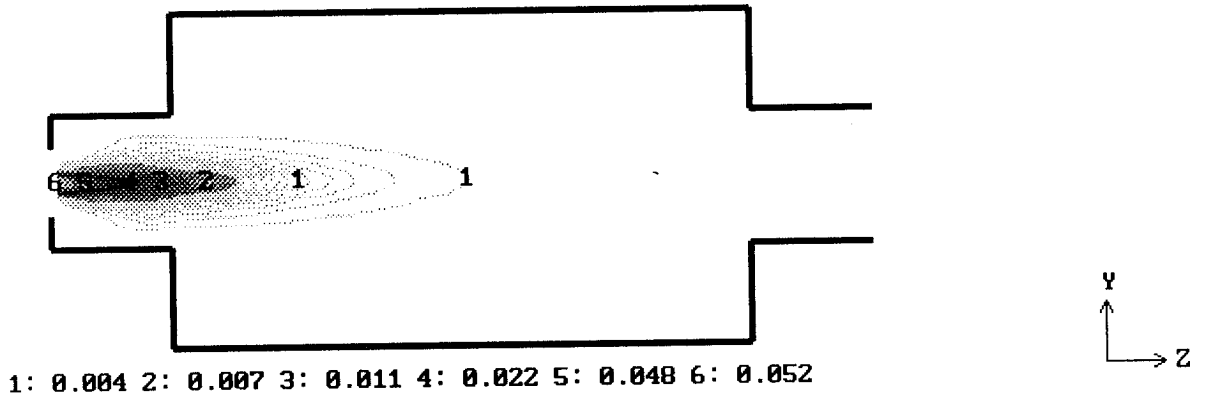

(b)

Figure 4.12 Fuel Concentration [kg/m^3] Distribution in Y-Z plane at λ=1
(a) Furnace only (b) Furnace with PCC

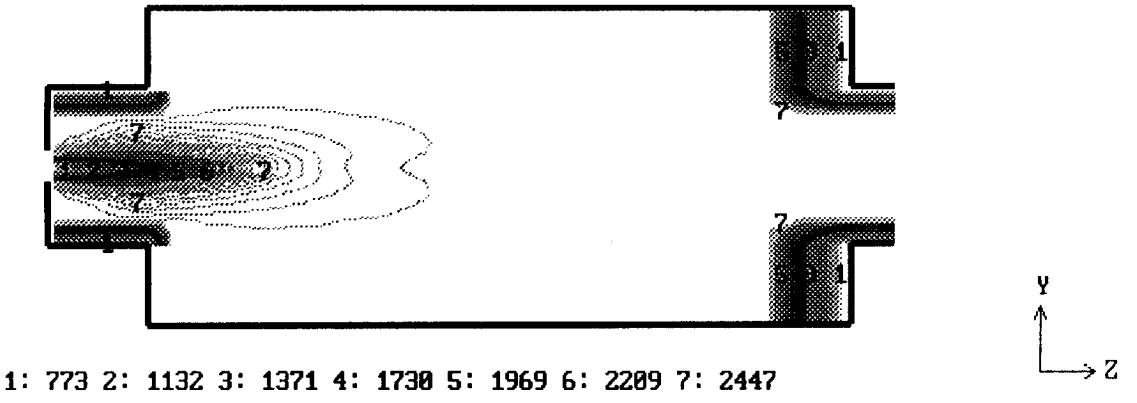

1: 773 2: 1132 3: 1371 4: 1730 5: 1969 6: 2209 7: 2447

(a)

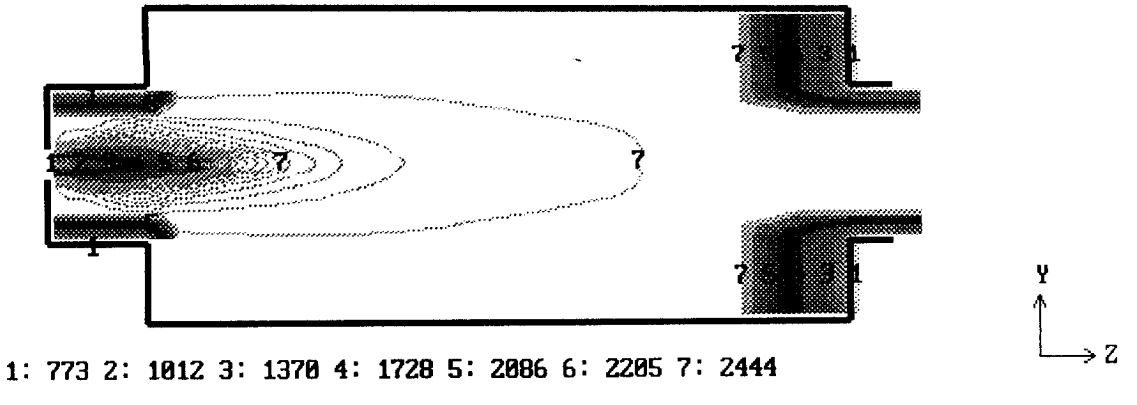

1: 773 2: 1012 3: 1370 4: 1728 5: 2086 6: 2205 7: 2444

(b)

Figure 4.13 Temperature Distribution in Y-Z plane at λ=1
(a) Furnace only (b) Furnace with PCC

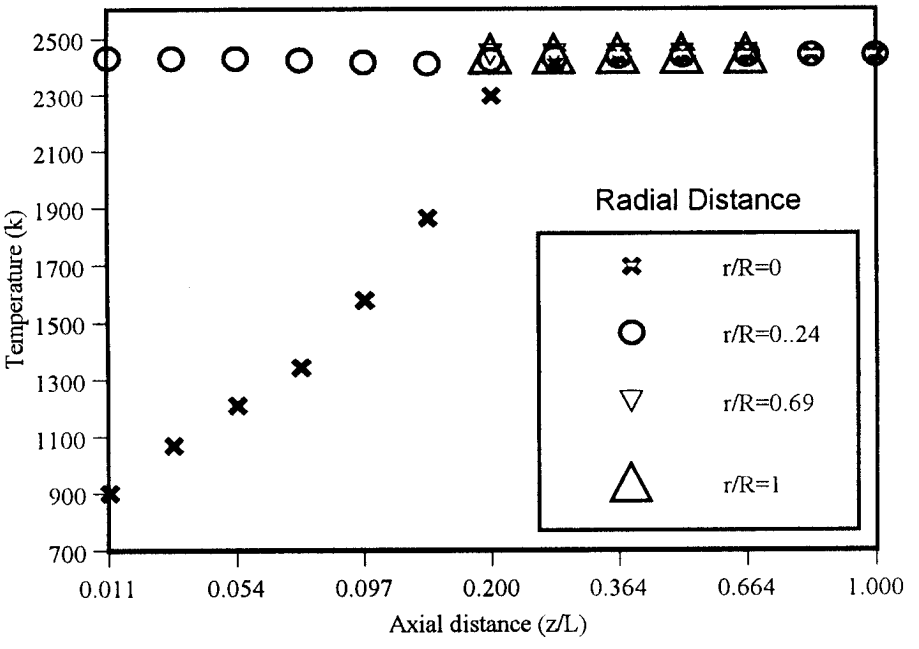

(a)

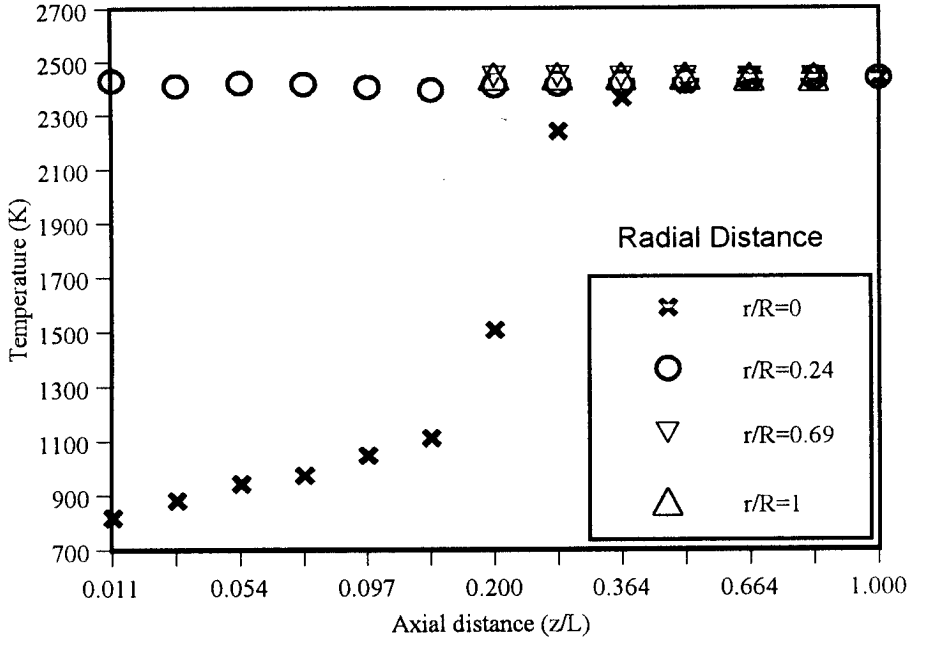

(b)

Figure 4.14 Temperature Distribution at various r/R and $\lambda = 1$ in Y-Z plane at $\theta = 0°$and 180° (a)Furnace only (b) Furnace with PCC

4.2.3 Radiation Field

To achieve a realistic modelling of enclosed fires, radiative heat transfer must be included. Using the shareware version of PHOENICS used, it is not possible to simultaneously predict the flow patterns and radiation for the three-dimensional flame. However, the shareware version incorporates the composite-flux model of radiation provided in subroutine GXRADI called from GREX2. It sets the absorption and scattering coefficient and the specific heat of the medium. It solves for the enthalpy, and the composite radiation fluxes in the x-, y-, and z-directions. It omits the convection and transient terms from the radiation equations. This way the program predicts radiation alone from a scattering, absorbing and emitting medium.

The radiation transfer was analysed without considering the turbulence-radiation interaction. The simulations were then performed for a case where only the products of combustion are strongly participating. These combustion gases emit about 40 percent of their energy by radiation [1]. Without emission of radiation, heat transfer from the gas to the load would be extremely small, and the exhaust gas would leave the furnace at almost the adiabatic flame temperature. The variation of irradiance in the combustion system is dependent on the absorption coefficient, emission (or absorption) of radiation by the gas, and emission (or absorption) of radiation by the refractory. The smaller the absorption coefficient, the more uniform is the radiation field. Also when the gas is a strong emitter of radiation and the boundaries strongly absorb the radiation emitted by the gas, the radiation field becomes highly non-uniform.

Figures 4.15 and 4.16 show the results for the prediction for the furnace without the post combustion chamber and the case with one. The results were plotted in cartesian co-ordinates for clarity. Radiation is six-dimensional in nature as stated is Section 2.6, this results in a voluminous radiant flux field. The radiation variables are the flux sums for the three directions: I+J, K+L, and M+N. Therefore, there is too much information to be graphically displayed in this one report. The figures therefore simply present the graphs for these three flux sums for the y-z plane at 0° and 180° along the combustor axis.

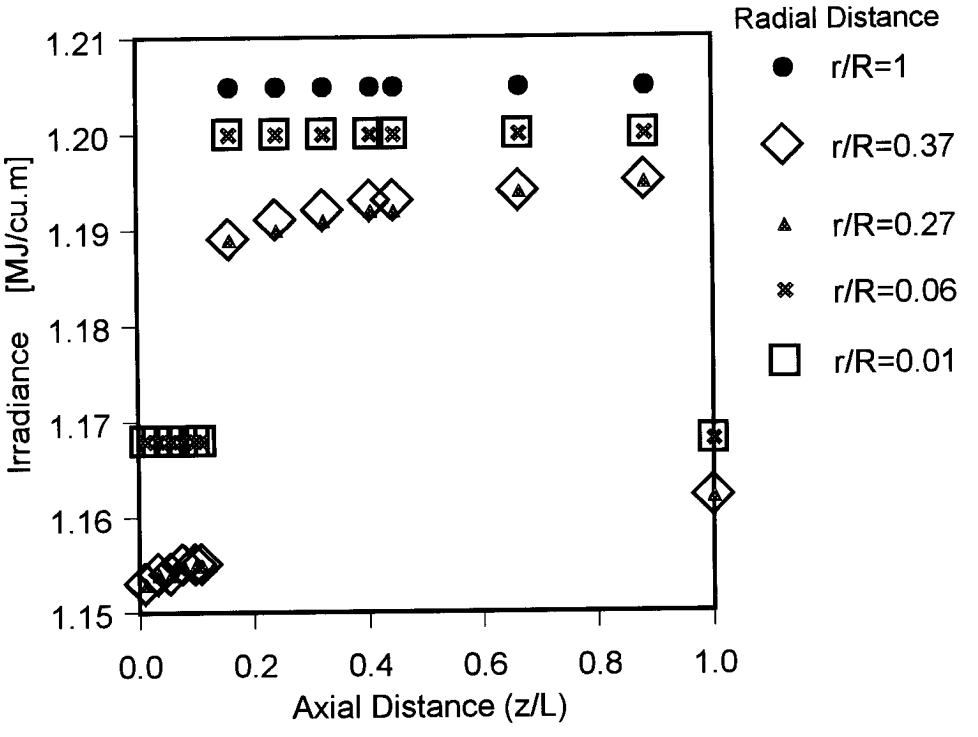

Figure 4.15(a) Radiation Flux Distribution for Furnace only in the x-direction.

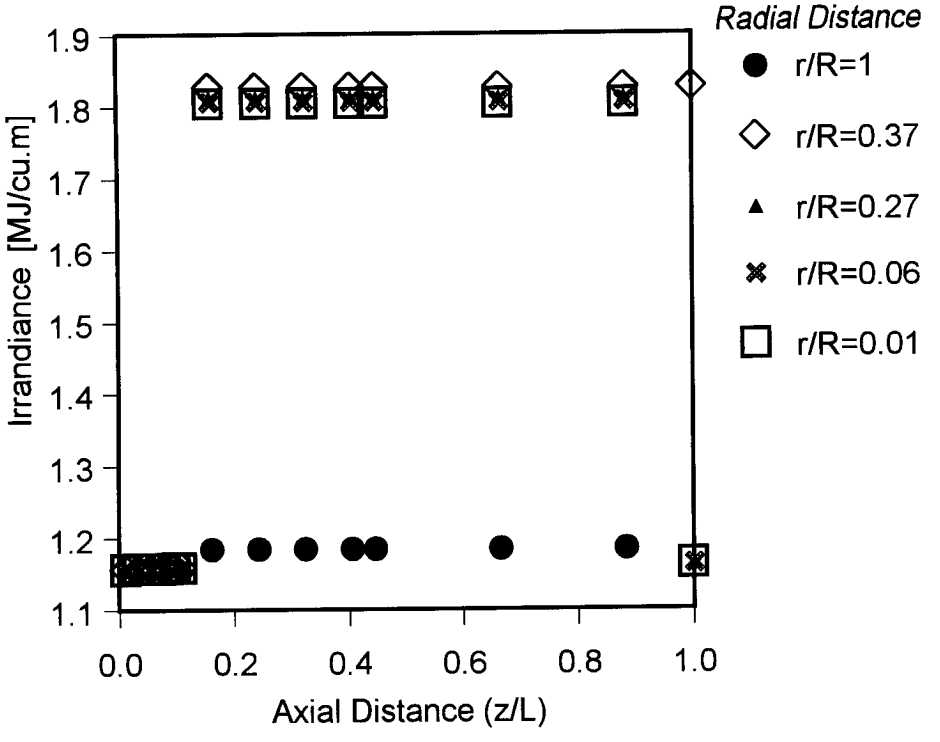

Figure 4.15(b) Radiation Flux Distribution for Furnace only in the y-direction.

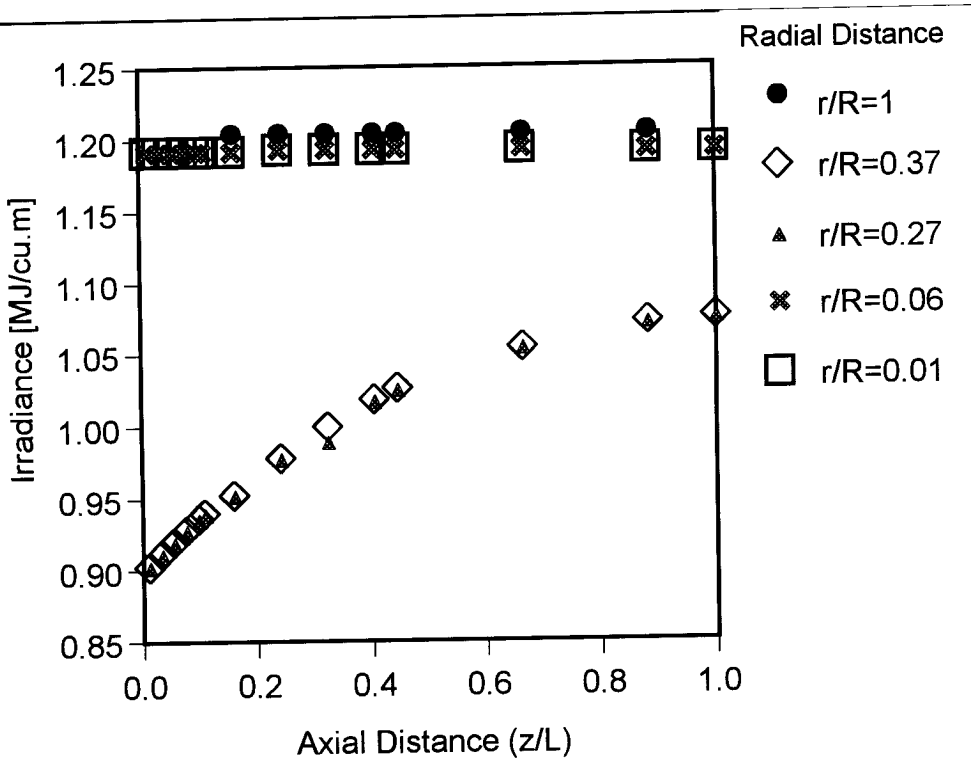

Figure 4.15(c) Radiation Flux Distribution for Furnace only in the z-direction

The largest values in the x-direction lie along the circumference of the furnace i.e. r/R=0.01, the reason is of course that there are no sinks of this kind of radiation at the boundaries of the integration domain, Fig.4.15 (a). The lower values in the y-direction are near the centre and are smallest at the wall. This type of radiation easily escapes to the relatively cooled wall, Fig.4.15 (b). This is desirable in order to transfer heat to the load in the furnace. The z-direction radiation also escapes, but it has a greater distance to travel, Fig.4.15 (c). It is observed that the irradiance near the wall is uniformly distributed and is 1.2 MJ/m^3.

Turbulence –radiation interaction is very important in the analysis of radiative heat transfer, especially when the flame size is comparable with the size of the combustion space. The heat flux at the wall may be underpredicted by as much as a few hundred percent if the turbulence-radiation interaction is neglected for long flames. For short flames in comparison to the furnace size, the difference between the predictions of radiative heat fluxes at the wall with and without turbulence-radiation interaction is only about ten percent [1].

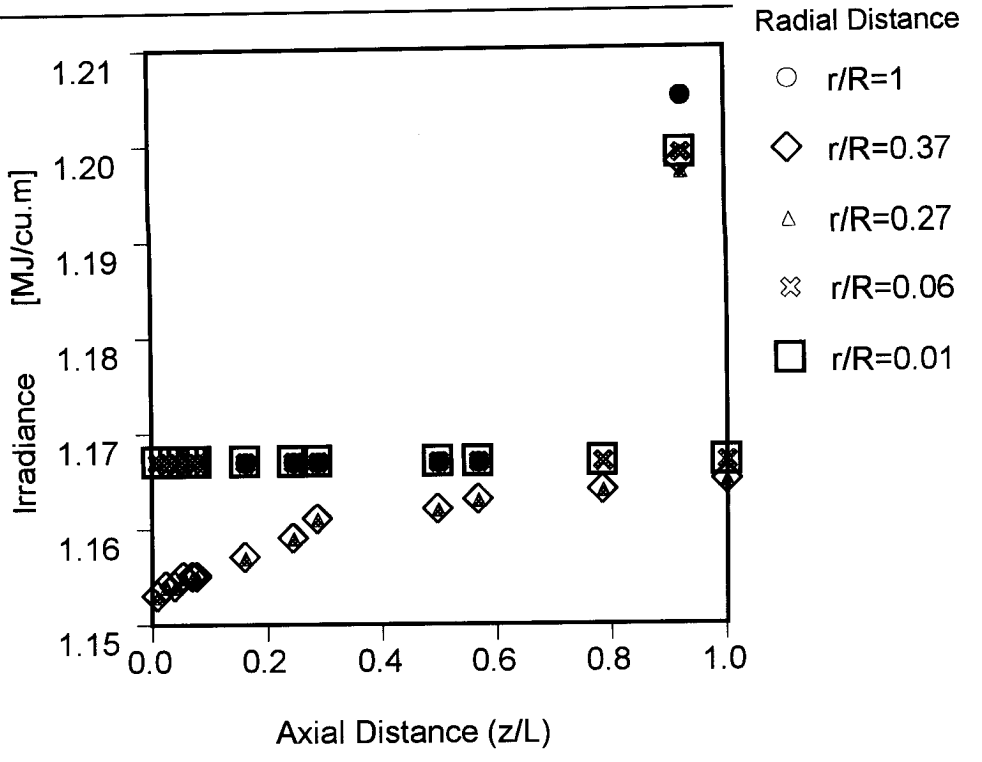

Figure 4.16(a) Radiation Flux Distribution for Furnace with PCC in the x-direction

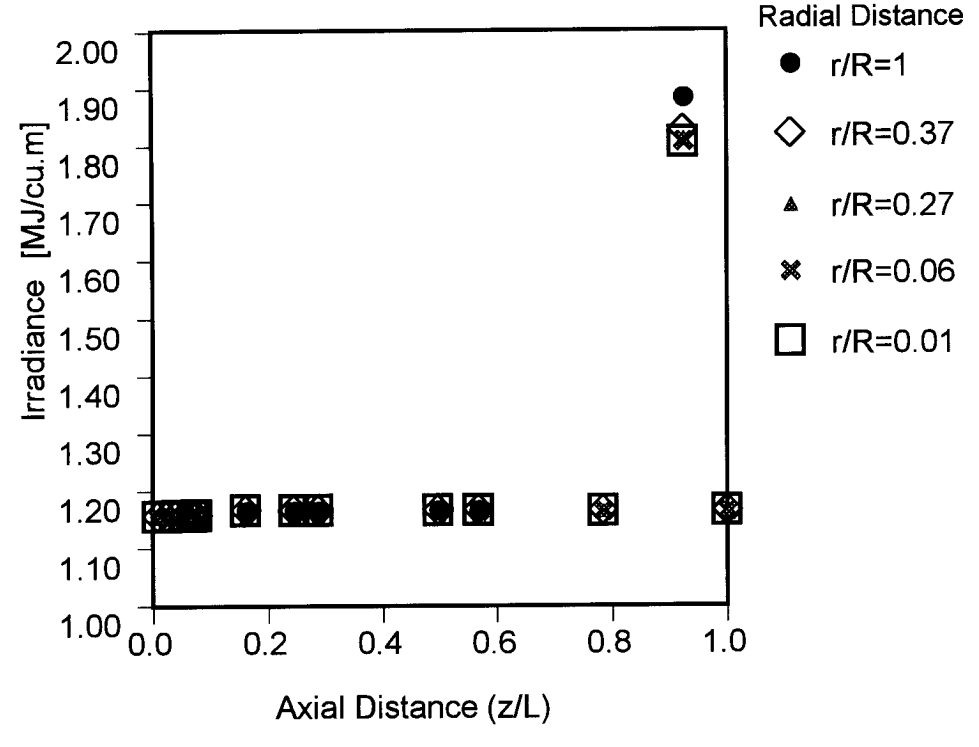

Figure 4.16(b) Radiation Flux Distribution for Furnace with PCC in the y-direction

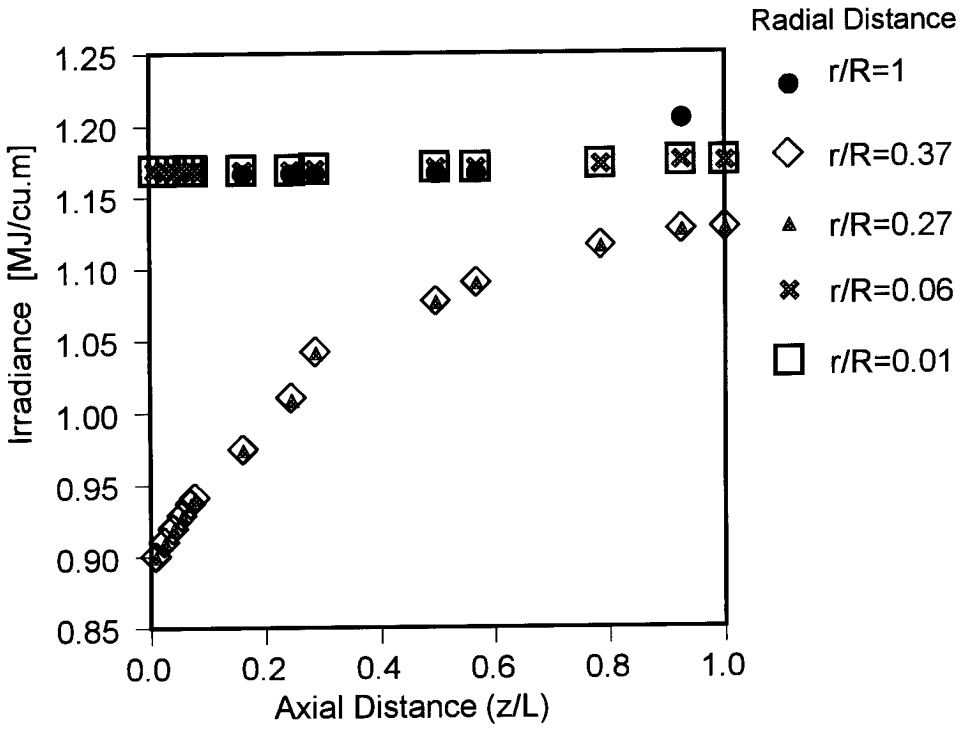

(c)

Figure 4.16(c) Radiation Flux Distribution for Furnace with PCC in the z-direction.

When the post combustion chamber is incorporated in the exhaust of the furnace, the average irradiance at the wall in the x-direction drops to 1.7MJ/m^3, due the increase in the area of the wall, Fig.4.16 (a). Addition of the post combustion chamber also increases radiation transfer in the horizontal direction. This is why the y-direction irradiance becomes uniformly distributed throughout the furnace chamber, Fig.4.16 (b). For the same reason, the z-direction irradiance in the mid region r/R=0.27 to 0.37, rises steadily from the burner end (0.9 MJ/m^3) to the exhaust (1.07 MJ/m^3). All the phenomena observed above are due to increase in total volume covered by the irradiance.

4.3 Effect of Optimisation of Post Combustion Chamber Results and Discussions

4.3.1 Model Parameters

Furnace design parameters and operating conditions affect its performance. Therefore, optimum design and operation are important from the viewpoint of energy efficiency and quality control of the product. Parametric simulations were performed by focusing on the flow features of turbulence, combustion and heat transfer characteristics. To determine the effect of the parametric changes, the furnace with normal post combustion chamber was considered as the reference case. Its size was varied in steps from the base case, for each simulation, in order to interpret the effect of each individual size. The size was varied by increasing the length in steps of 0.25 m from the normal 1 m length to 3.5 m length. The diameter of the post combustion chamber was kept constant. Details of the normal post combustion chamber were as shown in Table 4.2. The characteristics under study are herewith discussed in order to highlight the scientific phenomena at hand. The computational details are tabulated in Table 4.4.

Table 4.4 Some Computational details of the Simulation with optimised PCC

No.	Parameter	Furnace With Optimum PCC
1	Grid Employed	10 x 215 x 25
2	Memory Storage	18 KB
3	Computer used	Tulip 486 dx 50
4	Number of iterations	700
5	Typical Computer Time	15.1 Hours

Optimisation of the Post Combustion Chamber

Temperature was used as a criterion in selecting the optimum size of the post combustion chamber. Figure.4.17 shows the axial line temperature distributions along the furnace. The highest centre line temperature was obtained with a post combustion chamber of length 2.75 m. This particular post combustion chamber gave a high and uniform mean temperature distribution throughout the furnace space, Fig.4.22. The optimum post combustion chamber gave the temperature at the centre line of 2444 K in the injection zone, and maintained constant through to the exit of furnace.

Figure 4.17 shows the optimisation of the PCC with regards to maximum and uniform temperature distribution in the combustor. At 2.75 m length of the PCC, temperature distribution in the combustor is better than at other lengths of the PCC. Tangirala *et al* [3]

and Chisale *et al.* [2] have both confirmed that, keeping the fuel momentum constant and increasing the r.f.z intensity leads to improved mean temperature in the combustor.

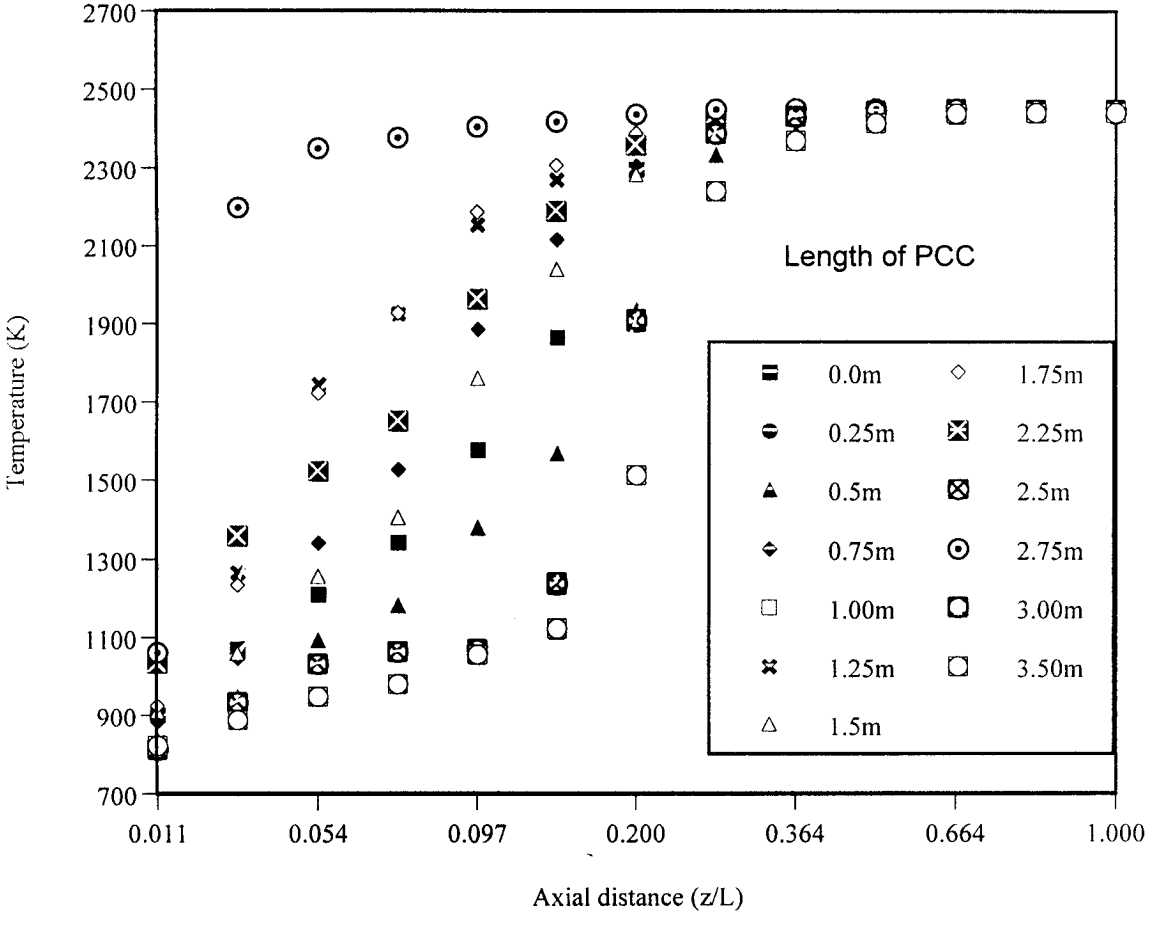

Figure 4.17 Temperature Distribution at Centre line of Furnace at $\lambda = 1$: for various lengths of PCC

4.3.2 Flow Field

Velocity

The results for the velocity field simulated with the optimum post combustion chamber showed very little variation (average of 2.8 percent) from the base case with normal post combustion chamber. Hence, the velocity vector plots, as in Section 4.2, have not been repeated here. However, the notable feature is that the intensity of the recirculation around the centre line (r/R = 0 to 0.15) of the furnace has shown a significant increase in size. The intensity is higher than the reference case and the base case with a normal post combustion chamber. Along the wall regions (r/R = 0 75 to 1.0), the intensity of recirculation is lower than in the other two cases.

The above condition promotes increased recirculation of vitiated gases in the central combustion region where mostly there is the incoming fresh mixture. The recirculation near the inlet is necessary for the efficient combustion. However, this makes the temperature in the furnace more uniform, increases the furnace temperature overall as well as residence time of the gas in the furnace.

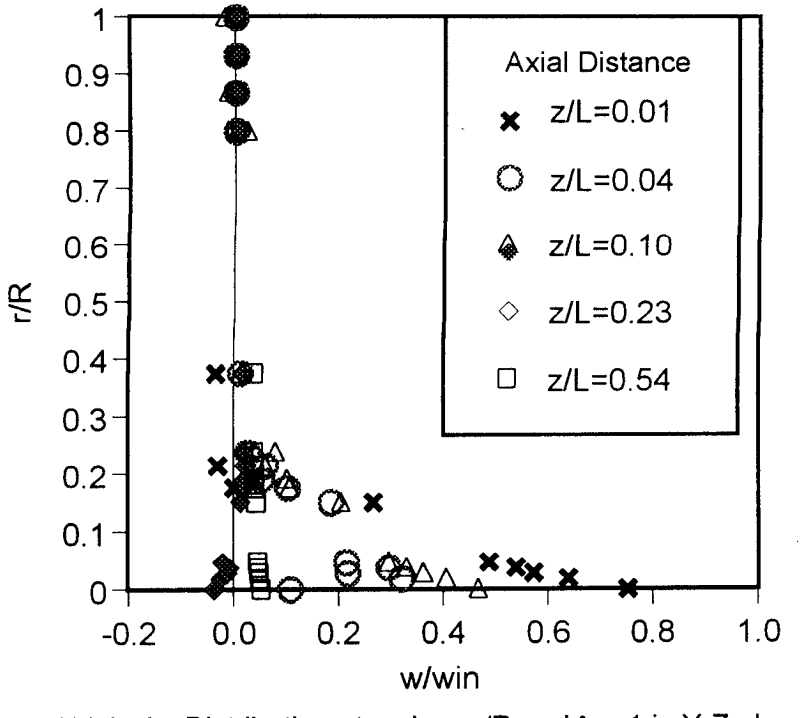

Figure 4.18 Axial Velocity Distribution at various r/R and λ = 1 in Y-Z plane at θ = 0°and 180°: Furnace with Optimised PCC

Turbulent Kinetic Energy k and its Dissipation ε

Figure 4.19 shows turbulent kinetic energy and its dissipation rate for the case with an optimised post combustion chamber. The turbulent kinetic energy intensity has very sharp rise and rapid drop in the region of the flame. Thereafter the kinetic energy along the centre line decreases gradually up to the exit of combustor. The high turbulent kinetic energy at the centre line is in agreement with the sharp velocity gradient around the centre line as explained above.

The dissipation is almost proportional to the turbulent kinetic energy as ascertained and explained in Section 4.2. The absolute values of k and ε are greater at the centre line than in the shear layer. This is due to advection of the quantities from upstream and the intense production of turbulence by high velocity gradient near the centre line. As a result, the recirculation is lower near the wall regions than the centre line

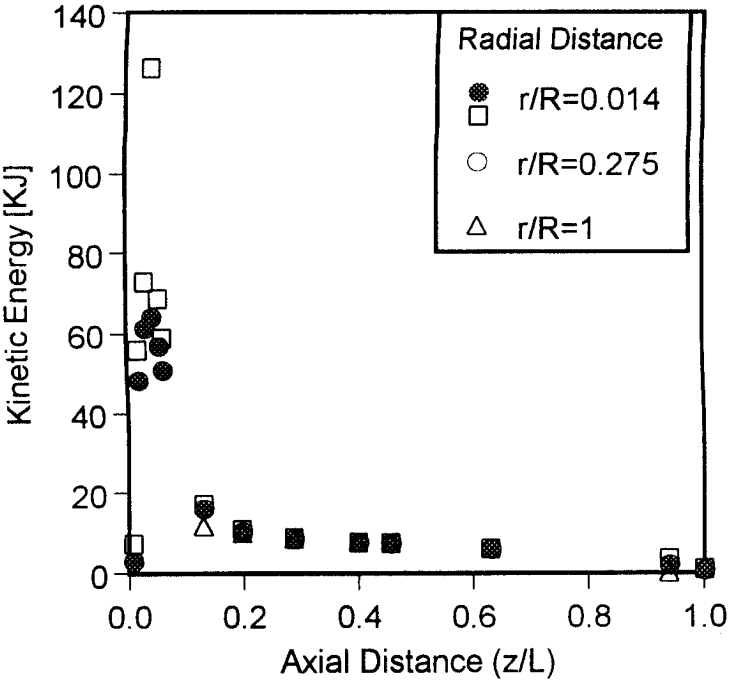

(a)

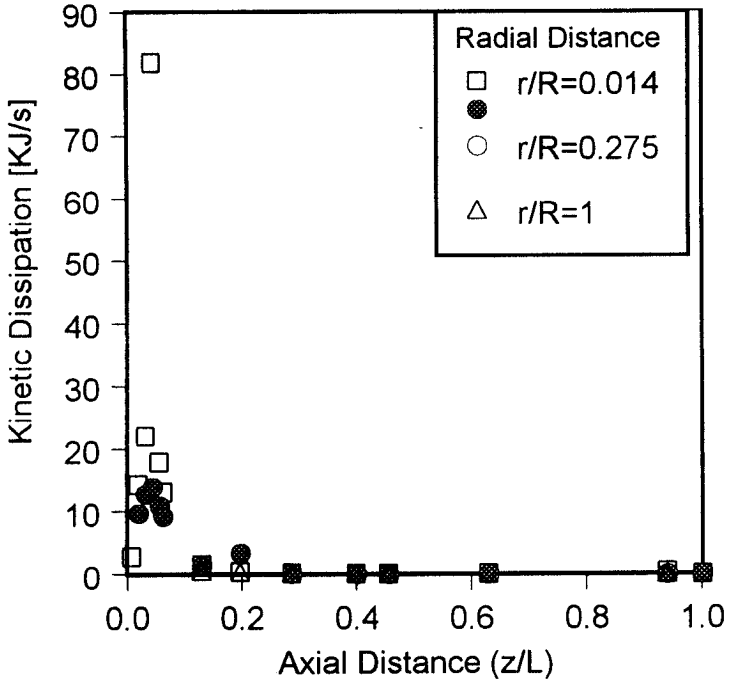

(b)

Figure 4.19 Turbulence in Furnace with Optimised PCC in Y-Z plane at λ=1
(a) Kinetic Energy *k* [KJ] (b) Dissipation ε [KJ/s]

4.3.3 Combustion and Temperature field

The mixture fraction and fuel concentration plots as shown in Fig.4.20, for the furnace with optimised post combustion chamber, show that fuel is consumed quite early around the inlet section. The mixture fraction drops sharply in a short distance of the combustor. An intense recirculation is revealed around the centre line and the inlet region by the flow field as observed in Section 4.3.2. This lead to reduced flame length in the flow direction and expansion in the transverse directions due to vigorous mixing. This results in a short flame along the flow direction (Fig.4.21). As a result, there is also rapid combustion of fuel close to the inlet and therefore increases the residence time for the hot gas to lose energy while in the furnace. This has a greater influence in that it decreases the local heat flux (both convective and radiative) near the inlet. Consequently, the heat flux is greater downstream the combustor (Fig.4.24). With an optimised post combustion chamber the mean temperature in the furnace is almost uniform at all radial and axial positions Fig.4.22.

Comparing the case for the optimised PCC, Fig.4.22, with the other two cases for furnace only and furnace with existing PCC, Figs 4.14(a)-(b), it is noticed that the axial temperature profiles are very different. In the primary combustion zone the temperature was slightly lower, by about 200 K and reached about 2500 K in the secondary combustion zone. This can be attributed to a longer residence time of the mixture in the primary combustion zone. The scenario, Fig.4. 22, is such that fuel, temperature and hence thermal load distribution in the combustor is better in comparison to the other two cases.

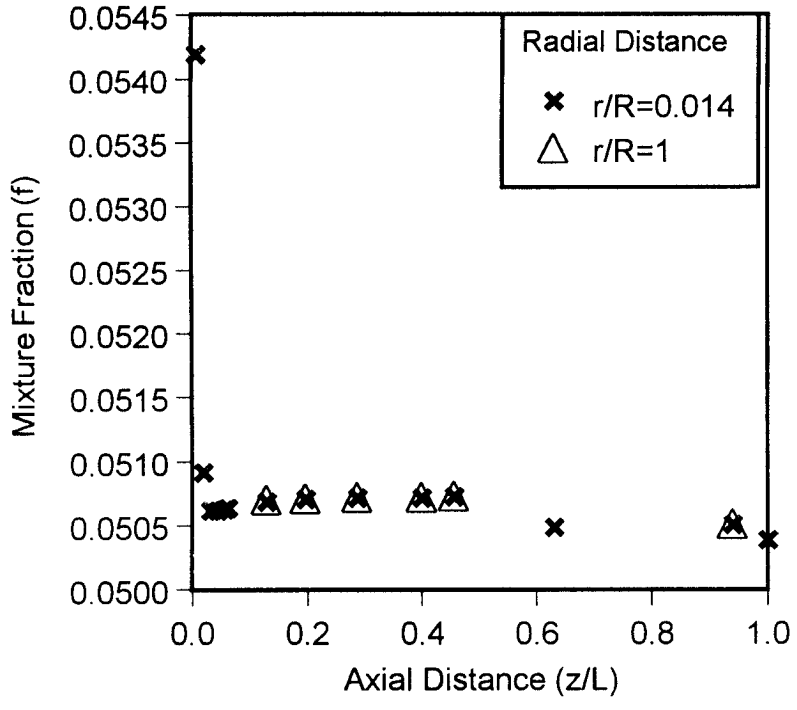

(a)

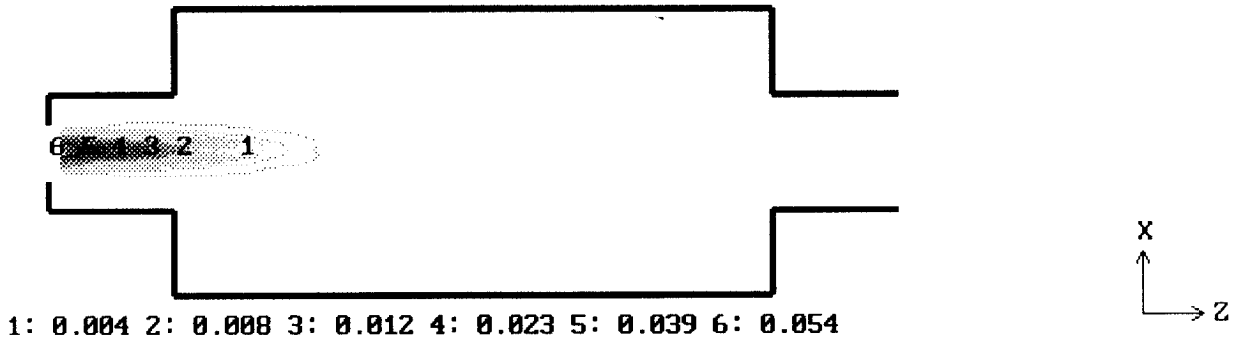

(b)

Figure 4.20 Combustion in Furnace with Optimised PCC
(a) Mixture Fraction (b) Fuel Concentration [kg/m^3]

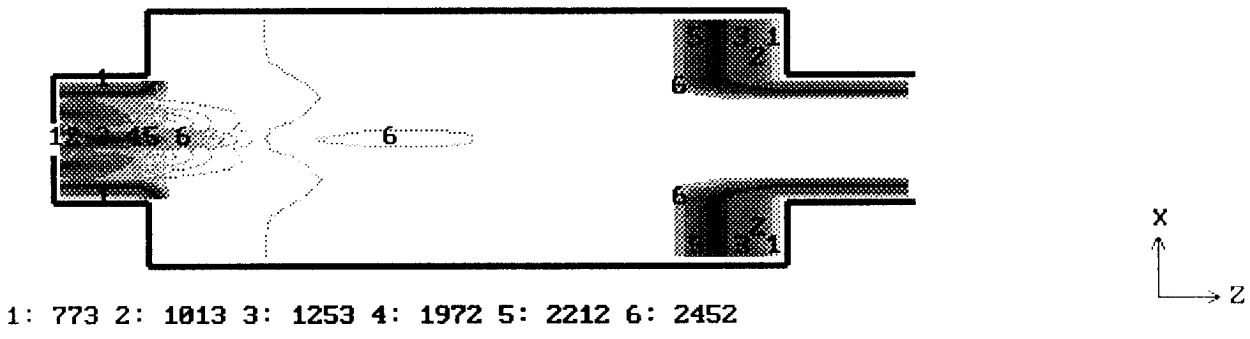

Figure 4.21 Temperature Distribution in Furnace with Optimised PCC in Y-Z plane:

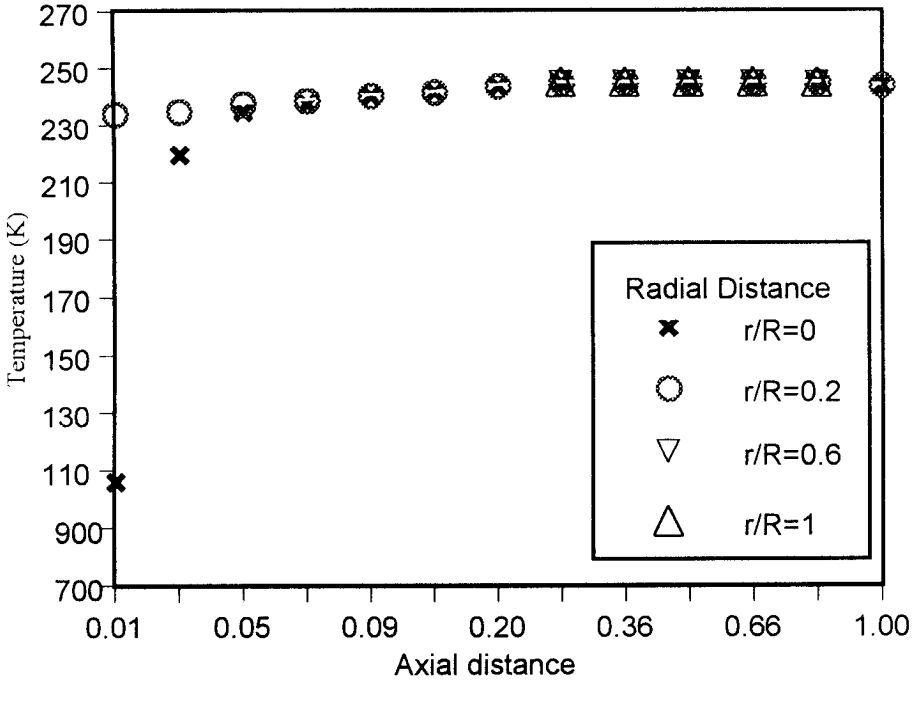

Figure 4.22 Temperature Distribution at various r/R and $\lambda = 1$ in Y-Z plane at $\theta = 0°$and 180°:For Furnace with Optimised PCC

4.3.4 Radiation Field

Figure 4.23 shows the irradiance in the x-, y-, and z-directions for the furnace with an optimised post combustion chamber.

The irradiance in the x or circumferencial irradiance is reduced from around 1.2 to 1.18 MJ/m^3 in the wall and centre line regions. The irradiance in the region r/R=0.69 to 0.375 rises gradually from 1.15 MJ/m^3 upstream to 1.18 MJ/m^3 downstream at the exit of combustor [Fig.4.23 (a)].

The radial or y-directed irradiance is uniform, 1.15 MJ/m^3, from upstream to downstream and from the axis to the wall region. This is most desirable for heating any load in the furnace since radiation accounts for the larger percentage of heat transfer to the load. For the rotary furnace under study, the heat to walls is redistributed to the load as the furnace wall rotates around, thereby increasing the heat to the load.

From Figs.4.15 and 4.23, it is clearly seen that the z-directed or axial irradiance is slightly affected by the optimisation of the post combustion chamber.

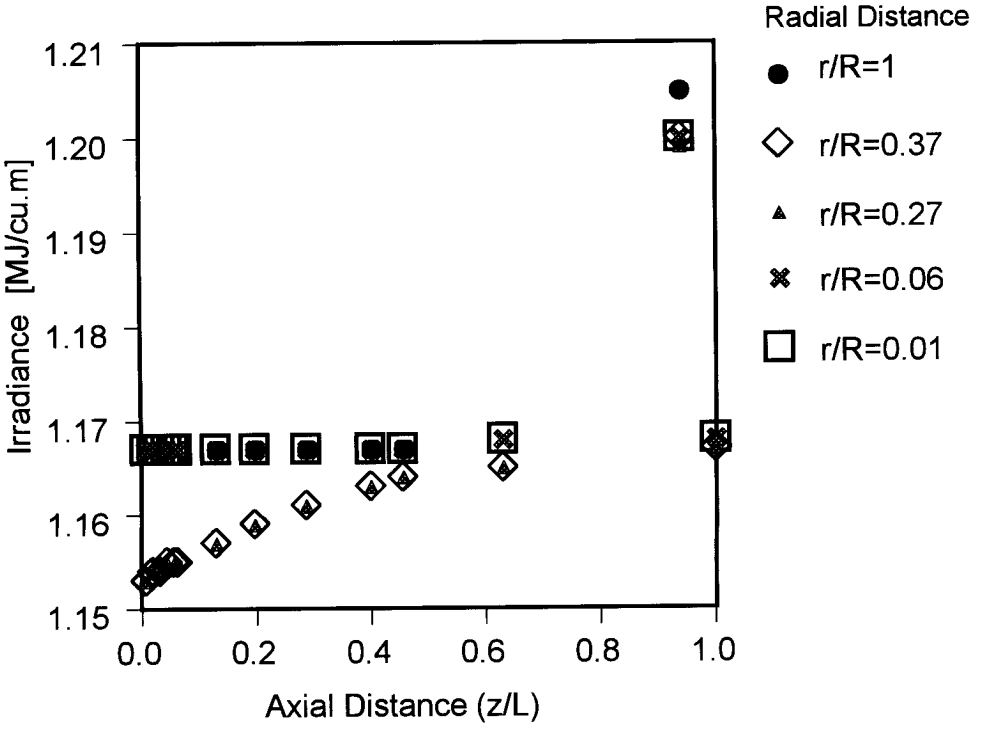

Figure 4.23(a) Radiation Flux Distribution for Furnace with Optimised PCC in the x-direction.

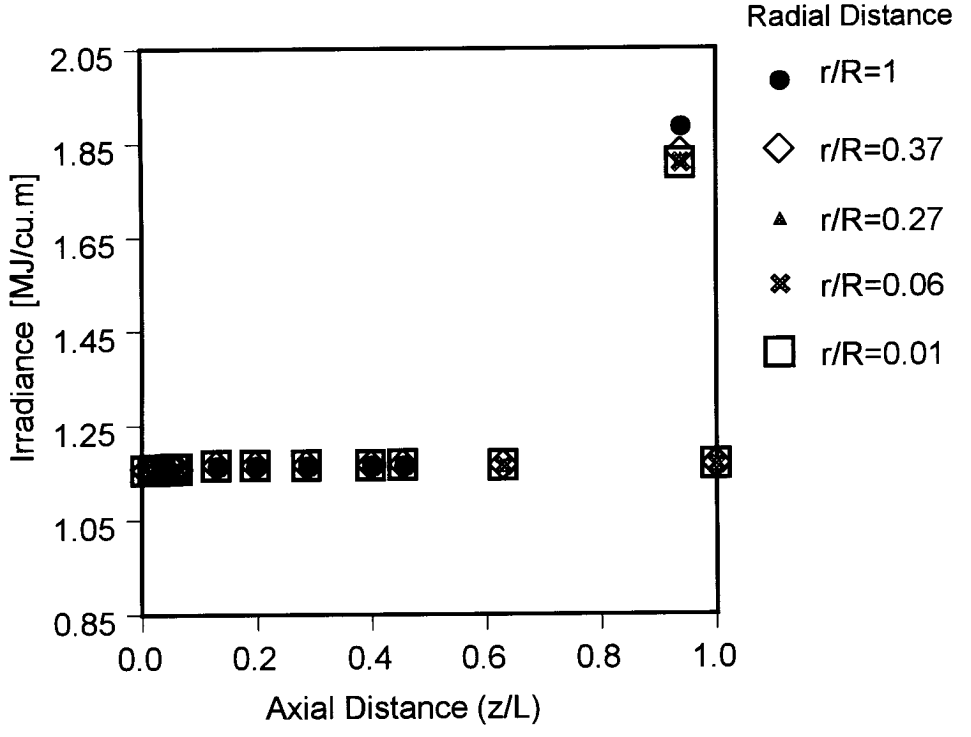

Figure 4.23(b) Radiation Flux Distribution for Furnace with Optimised PCC in the y-direction.

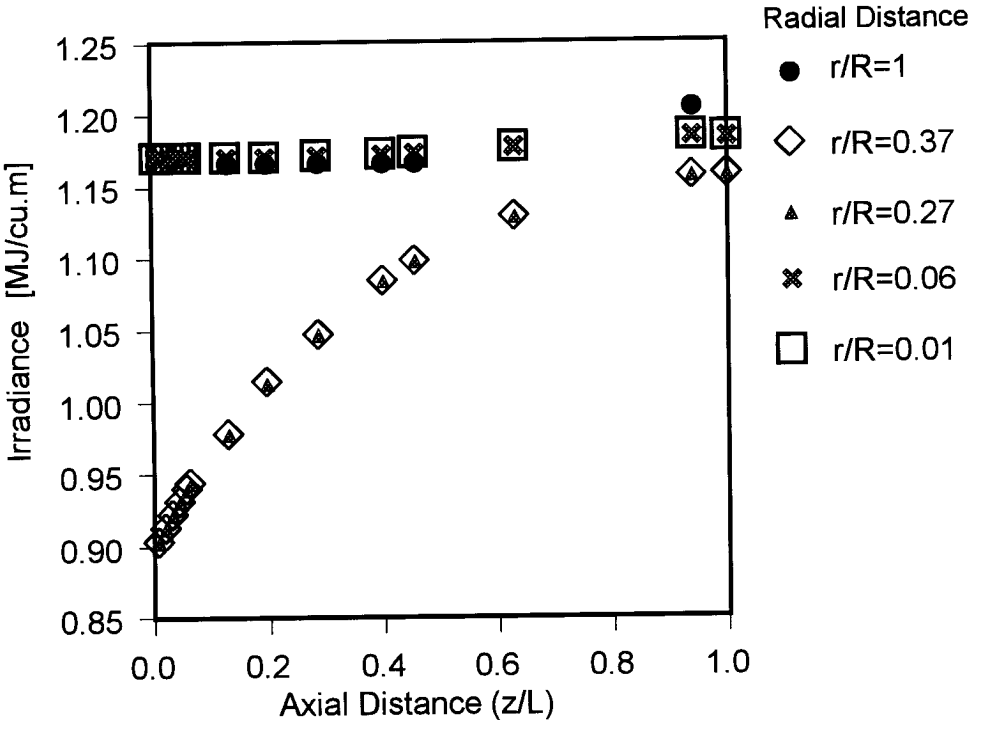

Figure 4.23(c) Radiation Flux Distribution for Furnace with Optimised PCC in the z-direction.

4.4 Heat Flux across Wall of Combustor

The furnace wall has a threefold function. The first is to ensure the necessary refractoriness withstand the effect of the flame and the slagging action of the dust in the furnace atmosphere. Second is heat insulation, and thirdly in certain processes, to provide a means of supplying heat to the stock by re-radiation. It is not always possible to obtain an ideal combination of these properties in any one material. Accordingly, composite wall of firebrick and insulating brick may be used. The effectiveness of the insulating material depends upon the minuteness and uniform distribution of the cells of air present in the material, the heat conductivity of which is extremely low. The temperature at which any insulating material can be used is limited. The higher the temperature the more important the structural losses become, thereby necessitating proper heat protection. When a refractory material forming a furnace lining is backed by insulation, the temperature of the outer surface of the refractory forming the interface between it and the insulation is raised, and so also is the average temperature of the brick. The interfacial temperature is the maximum temperature to which the insulation is heated and this must be less than the limiting temperature for that refractory. The effect of insulation is to bring the refractory within its temperature limit at which it can collapse under load. The insulation of furnaces is extremely important for fuel economy, but should only be undertaken under expert advice.

Figure 4.24 shows the heat flux across the wall of the combustor or furnace for the three cases under study. For the reference case, the heat flux is the highest in the inlet section and lowest in the secondary combustion zone, but has the highest temperature at exit. The furnace with a post combustion chamber has lower heat flux in the inlet section, but the heat flux is higher in the secondary combustion zone than the reference case and characterised by lower exit temperature. The furnace with an optimised post combustion chamber has the lowest heat flux in the inlet section and highest heat flux in the secondary combustion zone, of which region the heat load is located, and depicts the lowest temperature at exit.

The average values for the heat flux across the wall of combustor were 182.42 kW/m^2 for reference case, 182.1 kW/m^2 for the case with normal post combustion chamber, and 180.5 kW/m^2 for the case with an optimised post combustion chamber. The optimised

case gives the high and desirable heat flux transferable to the heat sink in the main space of combustor though it will call for proper insulation for walls in this region.

There is also better use of the heat within the main space of combustor in the case of optimised PCC as depicted in Fig.4.24. At length 3.50 m of the PCC, the maximum temperature in the combustor was achieved far downstream due to probably longer residence time of the mixture in the combustor. Similarly, at length 0 m of the PCC, the maximum temperature in the combustor was also achieved far downstream. However, a better and more or less uniform temperature distribution was achieved in the combustor at the optimum length of 2.75 m of the PCC.

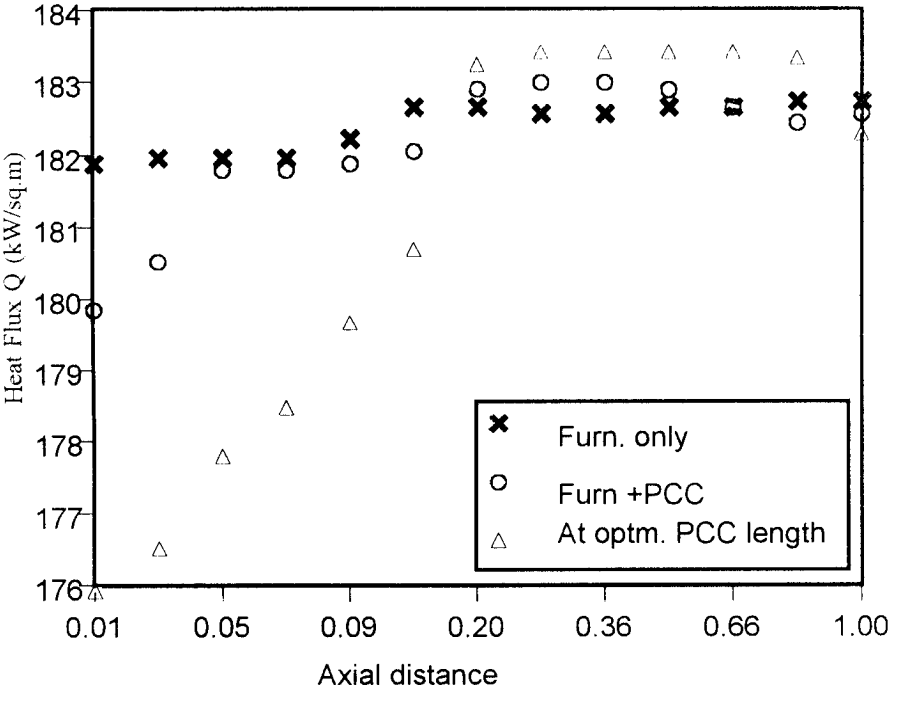

Figure 4.24 Heat Flux across Wall of Furnace at $\lambda = 1$

4.5 Exhaust Gas Loss

The total heat supplied to a furnace is divided into the useful heat, structural loss and exhaust gas loss. For constant fuel consumption and a constant structural loss, loss of useful heat can only take place through the exhaust gas. It is, therefore, important to know the temperature and composition of the gases leaving the furnace in order to ascertain the heat loss through the exhaust gas. Heat loss was quantified by the mass conservation law.

Figure 4.25 shows the heat loss in the exhaust gas for the reference case, furnace with normal PCC and case for furnace with an optimised PCC. The heat loss in exhaust for the case of furnace only is 0.8185 MW and for case with normal PCC is 0.8175 MW. This is equivalent to a recovery of 3.5 MJ/h as useful heat in the furnace, which can raise the slag temperature and improve the lead recovery process. When the length of the PCC is optimised, the heat loss is 0.8165 MW, an equivalent of 7 MJ/h heat recovery.

In terms of heat lost in the exhaust gases, it is noticed that the case of optimised PCC has less loss of heat, which corresponds well with the exhibited lowest temperature at exit. This means that fuel was better used and hence improved combustion efficiency in the case of the furnace fitted with the optimised PCC.

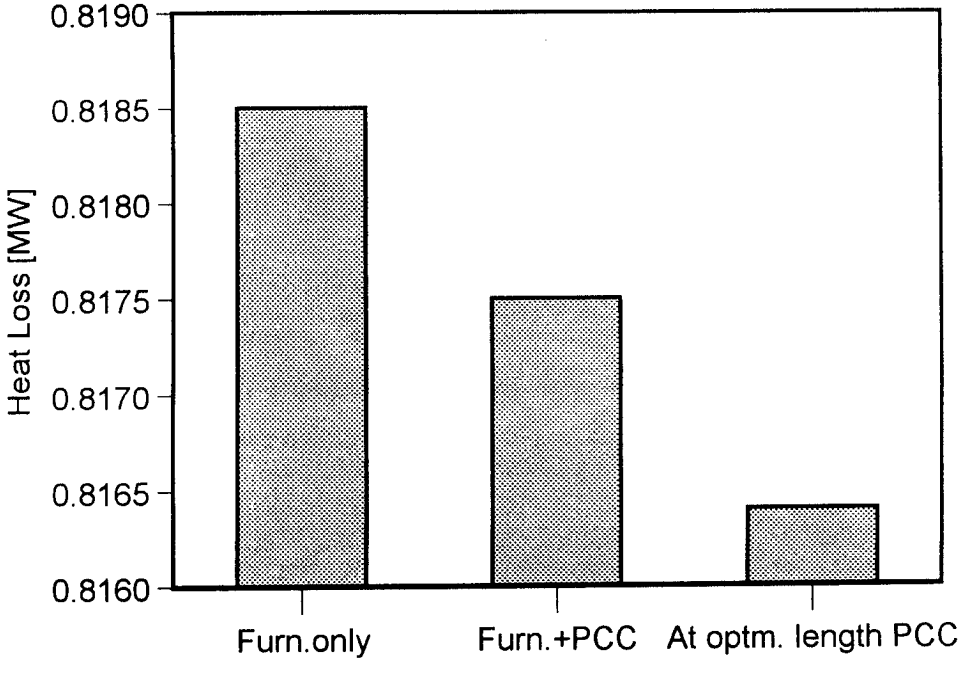

Figure 4.25 Heat Loss through Exhaust Gas at $\lambda = 1$

4.6 Combustion Efficiency

Ideally, all the energy released by combustion should be available for transfer across the boundary of the products system. In practise, not all the chemical reaction energy is made available owing to imperfections of mixing, incomplete combustion by local chilling, unusable heat flow through the system boundary, and so on. Consequently, Eq.1.1 is used to calculate the combustion efficiency. The equation applies for the case where the actual mixture strength can be stoichiometric or fuel weak. In the furnace application under study, the energy is required for direct transfer as heat to the molten lead in the furnace chamber. Consequently, a radiant flame is needed, which tends to favour high-density carbon-hydrogen ratio fuels and efficiency is based on the combined aspects of combustion and heat transfer to the load in the furnace.

Table 4.5 shows the combustion efficiencies for the three situations under study. The combustion efficiency changes by one percent from one case to the other. This rise only makes sense when associated with the heat recovered from the exhaust gases for each case under study as explained in Section 4.5.

Table 4.5 Combustion Efficiency

Parameter	Combustion Efficiency
Furnace only	94.1%
Furnace with normal post chamber	94.3%
Furnace with optimised post chamber	94.6%

4.7 Summary

The effect of the post combustion chamber incorporation in the exhaust system of the rotary furnace and geometric variations of the post combustion chamber size are summarised in Table 4.6. This table does not include either all of the possible geometric variations or their operating range. However, it is in the range of the reference furnace.

The noticeable improvement in the thermal performance of the furnace is made by reduction in excess air, incorporation of the post combustion chamber in the exhaust system of the furnace and largely by optimising the size of the post combustion chamber. Enomoto *et al.* [16] have concluded that excess air is one of the most important factors affecting the thermal performance of a furnace.

Table 4.6 Effect of Post Combustion Chamber on Thermal Performance of Furnace

FIELD	EFFECT	
	NORMAL POST COMBUSTION CHAMBER	OPTIMISED POST COMBUSTION CHAMBER
Flow	Recirculation intensity increases in the region r/R = 0 to 0.5. Mainstream velocity also slightly decreases.	Recirculation intensity increases in the region of r/R = 0 to 0.1 and almost disappears in the wall region.
Combustion and Temperature	The flame becomes long covering three quarters of the furnace length and temperature rise is gradual around centre line in the inlet plane	The flame becomes very short but expands in radial direction and the temperature throughout the furnace high and uniform
Radiation	The circumferencial irradiance significantly reduces in the region of r/R = 0.069 to 1 while the irradiance in the radial direction becomes uniform with the reduction which occurs from r/R = 0.069 to 0.375.Axial irradiance increases steadily downstream.	The irradiance in the radial, circumferencial and axial directions remains same as the case with the normal post combustion chamber.

5.0 CONCLUSIONS AND RECOMMENDATIONS

5.1 Conclusions

Flow and combustion characteristics and heat transfer in the combustor have been numerically modelled resulting in improved combustion efficiency. The focus has been on turbulent combustion. The computation and modelling was done for an industrial methane fired furnace. The primary aim was to achieve an in depth understanding of combustion fundamentals, their applications as well as examine the effects of the existing PCC and an optimised PCC on the overall thermal performance of the furnace.

The benefits of using numerical computer methods in analysing geometric and combustion parameters in a combustor, necessary for improving the performance cannot be overemphasised. The results obtained reveal the usefulness of PCC as a retrofit to the combustor.

Based on the results obtained, the following conclusions can be drawn on the effects of the existing PCC and an optimised PCC on the overall thermal performance of combustor:

1. Low excess air close to stoichiometric is desirable as it increases thermal efficiency. The low excess air results in longer residence time due to low mass flow rate, hence increasing thermal effectiveness and giving higher local heat flux. Little amount of excess air also increases the maximum attainable temperature in the combustor.

2 Incorporation of the post combustion chamber in the exhaust of the furnace elongates the size of recirculation region in the combustor. This also intensifies macro mixing of the fuel, air and combustion products leading to higher temperatures in the combustor at same fuel consumption. The macroscale mixing enhances flame stabilisation and overall mixing in the combustor.

3 The post combustion chamber, especially when optimised causes combustion to occur quite early in the primary combustion zone and therefore increasing the residence time of the combusting mixture and products of combustion in the furnace. The products of combustion then lose their energy while still in the furnace space therefore reducing exhaust gas loss and increasing the useful heat value. High temperatures within the furnace are therefore sustained.

4 The average heat flux across the wall of the combustion chamber is lower in the case with PCC, namely, 182.10 kW/m. It is 182.42 kW/m for the case without PCC. However it is much lower, 180.50 kW/m, when the length of the PCC is optimized.

5 The heat loss in exhaust gases for case without the post combustor is 2946.5 MJ/h. Heat loss in exhaust gases for case with PCC reduces to 2943 MJ/h. This is equivalent to recovery of 3.5 MJ/h as useful heat in the furnace, which raises the temperature in the combustor space and improve the combustion efficiency by 0.21 percent. Temperature rise in the combustor is critical for increment of Lead metal recovery from the slag. When the length of the PCC is optimized the heat loss is further reduced to 2939.5 MJ/h, an equivalent of 7 MJ/h heat recovery. This further reduction in heat loss in exhaust gases improve the combustion efficiency by 0.53 percent. This further gain in heat can translate in a far much improvement in Lead metal recovery.

6 The composite flux method is quite versatile, easy to use, compatible with any Radiation Transfer Equation approximation method. Its equations are handled by the numerical algorithms employed for flow equations. It is accurate and offers acceptable economy.

7 The present work demonstrates that numerical code like PHOENICS can readily be applied for rotary furnace combustion calculations. The features of the predictions are physically plausible.

5.2 Recommendations

Based on this analysis, the following recommendations are made for future work:

1. The main task for future work is validation of the program against reliable experimental data. Such an experimental study will also verify the model predictions of the thermal performance of the furnace.

2. The combustion chamber for the Rotary Furnace under study uses liquid fuel (Heavy Fuel Oil or Kerosene), that is injected, into the chamber by an atomiser. The present model may be used for such applications if the liquid droplets are assumed to

vaporise rapidly. Otherwise the modelling of droplets vaporisation in the primary zone must be included.

3. For more advanced predictions, it is necessary to combine the combustion space model with the energy model for the sink. An example of where coupling between combustion space and sink is strong, is a glass-melting tank.

4. For many applications, the model would need to be extended to include the effect of turbulence-radiation interaction as it affects the uniformity and values of temperature field results.

5. Finally, for the Rotary Furnace at Kabwe the post combustion chamber should be optimised as demonstrated in this study.

APPENDICES

APPENDIX A

Specifications for Rotary Furnace

Table A.1 Specifications for Rotary Furnace

PARAMETER	DETAILS
Dimensions	Diameter 1600 mm Length 4580 mm
Capacity	5.5 tonnes per charge
Feed	Manual
Drive motor	4 kW
Reduction gear box	40:1 and 20:1 ratios
Fuel	Heavy Fuel Oil (HFO), Light Fuel Oil (LFO), Kerosene, Diesel or Gas
Burner	Shiedrop size 4A

NB:

(i) The ends of the rotary furnace are slightly conical shaped.

(ii) The furnace is lined with refractory cement and refractory bricks.

(iii) The burner is located at the charging end.

APPENDIX B

Lead Recovery Data

Table B.1: Results for the Lead Smelting Trials

Trial No.	Dross Charged (kg)	Grade Dross Pb (%)	HFO (Litres)	Soda Ash (kg)	Input Metal (kg)	Output Metal (kg)	Pb Rec. (%)
1.	4000	56.30	563.0	275	2225	1518	67.4
2.	2000	68.00	424.0	125	1360	597	43.9
3.	4000	83.30	500.0	250	3332	2309	69.3
4.	4000	51.20	510.0	200	2048	1270	62.0
5.	4000	81.50	540.0	150	3260	2650	81.3
6.	4000	81.60	542.0	150	3264	2508	76.8
7.	4000	80.00	520.0	100	3200	2390	74.7
TOTALS	26000	71.7	3,599.0	1250	18716	13242	70.8

NB: Only the high cost inputs like HFO fuel and Soda Ash have been depicted here.

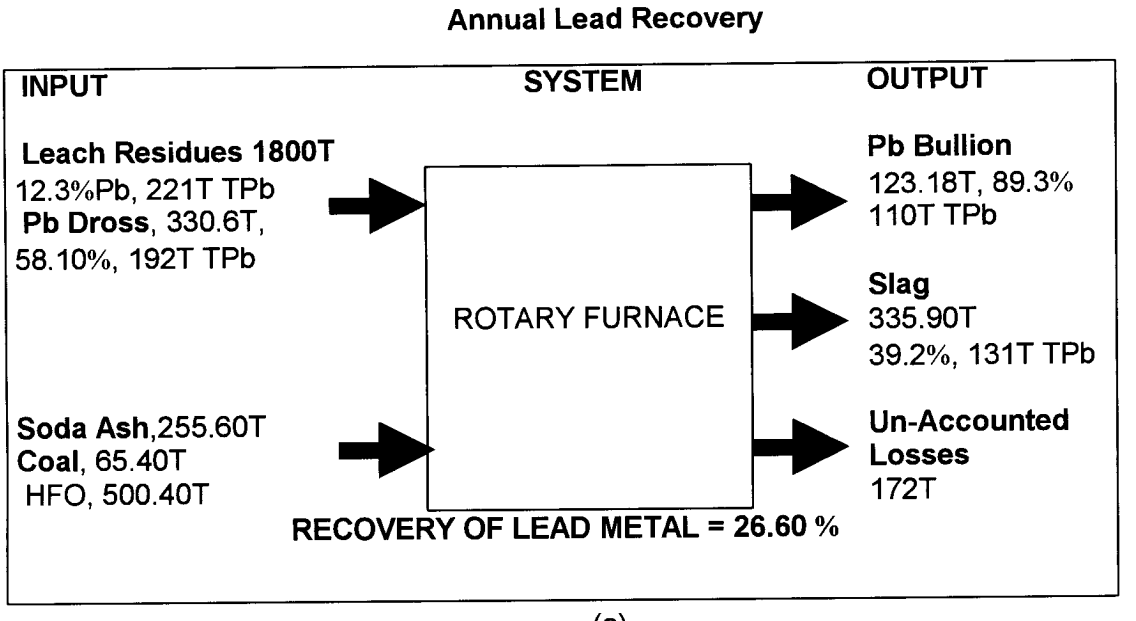

(a)

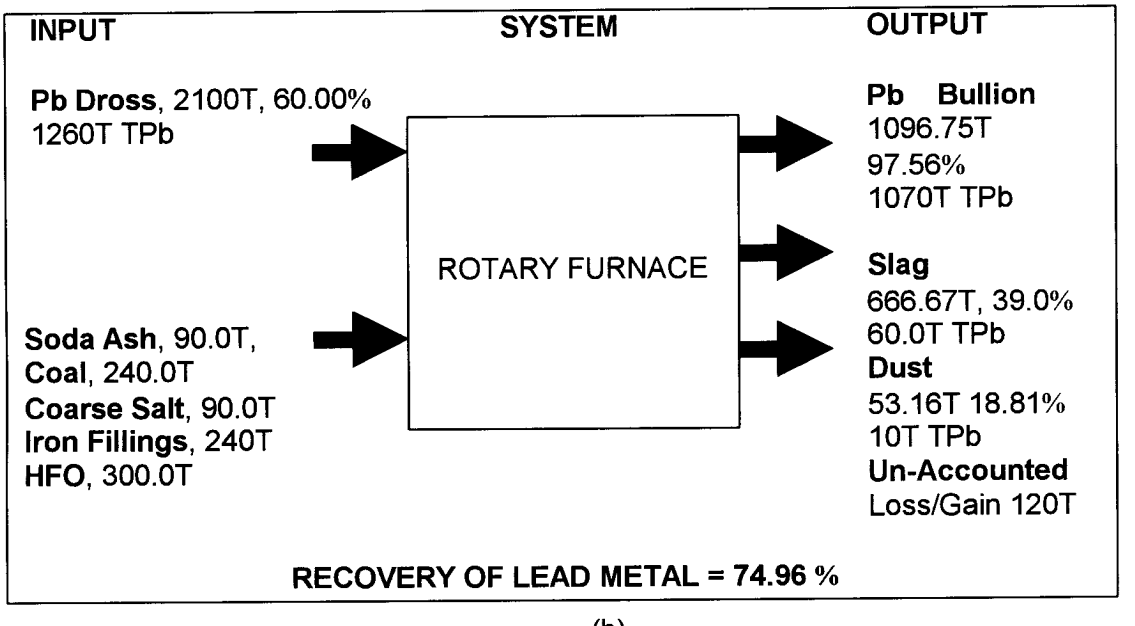

(b)

Figure B.1 (a) Before the PCC Project and (b) After the PCC Project

APPENDIX C

Verification of Numerical Computer Program

The numerical computer code PHOENICS which has been used for the solution of the governing equations is capable of solving the convective transport equation as well as diffusion equations in three-dimension. The verification of this code is best made for a problem for which an exact analytical solution is available. The problem can be solved numerically and the results can be compared with the exact solution. A convection problem is more desirable for verification as it includes flow, which is predominant in this study. Consequently, a one-dimensional convection-diffusion problem is chosen as sketched in Fig. C.1 due to scarcity of analytically solved three-dimensional convection-diffusion problems.

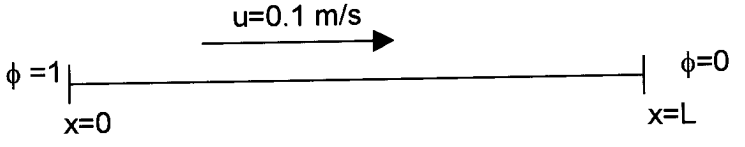

Figure C.1 Test problem for verifying the computer code.

The governing equation and boundary conditions for an arbitrary property ϕ distribution are:

$$\frac{d}{dx}(\rho u \phi) = \frac{d}{dx}\left(\Gamma \frac{d\phi}{dx}\right) \qquad \text{Eq.C.1}$$

ϕ_0=1 at x=0 and ϕ_l=0 at x=L. Also following data applies: L=1.0 m, ρ=1.0kg/m^3, Γ =0.1 kg/m/s
The flow must also satisfy the continuity equation:

$$\frac{d}{dx}(\rho u) = 0 \qquad \text{Eq.C2}$$

An exact analytical solution is obtained from the following equation after substitution of data.

$$\frac{\phi - \phi_0}{\phi_L - \phi_0} = \frac{\exp\left(\rho u x/\Gamma\right) - 1}{\exp\left(\rho u L/\Gamma\right) - 1} \qquad \text{Eq.C.3}$$

Considering the one-dimensional control volume shown in Fig.C.2 and use the notation introduced in Section 2.2, of Chapter Two. Consider a general node P. The neighbouring nodes are identified by W and E and control volume faces by w and e.

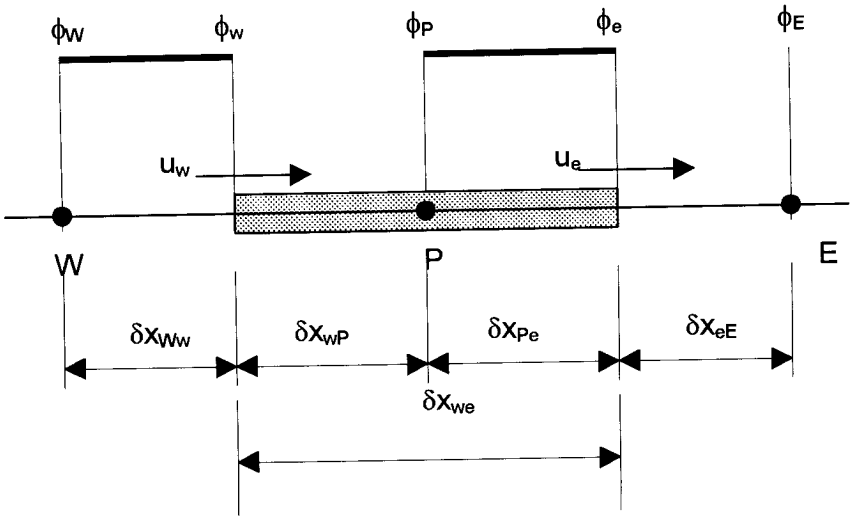

Figure C.2 A control volume around node P.

Integration of transport Eq.C.1 over the control volume Fig.C.2 gives:

$$(\rho\, u\, A\, \phi)_e - (\rho\, u\, A\, \phi)_w = \left(\Gamma\, A\, \frac{\partial \phi}{\partial x}\right)_e - \left(\Gamma\, A\, \frac{\partial \phi}{\partial x}\right)_w \qquad \text{Eq.C.4}$$

And integration of the continuity Eq.C.2 yields:

$$(\rho\ u\ A\ \phi)_e - (\rho\ u\ A\ \phi)_w = 0 \qquad \text{Eq.C.5}$$

To obtain discretised equations for the convection-diffusion problem we must approximate the terms in Eq.C.4. It is convenient to define two variables F and D to represent the convective mass flux per unit area and diffusion conductance at cell faces:

$$F = \rho\, u \qquad \text{and} \qquad D = \frac{\Gamma}{\delta\, x} \qquad \text{Eq.C.6}$$

The cell face values of the variables F and D can be written as:

$$F_w = (\rho u)_w, \qquad F_e = (\rho u)_e \qquad \text{Eq.C.7(a)}$$

$$D_w = \frac{\Gamma_w}{\delta x_{WP}}, \qquad D_e = \frac{\Gamma_e}{\delta x_{PE}} \qquad \text{Eq.C.7(b)}$$

We develop techniques assuming that $A_w = A_e = A$ and employ the central differencing approach to represent the contribution of the diffusion terms on the right hand side. The integrated convection-diffusion Eq.C.4 can now be written as:

$$F_e\phi_e - F_w\phi_w = D_e(\phi_E - \phi_P) - D_w(\phi_P - \phi_w) \qquad \text{Eq.C.8}$$

And the integrated continuity Eq.C.6 as:

$$F_e - F_w = 0 \qquad \text{Eq.C.9}$$

We also assume that the velocity field is 'somehow known', which takes care of the values of F_e and F_w. In order to solve Eq.C.8 we need to calculate the transported property ϕ at the e and w faces. The upwind differencing or 'donor cell' differencing scheme, embodied in PHOENICS by default, is used here to determine these values at the faces.

Since the flow is in the positive direction, $u_w>0$, $u_e>0$ ($F_w>0$, $F_e>0$), the upwind scheme sets

$$\phi_w = \phi_W \text{ and } \phi e = \phi_P \qquad \text{Eq.C.10}$$

and the discretised Eq.C.8 becomes

$$F_e\phi_P - F_w\phi_w = D_e(\phi_E - \phi_P) - D_w(\phi_P - \phi_W) \qquad \text{Eq.C.11}$$

which can be re-arranged as

$$(D_w + D_e + F_e)\,\phi_P = (D_w + F_w)\,\phi_W + D_e\phi_E \qquad \text{Eq.C.12}$$

to give

$$[(D_w + F_w) + D_e + (F_e - F_w)]\,\phi_P = (D_w + F_w)\,\phi_W + D_e\phi_E \qquad \text{Eq.C.13}$$

Identifying the coefficients of ϕ_W and ϕ_E as a_W and a_E the Eq.C.13 can be written in the usual general form

$$a_P\phi_P = a_W\phi_W + a_E\phi_E \qquad \text{Eq.C.14}$$

with central coefficient

$$a_P = a_W + a_E + (F_e - F_w)$$

and neighbour coefficients for $F_w>0$ and $F_e>0$ are

$$a_W = D_w + F_w \quad \text{and} \quad a_E = D_e$$

A numerical solution of the given problem is obtained using five control volumes for the discretisation shown in Fig.C.3 below:

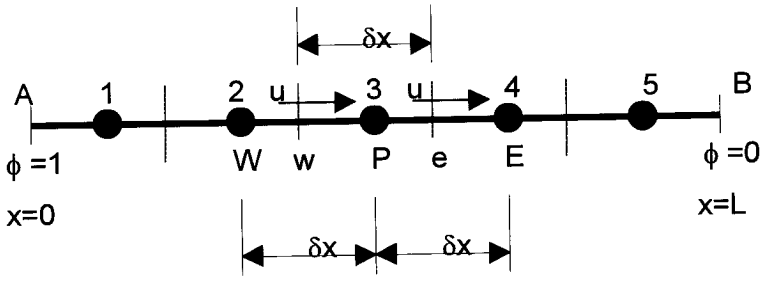

Figure C.3 The grid used for discretisation.

The division gives $\delta x = 0.2$ m. Note that $F = F_e = F_w = \rho u$ and $D = D_e = D_w \Gamma/\delta x$ everywhere. The boundaries are denoted by A and B. The discretisation Eq.C.14 and its coefficients apply at internal nodal points 2, 3, 4, but control volumes 1 and 5 need special treatment since they are adjacent to the domain boundaries.

At the boundary node 1, the use of upwind differencing for the convective terms gives

$$F_e\phi_P - F_A\phi_A = D_e(\phi_E - \phi_P) - D_A(\phi_P - \phi_A) \qquad \text{Eq.C.15}$$

And at node 5

$$F_B\phi_P - F_w\phi_W = D_B(\phi_B - \phi_P) - D_w(\phi_P - \phi_W) \qquad \text{Eq.C.16}$$

At the boundary nodes we have $D_A = D_B = 2\Gamma/\delta x = 2D$ and $F_A = F_B = F$ and as usual the boundary conditions enter the discretised equations as source terms combinations:

$$a_P\phi_P = a_W\phi_W + a_E\phi_E + S_u \quad \text{with} \quad a_P = a_W + a_E + (F_e - F_w) - S_P \qquad \text{Eq.C.17}$$

The neighbour coefficients are then given below.

Node	a_W	a_E	S_P	S_u
1	0	D	-(2D + F)	$(2D + F)\phi_A$
2, 3, 4	D + F	D	0	0
5	D + F	0	-2D	$2D\phi_B$

The coefficients values are summarised in Table C.1 below.

Table C.1 Values of Coefficients

Node	a_W	a_E	S_u	S_p	$a_P = a_W + a_E - S_P$
1	0	0.5	-1.1	1.1	-0.6
2	0.6	0.5	0	0	1.1
3	0.6	0.5	0	0	1.1
4	0.6	0.5	0	0	1.1
5	0.6	0	-1.0	0	0.6

The resulting set of algebraic equations for this example is:

$$
\begin{aligned}
-0.6\,\phi_1 &= 0.5\,\phi_2 + 1.1 \\
1.1\,\phi_2 &= 0.6\,\phi_1 + 0.5\,\phi_3 \\
1.1\,\phi_3 &= 0.6\,\phi_2 + 0.5\,\phi_4 \\
1.1\,\phi_4 &= 0.6\,\phi_3 + 0.5\,\phi_5 \\
0.6\,\phi_5 &= 0.6\,\phi_4
\end{aligned}
\qquad \text{Eq.C.18}
$$

This set of equations can be rearranged in matrix form below:

$$
\begin{bmatrix}
-0.6 & -0.5 & 0 & 0 & 0 \\
-0.6 & 1.1 & -0.5 & 0 & 0 \\
0 & -0.6 & 1.1 & 0 & 0 \\
0 & 0 & -0.6 & 1.1 & -0.5 \\
0 & 0 & 0 & -0.6 & 0.6
\end{bmatrix}
\begin{bmatrix}
\phi_1 \\ \phi_2 \\ \phi_3 \\ \phi_4 \\ \phi_5
\end{bmatrix}
=
\begin{bmatrix}
1.1 \\ 0 \\ 0 \\ 0 \\ 0
\end{bmatrix}
\qquad \text{Eq.C.19}
$$

Using the Gaussian elimination designed in the code used, the solution of the above system is

$$
\begin{bmatrix}
\phi_1 \\ \phi_2 \\ \phi_3 \\ \phi_4 \\ \phi_5
\end{bmatrix}
=
\begin{bmatrix}
0.9337 \\ 0.7879 \\ 0.6130 \\ 0.4031 \\ 0.1512
\end{bmatrix}
$$

The results are at Peclet number Pe = $\rho u \delta x / \Gamma$ = 1.0 x 0.1 x 0.2/ 0.1 = 0.2

Table C.2 Results for the Test Problem for Verifying the Computer Code

Node	Distance	Numerical Solution	Exact solution	Difference	Percentage error
1	0.1	0.9337	0.9387	0.005	0.53
2	0.3	0.7879	0.7963	0.008	1.05
3	0.5	0.6130	0.6224	0.009	1.51
4	0.7	0.4031	0.4100	0.007	1.68
5	0.9	0.1512	0.1505	-0.001	-0.02

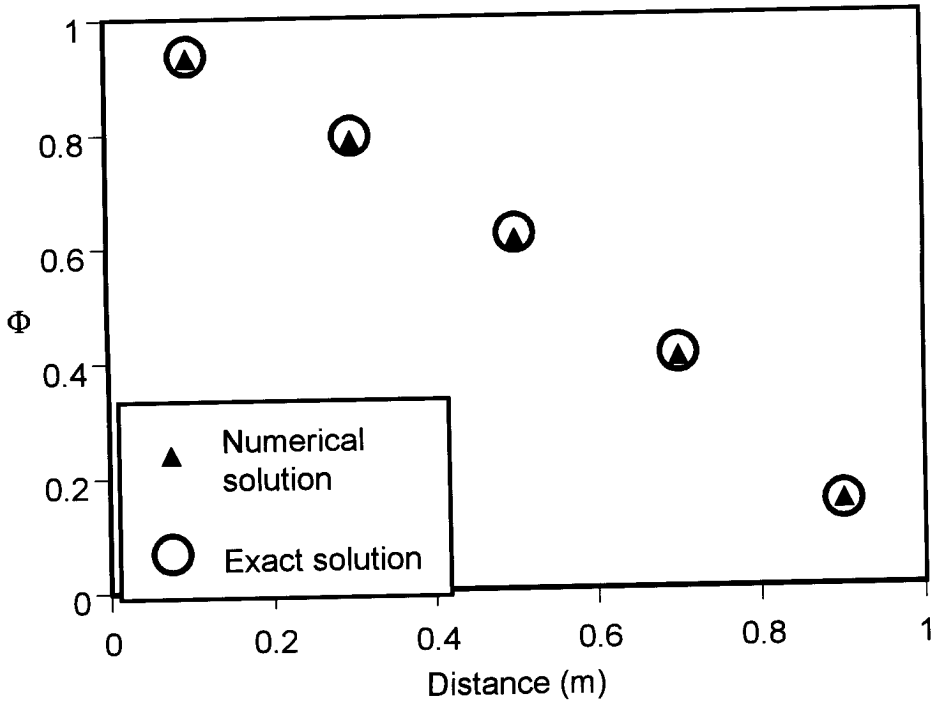

Figure C.4 Numerical and exact solutions of the problem shown in Figure C.1.

The analytical solution is again given by Eq.C.3 and is compared with the numerical, upwind differencing, solution. The results as summarised in Table C.2 and Fig.C.4 show that the upwind differencing scheme produces good results at this Peclet number. More accurate numerical solution can be obtained when larger number of control volumes is employed. However, even with the five control volumes, the accuracy is good enough to verify the validity of the computer code.

APPENDIX D

Verification of Turbulence Model

The Test Problem

The k-ε turbulence model is widely used for the prediction of turbulent flow. It is generally accepted as a good compromise between accuracy and computability. Its validity is examined by comparing the numerical predictions with the experimental data for a specific problem. A recirculating flow is of special interest to this study. Thus, an experimental fire test as shown in Fig.D.1 was chosen as the test case. The experimental data were obtained by the Lawrence Livermore National Laboratory (LLNL) in the test room shown in Fig.D.1. The details of the experiments have been reported in [1]. The fire was at the centre of the floor and clean air was introduced along the floor of the test cell, which is approximated in the model by 0.12 m high and 2 m long slot for air entry, located 0.1 m above the floor. The fire sources in the experiments were a burner, a spray and a pool of fuel in a tray. The products of combustion were extracted near the top of the cell using an axial flow fan through a rectangular 0.65 m square duct placed 3.6 m above the floor as shown in Fig. D.1. The Test designated MOD08 has been selected for CFD modelling here. A spray of isopropyl alcohol from an opposed-jet nozzle located at the centre of the pan was used, and the fuel evaporated quickly to burn like a natural pool fire. The fuel injection rate was 13.1 g/s with a total heat release of 400kW. These data were used to specify burner conditions at the fire source. The measured extraction rate, 400l/s in steady state, was used to specify the outflow. The mass flow rate of air into the domain and the inlet and outlet velocities are calculated as part of the solution.

The walls, the floor and the ceiling of the compartment were of 0.1 m thick refractory. The estimated thermal conductivity, density and specific heat were, respectively, 0.39 W/m/K, 1400 kg/m^3 and 1 kJ/kg/K for the walls and 0.63 W/m/K, 1920 kg/m^3 and 1 kJ/kg/K for the ceiling and the floor. The walls were assumed to be perfectly black for radiation calculations.

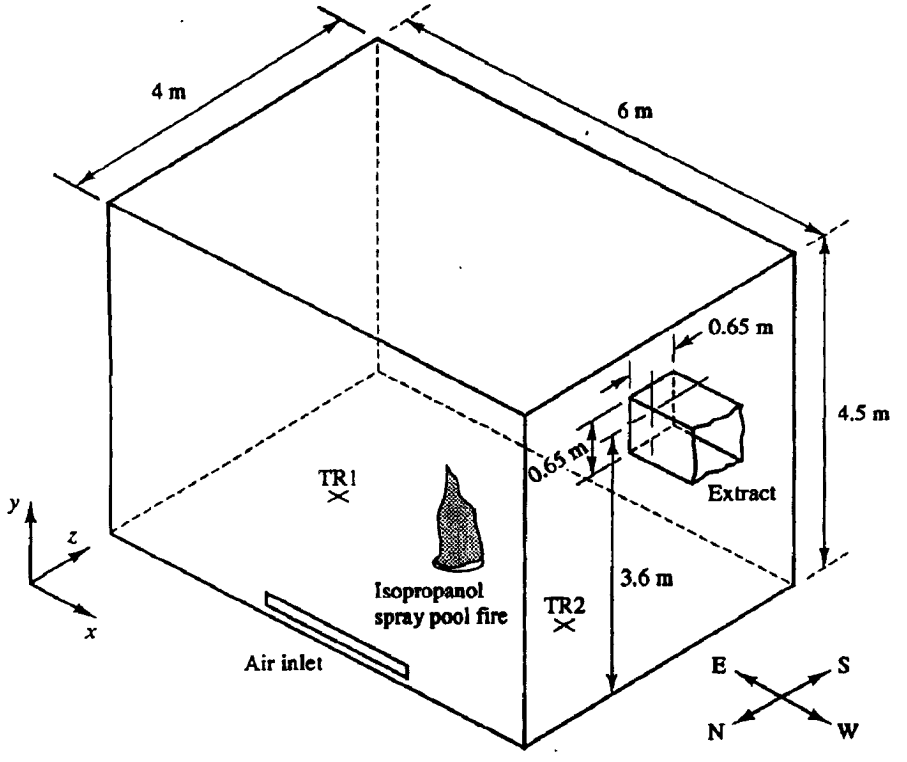

Figure D.1 Schematic diagram of the Lawrence Livermore National Laboratory (LLNL) test cell.

CFD Simulation

The simulation of the aerodynamics and combustion was carried out using a three-dimension CFD procedure based on the SIMPLE algorithm and the hybrid-differencing scheme for discretisation. Turbulence was modelled with the k-ε turbulence model with buoyancy terms and combustion modelling assumed fast chemistry (SCRS). The discrete transfer model of thermal radiation [2] was used to calculate radiative heat transfer. The wall temperatures were obtained from one-dimensional wall heat transfer model. A numerical grid of 14 x 13 x 12, although not very fine, was considered adequate to predict the overall properties of the fire. Further details of the model can be found in [3] and [4]. Some specimen results are presented below.

Specimen Results

Figure D.2 shows the predicted steady state flow pattern in the Y -Z plane at X = 3.25 m. The buoyancy-generated flow is clearly reproduced by the simulation which also shows the entrainment induced by the strong buoyancy effects. The predicted temperature distribution in the Y -Z plane at X = 3.00 m (Fig. D.3) shows the hot gases around the central flame and the formation of a hot layer at ceiling level. The flame structure and tilt due to induced air flow are also clearly visible. Figure D.4 compares the room temperature predictions with the experimental data of [1]. The experimental temperatures were recorded using two thermocouple rakes (TR1-east rake and TR2-west rake) with 15 thermocouples each placed 1.5 m on either side of the fire and located in the central plane as shown in Fig.D.1 The predictions reproduce the main features of the experiments and, despite the coarse grid, the predictions agree well with the experimental data.

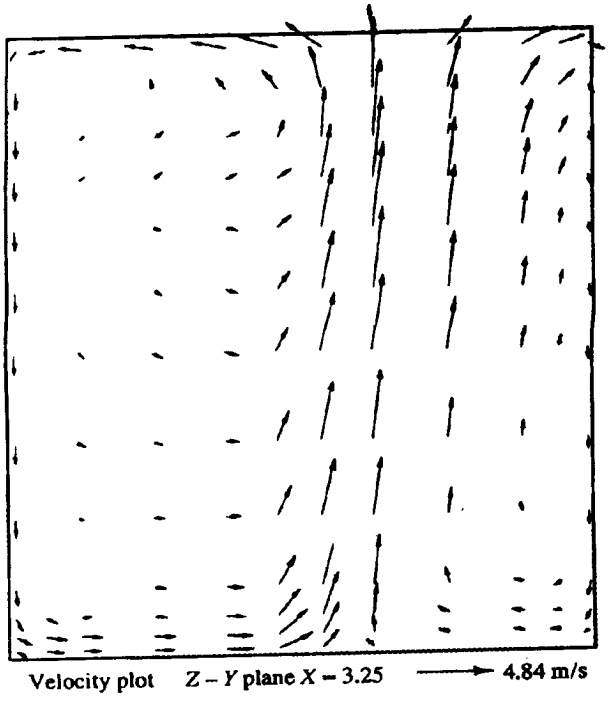

Figure D.2 Predicted flow inside compartment: velocity vectors plots in Z-Y plane , X=5.25 m.

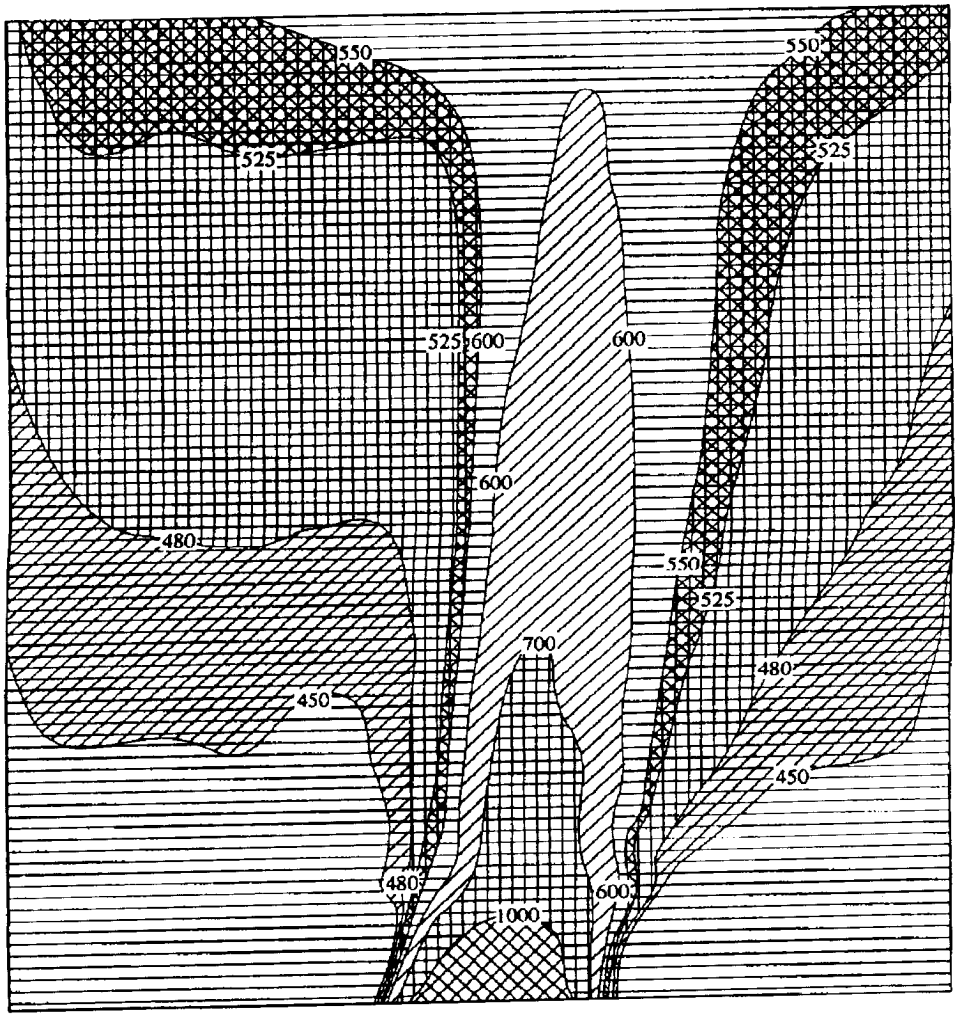

Figure D.3 Predicted Temperature (K) Field in the Y-Z Plane at X=3.00 m.

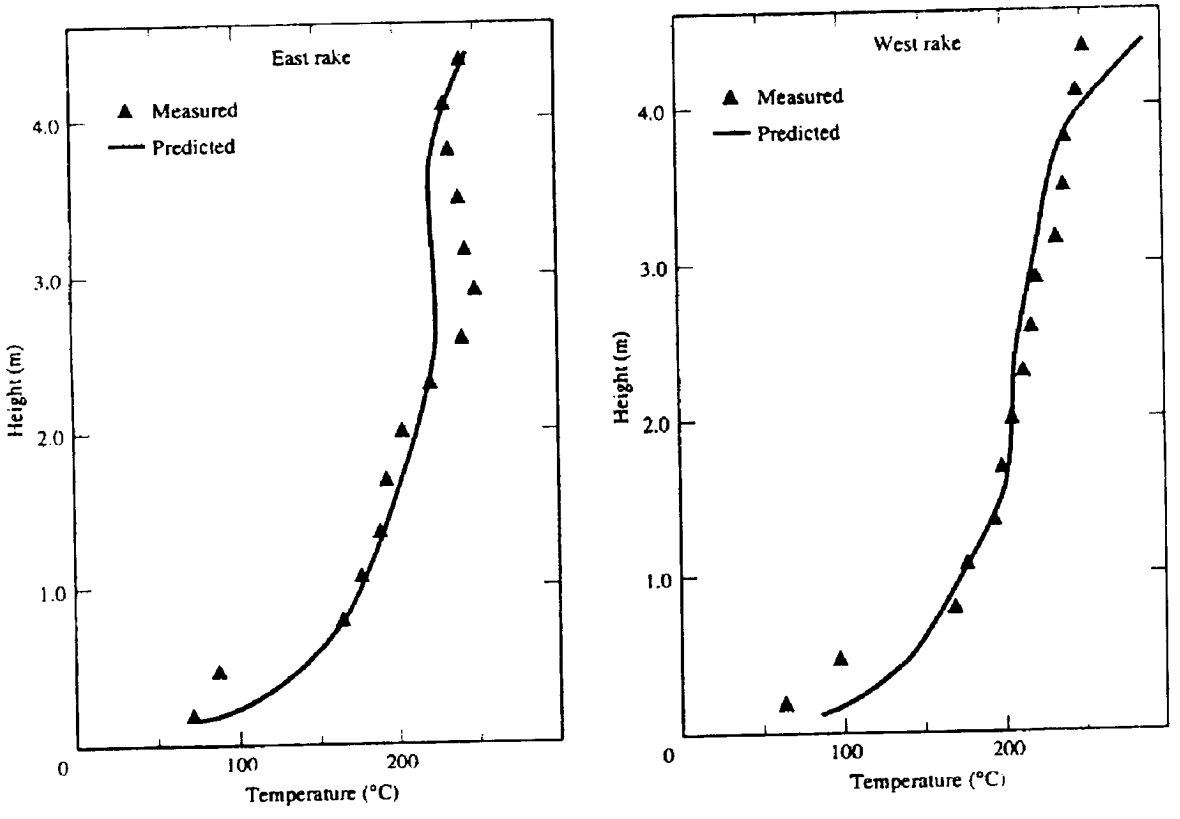

Figure D.4 Comparison of Temperature Distribution between Experiment and k-ε.

APPENDIX E

Relaxation of sources

The solver EARTH sets final discretisation equation for ϕ_p with conventional relaxation factor α as:

$$\phi_p = \alpha.\phi_p + (1 - \alpha).\phi_{po} \qquad \text{Eq.E.1}$$

where ϕ_p is the calculated value of the conservation equation for ϕ in the point P and ϕ_{po} is the old value of ϕ_p from the former iteration cycle. Values for α range from 0 to 1 in the case of under-relaxation. Under-relaxation is required in this steady flow simulation due to the likelihood of exceeding the Courant limit. The Courant limit is the width of the cell divided by the velocity through it. The Courant limit can be so small that a very large number of time steps have to be computed for this flow of practical interest, therefore, entailing unacceptably large computing time. PHOENICS, because of its fully implicit formulation of the finite-volume equations, can take time steps which exceed the Courant limit by many orders of magnitude; and this is why under-relaxation is required in order to ensure smooth convergence of the iterative procedure. The under-relaxation was applied to dependent variables of the differential equations namely: velocity components, density which is varying appreciably with temperature and the effective viscosity which is computed from turbulent quantities. In this code used, the 'false time step' is used for under-relaxation especially for the velocities, since the coefficients for the pressure-correction equation are directly influenced by the increased "stiffness" of the velocity equations, with the consequence that the plausible pressure fields are quickly created. Same under-relaxation was applied to the constant part of the linearised source terms. False time steps have also been used for under-relaxing of turbulent quantities and concentrations of chemical species since the system is undergoing chemical transformations. Values for the false time steps were selected for the variables in question.

The recommended [1] values of the relaxation factor α are given in Table 3.2 below. In this study heavy under relaxation was started with. Typical values used were in the range of 10^{-6} and the convergence was very slow. The values of α were then gradually increased to a range of 0.1 to 0.9 and convergence was attained much more rapidly at 500 to 700 iterations.

When $\alpha > 1$, over-relaxation results, but it is limited to applications involving whole-field linear equation solver not used in this case.

Table E.1 Recommended Relaxation Factors (α)

Φ	U	V	W	P	k	ε	f	M_{fu}	H
$\alpha_{initial}$	0.3	0.2	0.2	1	0.8	0.8	0.9	0.9	0.9
α_{max}	0.7	0.6	0.6	1	1.0	1.0	1.0	1.0	1.0

REFERENCES

CHAPTER ONE

[1] Hinze, J. O. Turbulence. Second Edition, McGraw-Hill, New York, 1975.

[2] Jones, W. P. Models for Turbulent Flows with Variable Density and Combustion, in Prediction Methods for Turbulent Flows. Edited by W. Kollmann, Hemisphere Publishing Corp., Washington, pp. 379-422, 1980.

[3] Tae-Ho, S. Simulation of Flow, Combustion and Heat Transfer in a Two-Dimensional Natural Gas-Fired Industrial Furnace. Thesis, Ph.D. Purdue University. pp. 1-4, 1986.

[4] Khalil, E. E., Spalding, D. E and Whitelaw, J. H. The Calculation of Two Dimensional Flow Properties in Two-Dimensional Furnaces. Int. J. Heat and Mass Transfer, Vol. 18, pp. 775-791, 1975.

[5] Pai, B. R., Michefelder, S. and Spalding D. B. Prediction of Furnace Heat Transfer with Three-Dimensional Mathematical Model. Int. J. Heat Mass Transfer, Vol. 23, pp. 5771-580,1978.

[6] Serag-Eldin, M. A. and Spalding, D. B. Computation of Three-Dimensional Gas-Turbine Combustion Chamber Flows. J. Engineering for Power, Vol. 101, pp. 327-336, 1979.

[7] Khalil, E. E. Flow and Combustion Characteristics of Turbulent Reacting Flames, in Mechanics of Combustion Systems, ASME, New York, pp. 217-225, 1981.

[8] Abou-Ellail, M. M. M., Goodman, A. D., Lockwood, F. C. and Megahed, I. E. A. Description and Validation of a Three-Dimensional Procedure for Combustion Chamber Flows, in Progress in Astronautics and Aeronautics, Turbulent Combustion, Volume 58, AIAA, New York, pp. 163-190, 1978.

[9] Abou Ellail, M. M. M. and Elkotb, M. M. Prediction and Measurement of Flow and Heat Transfer in Motored Diesel Engine Swirl Chamber. Third Symposium on Turbulent Shear Flows, Sep. 9-11, University of California, Davis, pp. 5.1-5.7, 1981.

[10] Launder, B. E. and Spalding, D. B. Mathematical Models of Turbulence. Academic Press, 1972.

[11] Khalil, E. E. Modelling of Furnaces and Combustors. Abacus Press, Hampshire, 1982.

[12] Spalding, D. B. Development of the Eddy-Break-Up Model of Combustion, in The Sixteenth Symposium (International) on Combustion, The Combustion Institute, Pittsburgh, pp. 1657-1663, 1973.

[13] Pope, S. B. The Implications of the Probability Equations for Turbulent Combusting Flows, Combustion and Flame, Vol. 29, pp. 235, 1977.

REFERENCES:

[14] Jones, W. P. and Whitelaw, J. H. Calculation Methods for Reacting Flow, in Prediction of Turbulent Reacting Flows in Practical Systems, ASME, New York, pp. 9-22, 1981.

[15] Bray, K. N. C. Turbulent Flows with Premixed Reactants, in Topics in Applied Physics. Vol. 44, edited by P. A. Libby and F. A. Williams, Springer-Verlag, New York, pp. 115-183, 1980.

[16] Borghi, R. Models of Turbulent Combustion for Numerical Predictions, in Prediction Methods for Turbulent Flows. Edited by W. Kollmann, Hemisphere Publishing Corp., Washington, pp. 423-458, 1980.

[17] O'Brien. The Probability Density Function (pdf) Approach to Reacting Turbulent Flows, in Topics in Applied Physics. Vol. 44, edited by P. A. Libby and F. A. Williams, Springer-Verlag, New York, pp. 185-218, 1980.

[18] Spalding, B. D. Combustion and Mass Transfer. Pergamon Press, London, 1979.

[19] Viskanta, R. Radiative Heat Transfer, Fortschritte der Verfahrenstechnik. Vol. 25A, pp. 51-81, 1984.

[20] Hottel, H. C. and Sarofim, A. F. Radiattive Transfer. MacGraw Hill, New York, 1967.

[21] DeMarco, A. G. and Lockwood, E. C. A New Flux Model for the Calculation of Radiation in Furnaces, Italian Flame Day, La Rivisa del combustibili', Vol. 29, No. 5-6, pp. 184-96, 1975.

[22] Chandrasekhar, S. Radiative Transfer. Dover Publications, New York, 1960.

[23] Menguc, M. P. and Viskanta, R. Radiative Transfer in Three-Dimensional Rectangular Enclosures Containing Inhomogeneous, Anisotropic Scattering Media. J. Quant. Spectrosc. Radiat. Transfer. Vol. 33, pp. 533-549, 1985.

[24] Crosbie, A. L. and Viskanta, R. Effect of Band or Line Shape on the Radiative Transfer in a Non-Gray Planar Medium. J. Quant. Spectrosc. Radiative Transfer, Vol. 10, pp. 487-509, 1970.

[25] Grant, I. P. On the Representation of Frequency Dependence in the Radiative Transfer. J. Quant. Spectrosc. Radiat. Transfer. Vol. 105, pp. 227-243, 1965.

[26] Abu-Romis, M. M. and Tien C. L. Appropriate Mean Absorption Coefficients for Infrared Radiation of Gases, J. Heat Transfer, Vol. 89, pp. 321-327, 1967.

[27] Goody, R. M. Atmospheric Radiation, Clarendon University Press, Oxford, 1964.

[28] Chan, S. H. and Tien C. L., Total Band Absorptance of Non-Isothermal Infrared-Radiating Gases, J. Quant. Spectrosc. Radiat. Transfer. Vol. 9, pp. 1261-1271, 1969.

REFERENCES:

[29] Buckius, R. O. and Tien, C. L. Infrared Flame Radiation. Int. J. Heat Mass Transfer, Vol. 20, pp. 93-106, 1977.

[30] Ministry of Power, Efficient Use of Fuel, London, Her Majesty's Stationery Office, pp. 453, 1958.

[31] Trinks, W. and Mawihinney, M. H. Industrial Furnaces. New York; John Wiley and Sons Inc., Vol. 2: 4th ed., pp. 179, 181, 193, 1961.

[32] Carroll, C. Energy Management for Industrial Furnaces. New York: John Wiley & Sons Inc., pp. 22, 43, 1980.

[33] Stephen, R. T. An Introduction to Combustion, Concepts and Applications. New York, McGraw-Hill, Inc., pp. 51-55, 1996.

[34] Mutoka, W. M., Musonda, G., Kaacha, B. and Njovu, E. Lead-Smelting. Report: Kabwe Power and Metals Ltd, Kabwe, March.1998.

[35] Khalil, E. E., Hutchinson, P. and Whitelaw, J. H. The Calculation of Flow and Heat Transfer Characteristics of Gas-Fired Furnaces. Imperial College Report FS/79/15, 1979.

[36] Jones, W. P. and McGuirk, J. J. Mathematical Modelling of Gas-Turbine Combustion Chamber, Advisory Group for Aerospace Research and Development, Conference Proceedings No. 275, pp. 4.1-4.11, 1979.

[37] Enomoto, Y. W. Tsai and Essenhigh, R. H. Heat Transfer in a Continuos Model Furnace: A Comparison of Theory and Experiment, ASME Paper No. 75-HT-5, pp. 12-13.

[38] Patankar, S. and Spalding, D. B. Simultaneous Predictions of Flow and Radiation for Three-Dimensional Flames, in Heat Transfer in Flames, edited by N. Afgan *et al.,* New York, pp. 73-94, 1974.

[39] Goodger, E. M. Combustion Calculations, Theory, Worked Examples and Problems. London: The MacMillan Press

REFERENCES:

CHAPTER TWO

[1] Rhine, J. M. and Tucker, R. J. Modelling of Gas-Fired Furnaces and Boilers, and other Industrial Heating Processes, London, McGraw Hill Book Company, pp. 2-3, 1991.

[2] Khalil, E. E. Modelling of Furnaces and Combustors. Cairo, Abacus Press, pp. 1-3, 13, 1982.

[3] Versteeg, H. K. and Malalasekera, W. An Introduction to Computational Fluid Dynamics, The Finite Volume Method. Malaysia: Longmans. Reprint, pp. 11, 21-24, 212-213, 1996.

[4] Bird, R. B., Steward, W. E. and Lightfoot, E. N. Transport Phenomena. J. Wiley and Sons, New York, 1960.

[5] Hirschfelder, J. O. Curtis, C. F. and Bird, R. B. Molecular Theory of Gases and Liquids. Wiley, New York, 1964.

[6] Wamatz, J. Maas, U. and Dibble, R. W. Combustion *Physical and Chemical Fundamentals, Modelling and Simulation, Experiments, Pollutant Formation.* Springer-Verlag, New York, 1996.

[7] Lamers, A. P. G. G. Physical Models and Numerical Methods for Fluid Dynamical Problems. Lecture Notes Series. Technology University of Eindhoven, Netherlands, Lecture 4.S.410, pp. 7, 46, 152-164, 1999.

[8] Reynolds, O. An Experimental Investigation of the Circumstances which Determine whether the Motion of Water shall be Direct or Sinuous, and the Law of Resistance in Parallel Channels. Phil. Trans. Royal Society of London, 174, pp. 935-982, 1883.

[9] Tennekes, H. Simple Model for the Small-Scale Structure of Turbulence. Physics of Fluids, 11, pp. 669-671, 1968.

[10] Townsend, A. A. On the Fine-Scale Structure of Turbulence. *Proceedings of the Royal Society of London Series* A. 208, pp. 534-542, 1951.

[11] Stephen, R. Turns. An Introduction to Combustion, *Concepts and Applications.* Mc-Graw Hill. New York, pp. 363, 1996.

[12] Libby, P. A. and Williams, F. A. Fundamental Aspects, in *Turbulent Reacting Flows.* (P.A. Libby, and F. A. Williams, eds.) Springer-Verlag, New York, 1980.

[13] Speziale, C. G. Analytical Methods for the Development of Reynolds-Stress Closure in Turbulence. *Annu. Rev. Fluid Mech.* Vol. 23, pp. 107-157, 1991.

[14] Lazonova, M., Markov, D. and Denev, J. Turbulent Modelling in Fluid Dynamics. Lecture course, Computational Fluid Dynamics Centre. Technical University. Sofia, pp. 17-18, 1997.

REFERENCES:

[15] Reynolds, O. On the Dynamical Theory of Incompressible Viscous Fluids and the Determination of the Criterion. Philosophical Transactions of the Royal Society of London, Series A, Vol. 186, pp. 123, 1895.

[16] Jones, W. P. and Whitelaw, J.H. Calculations Methods for Reacting Turbulent Flow, in Prediction of Turbulent Reacting Flows in Practical Systems. ASME, New York, pp. 9-22, 1981.

[17] Favre, A. Statistical Equations of Turbulent Gases in Problems of Hydraulics and Continuum Mechanics. (Society of Industrial and Applied Mechanics, Philadelphia), pp. 31, 231, 1969.

[18] Hinze, J. O. Turbulence. Second edition, McGraw-Hill, New York, 1975.

[19] Bradshaw, P., Cebeci, T. and Whitelaw, J. H. Engineering Calculation Methods for Turbulent Flow, Academic Press, London, pp. 50-51, 1981.

[20] Anderson, D. A., Tannehill, J. C. and Pletcher, R. H. Computational Fluid Mechanics and Heat Transfer, Hemisphere Publishing Corporation, Taylor and Francis Group, New York, 1984.

[21] Boussinsq, V. J. The rie de le coulement tourbilleant. Mem. Press. Acad. Sci. 23, pp. 46, 1877.

[22] Launder, B. E., Morse, A. P., Rodi, W. and Spalding, D. B. The prediction of Free Shear Flows, a Comparison of Six Turbulence Models. NASA Report SP-311, pp.361, 1972.

[23] Schlichting, H. Boundary Layer Theory. 7th ed., McGraw-Hill, New York, 1979.

[24] Launder, B. E. and Spalding, D. B. The Numerical Computations of Turbulent Flows, Computer methods in Applied Mechanics and Engineering, Vol. 3, pp. 269-289, 1974.

[25] Launder, B. E. and Spalding, D. B. Mathematical Models of Turbulence. Academic Press, London, 1972.

[26] Bradshaw, P. (ED): Topics in Applied Physics Turbulence, 12, Springer-Verlag, 1976.

[27] Jones, W. P. Models for Turbulent Flows with Variable Density and Combustion, in Prediction Methods for Turbulent Flows. Edited by W. Kollmann, Hemisphere Publishing Corp., Washington, pp. 379-422, 1980.

[28] Khalil, E. E., Spalding, D. E. and Whitelaw, J.H. The Calculation of Local Flow Properties in Two-dimensional Furnaces, Int. J. Heat Mass Transfer. Vol. 18, pp. 5-12, 1975.

[29] Dimiter, M., Dobrin, T. and Stefan, Y. CFD Support in Combustion Modelling. Edited by Assoc. Prof. Peter, S. Ph.D. D. Computational Fluid Dynamic Centre, pp. 7-8, 1997.

[30] Chisale, P. C. Characteristics of Methane Swirl Combustion with Pre-Heated Air. Ph.D. Thesis, Kobe University, pp. 28-35, 1997.

REFERENCES:

[31] Spalding, D. B. Mixing and Chemical Reaction in Steady Confined Turbulent Flames. *Thirteenth Symposium (International) on Combustion,* The Combustion Institute, pp. 649-657, 1971.

[32] Hutchinson, p., Khalil, E. E., Whitelaw, J. H. and Wigley, G. The Calculation of Furnace Flow Properties and their Experimental Verification. J. Heat Transfer. **98,** pp. 276, 1976.

[33] Pope, S. B. The Calculation of the Flows Behind Bluff Bodies With and Without Combustion. Ph.D. Thesis. London University, 1976.

[34] Khalil, E. E. Flow and Combustion in Axisymmetric Furnaces. Ph.D. Thesis, London University, 1977.

[35] Bilger, R. A. Note on Favre Averaging in Variable Density Flows. Combustion Science and Technology, **11**, pp. 215, 1975.

[36] Bray, K. N. C. Kinetic Energy of Turbulence in Flames. Proc. AGARD Panel Meeting, April 1974: See also: AASU report, pp. 332, 1974.

[37] Khalil, E. E. Aerodynamic and Heat Transfer Characteristics of Axisymmetric Confined Gaseous-Flames. Proc. 6th Int. Heat Transfer Conference, pp. 25, 1978.

[38] Khalil, E. E. Numerical Computations of Turbulent Reacting Combustor Flows in Numerical Methods in Heat Transfer, edited by Lewis et al (Pineridge Press), pp. 548, 1981.

[39] Pun, W. M. and Spalding, D. B. A Procedure for Predicting the Velocity and Temperature Distributions in Confined, Steady, Turbulent, Gaseous Diffusion Flames, *Proc. Int. Astronautical Federation Meeting, Belgrade,* 1967.

[40] Lockwood, F. C and Naguib, A. S. Combustion and Flame. **24**, 1975.

[41] Lockwood, F. C. and Monib, H. A. Fluctuating Temperature Measurements in a Heated Round Free Jet, Combust. Sci. Technol., Vol. 22, pp. 183, 1980.

[42] Pope, S. B. PDF Methods for Turbulent Reacting Flows, Prog. Energ. Combust. Sci., Vol. 11, pp. 119-192.

[43] Jones, W. P. Models for Turbulent Flows with Variable Density, in W. Kollmann (ed.) *Prediction Methods for Turbulent Flows.* VKI Lecture Series, pp. 378-421 Hemisphere Publishing Corporation, New York, 1979.

[44] Magnussen, B. F. and Hiertager, H. 16th Symposium (Interl.) and Combustion, The Combustion Institute, pp. 719, 1976.

[45] Borghi, R. Turbulent Combustion Modelling. Prog. Energy Combust. Sci., Vol. 14, pp. 245-292, 1988.

REFERENCES:

[46] Gosman, A. D., Lockwood, F. C. and Salooja, A. P. The Prediction of Cylindrical Furnaces Gaseous Fuelled with Premixed and Diffusion Burners, *Seventeenth Symposium (International) on Combustion,* The Combustion Institute, pp. 747-760, 1978.

[47] Tae-Ho Song, Simulation of Flow, Combustion and Heat Transfer in a Two-Dimensional Natural Gas-Fired Industrial Furnace. Thesis, Ph.D. Purdue University, pp. 97-103, 180, 1986.

[48] Hottel, H. C. and Sarofim, A. F., Int. J. Heat Mass Transfer, vol. **8** York, MacGraw pp. 1153, 1965.

[49] Afgan, N. H. and Beer, J. M. Heat Transfer in Flames; International Centre for Heat and Mass Transfer, Washington D.C., pp. 184, 1974.

[50] Viskanta, R. Advances in Heat Transfer. Vol. **3,** pp. 175, 1966.

[51] Rhine, J. M. and Tacker, R. J. Modelling of Gas-fired Furnaces and Boilers. McGraw Hill Book Company, pp. 214, 1991.

[52] Lockwood, F.C. and Shah, N. G. Eighteenth Symp. (Intl) on Combustion, The Combustion Institute, Pittsburgh, pp. 1405-1414, 1981.

[53] Hottel, H. C. and Cohen, E. S. Radiant Heat Transfer in a Gas Filled Enclosure. Allowance for Non-Uniformity of Gas Temperature. American Institute of Chemical Engineers. J., 4, pp. 3, 1958.

[54] Hottel, H. C. and Sarofim, A. F. Radiattive Transfer. MacGraw Hill, New York, 1967.

[55] Steward, F. R. and Cannon, P. The Calculation of Radiation Heat Flux in a Cylindrical Furnace using the Monte Carlo Method. Intl. J. Heat Mass Transfer, 14, pp. 245-262,1971.

[56] Viskanta, R. Radiation Transfer and Interaction of Convection with Radiation Heat Transfer. Chapter in "Advanced Heat Transfer. Vol. 3" Editors: Irvine, T.F. and Hartnett, J. P., 1966.

[57] Siddall, R. G. The Flux Method of Furnace Heat Transfer Analysis. Fourth Symp. On Flames and Industry. Brit Flame Res. Com. and Inst. Fuel at Imperial College, Sept. 1972.

[58] Siegel, R. and Howell, J. R. Thermal Radiation Heat Transfer. MacGraw Hill, New York, 1981.

[59] DeMarco, A. G. and Lockwood, F. C. A New Flux Model for the Calculation of Radiation in Furnaces. Italian Flame Day, La Rivisa dei Combustibili, Vol. 29, No. 5-6, pp. 184-196, 1975.

CHAPTER THREE

[1] Antonopoulos, K. A Comparison of Finite Difference And Finite Element Methods of Solution of Convective Transport Equation. MSc. Thesis. London University, 1975.

[2] Patankar, S. V. and Spalding, D. B. Heat and Mass Transfer in Boundary Layer. (Academic Press), 1967.

[3] Spalding, D. B. Germix-A General Computer Program for Two-Dimensional Parabolic Phenomena. (Pergamon Press), 1977.

[4] Spalding, D. B. Combustion as Applied to Engineering. J. Inst. Fuel, Vol. 44, pp. 196-203, 1971.

[5] Patankar, S. and Spalding, D. B. Simultaneous Predictions of Flow Patterns and Radiation for Three-Dimensional Flames, in Heat Transfer in Flames, edited by N. Afgan et al., New York, pp. 73-94, 1974.

[6] Patankar, S.V. Numerical Heat Transfer and Fluid Flow. London, McGraw Hill, 1980.

[7] Spalding, D. B. A Novel Finite-Difference Formulation for Differential Expressions involving both First and Second Derivatives. *Int. J. Num. Meth. Engng,* 4, pp. 551-559, 1972.

[8] Caretto, L. S., Gosman, A. D., Patankar, S. V. and Spalding, D. B. Two Calculation Procedures for Steady Three-Dimensional Flows with Recirculation, *Proc. 3rd Int. Conference on Numerical Methods in Fluid Mechanics.* 1972.

[9] Patankar, S. V. and Spalding, D. B. A Calculation Procedure for Heat, Mass and Momentum Transfer in Three Dimensional Parabolic Flows. *Int. J. Heat and Mass Transfer,* 15. pp. 1787, 1972.

[10] Versteeg, H. K. and Malalasekera, W. An Introduction to Computational Fluid Dynamics, The Finite Volume Method'. Malaysia: Longmans. Reprint, pp. 142-150, 1996.

[11] Lamers, A. P. G. G. Physical Models and Numerical Methods for Fluid Dynamical Problems. Lecture Notes Series. University of Technology, Eindhoven, Lecture 4.S.410, pp.140-141, 1999.

[12] Serag-Eldin, M. A. The Numerical Prediction of the Flow and Combustion Processes in a Three-Dimensional Can Combustor. Ph.D *Thesis,* London University, 1977.

[13] Jones, W. P. and Whitewall, J. H. Modelling and measurements in turbulent Combustion. Imperial College, London SW7 2BV. 20TH Symp. (Intl.) The Combustion Institute, pp. 245, 1984.

[14] Gosman, A. D. and Pun, W. M. Calculation of Recirculating Flows. Imperial College, Dept. of Mechanical Engineering, Report HTS/74/2. 1974.

REFERENCES:

[15] JANAF. Thermochemical Tables. National Bureau of Standards, NSRDS 377, Com-71, 50363,1977.

[16] Khalil, E. E. Flow and Combustion in Axisymmetric Furnaces. Ph.D. Thesis, London University. 1977.

[17] Rhine, J. M. and Tucker, R. J. Modelling of Gas-Fired Furnaces and Boilers, *and other Industrial Heating Processes.* McGraw-Hill, pp. 394-396, 1991.

[18] Roache, P. J. Computational Fluid Dynamics. (Hermosa).

[19] Gosman, A. D., Khalil, E. E. and Whitelaw, J. H. The Calculation of Two Dimensional Flows, in *Turbulent Shear Flows,* edited by Durst *et al.,* (Springer Verlag), pp. 2377, 1979.

[20] Khalil, E. E. Numerical Computations of Turbulent Reacting Combustor Flows, *in Numerical Methods in Heat Transfer,* edited by Lewis *et al. (John Wiley),* pp. 526, 1981.

[21] Khalil, E. E. Modelling of Furnaces and Combustion. Abacus Press, pp. 27-30, 1982.

[22] Pope, S. B. and Whitelaw, J. H. The Calculation of near Wake Flows. *J. Fluid Mechanics.* 73, pp. 9, 1976.

[23] Baker , R. J., Hutchinson, P., Khalil, E. E. and Whitelaw, J. H. Measurements of Three Velocity Components in Model Furnace with and without Combustion. *Pro. 15th Symp. (Int.) on Combustion,* pp. 553, 1972.

[24] Hutchinson, P. Khalil, E. E. and Whitelaw, J. H. Measurement and Calculation of Furnace Flow Properties. *J. Energy,* 1, pp. 212. 1977.

[25] Dovark, N. and Chigier, N. A. (*Proc. 15th Symp. Int.) on Combustion,* pp. 565, 1974.

[26] Baker, R. J., Hutchinson, P. Khalil, E. E. and Whitelaw, J. H. Preliminary Measurements of Instantaneous Velocity in a 2 m Square Furnace Using Laser Anemometry. *J. Heat Transfer* 96, pp. 410.

[27] Khalil, E. E., Spalding, D. E. and Whitelaw, J. H. The Calculation of Local Flow Properties in Two-Dimensional Furnaces, Int. J. Heat Mass Transfer, Vol. 18, pp. 775-791, 1975.

REFERENCES:

CHAPTER FOUR

[1] Tae-Ho Song, Simulation of Flow, Combustion and Heat Transfer in a Two-dimensional Natural Gas-Fired Industrial Furnace. Thesis, Ph.D. Purdue University, pp. 87, 180, 1986.

[2] Chisale, P.C. and Nakajima, T., 1997, " Effects of fuel Injection Mode and Combustor Exit Geometry on Swirl Combustion with Preheated Air" Kobe University Memoir Vol. 15 pp.1-9, 1996

[3] Tangirala, V. and Driscoll, J. F., 1988, "Temperatures within Non-premixed Flames: Effects of Rapid Mixing Due to Swirl; Combust. Sci. and Tech., 1988, Vol. 60. pp. 143-162.

[4] Khalil, E. E., Spalding, D. B. And Whitelaw, J. H. The Calculation of Local Flow Properties in Two-dimensional Furnaces, Int. J. Heat Mass Transfer. Vol 18, pp. 5-12, 1975.

[5] Pai, B. R., Michelfelder, S and Spalding, D. B. Prediction of Furnace Heat Transfer with a Three-dimensional Mathematical Model. Int. J. Heat Mass Transfer, Vol. 23, pp. 571-580, 1978.

[6] Abou Ellail, M. M. M., Goodman, A. D. Lockwood, F. C. And Megahed, I. E. A. Description and Validation of a Three-dimensional Procedure for Combustion Chamber Flows, in Progress in Astronautics and Aerodynamics, Turbulent Combustion, Vol. 58, AIAA, New York, pp. 163-190, 1978.

[7] Moss, W. D. Baker, S. And Bradbury, L. J. S. Measurement of Mean Velocity and Reynolds Stresses in Some Regions of Recirculating Flow, in Turbulent Shear Flows I, edited by F. Durst *et al.,* Springer-Verlag, Berlin, 1979.

[8] Patankar, S. V. Numeircal Heat transfer and Fluid Flow, McGraw-Hill, New York, 1980.

[9] Launder, B. E. AND Spalding, D. B. The Numerical Computation of Turbulent Flows, computer Methods in Applied Mechanics and Engineering, Vol. 3, pp. 269-289, 1974.

[10] Damkohler, G. Der Einfluss der Turbulence auf die Flamengeschwindigeit in gas gemischen, Z. Elektrochem. Vol. 64, pp. 601-626, 1940.

[11] Karlovitz, B. Denniston, P. W. J. And Wells, F.E. Investigation of Turbulent Flames, J. Chem. Phys., Vol. 19, pp. 541, 1951.

[12] Dugger, G. L. Effect of Initial Mixture Temperature on Flame Speed of Methane-Air, Propane-Air, and Ethylene-Air Mixtures at Low Initial Temperatures, NACA TN 2374, 1951.

[13] Lefebvre, A. H. Personal Communication, 1985.

REFERENCES:

[14] Chisale, P. C. Characteristics of Methane Swirl Combustion with Pre-Heated Air. Ph.D. Thesis, Kobe University, pp. 28-35, 1997.

[15] Lefebvre, A. H. The Role of Fuel Preparation in Low-emission Combustion. Journal for Gas Turbine and Power, October 1995. Vol. 117, pp. 623-624.

[16] Chisale, P.C. and Nakajima, T. Flame Stability in a Swirl Combustor. Paper in The Zambian Engineer, Vol.34 No.1, pp.146-147, 1999.

[17] Enomoto, H., Tsai, Y. W. and Essenhigh, R. H. Heat Transfer in a Continuous Model Furnace: A Comparison of Theory and Experiment, ASME Paper No. 75-Ht-5.

APPENDIX D

[1] Alvarez, N. J., Foote, K. L. and Pagni, P. J. Forced Ventilated Enclosure Fire, Combust. Sci. Technol., Vol. 39, pp. 55, 1984.

[2] Lockwood, F. C. and Shah, N. G. A New Radiation Solution Method for Incorporation in General Combustion Prediction Procedures, *Eighteenth Symposium (International) on Combustion.* The Combustion Institute, pp. 1405-1414, 1981.

[3] Malasekera, W. M. G. Mathematical Modelling of Fires and Processes, Ph. D. Thesis Imperial College London, 1988.

[4] Lockwood, F. C. and Malalasekera, W. M. G. Fire Computation: The Flashover Phenomenon, *Twenty-Second Symposium (International) on Combustion,* The Combustion Institute, pp. 1319-1328, 1988.

APPENDIX E

[1] Khalil, E. E. Numerical Computations of Turbulent Reacting Combustion s, in Numerical Methods in Heat Transfer, edited by Lewis et al. (John Wiley), pp. 526, 1 981.